NAVAL SHIP RESEARCH AND DEVELOPMENT CENTER
NAVAL SHIP RESEARCH AND DEVELOPMENT LABORATORY
ANNAPOLIS, MARYLAND 21402

TURBULENT FLOW DRAG-REDUCTION BY DILUTE POLY(ETHYLENE OXIDE) SOLUTIONS IN CAPILLARY TUBES

By
Ira Michael Felsen

Approved for public release;
distribution unlimited.

DEPARTMENT OF MATERIALS TECHNOLOGY

RESEARCH AND DEVELOPMENT REPORT

March 1971

Report 3240

Report 3240

Turbulent Flow Drag-Reduction by Dilute Poly(Ethylene Oxide) Solutions in Capillary Tubes

The Naval Ship Research and Development Center is a U.S. Navy center for laboratory effort directed at achieving improved sea and air vehicles. It was formed in March 1967 by merging the David Taylor Model Basin at Carderock, Maryland and the Marine Engineering Laboratory (now Naval Ship R & D Laboratory) at Annapolis, Maryland. The Mine Defense Laboratory (now Naval Ship R & D Laboratory) Panama City, Florida became part of the Center in November 1967.

Naval Ship Research and Development Center
Washington, D.C. 20007

MAJOR NSRDC ORGANIZATIONAL COMPONENTS

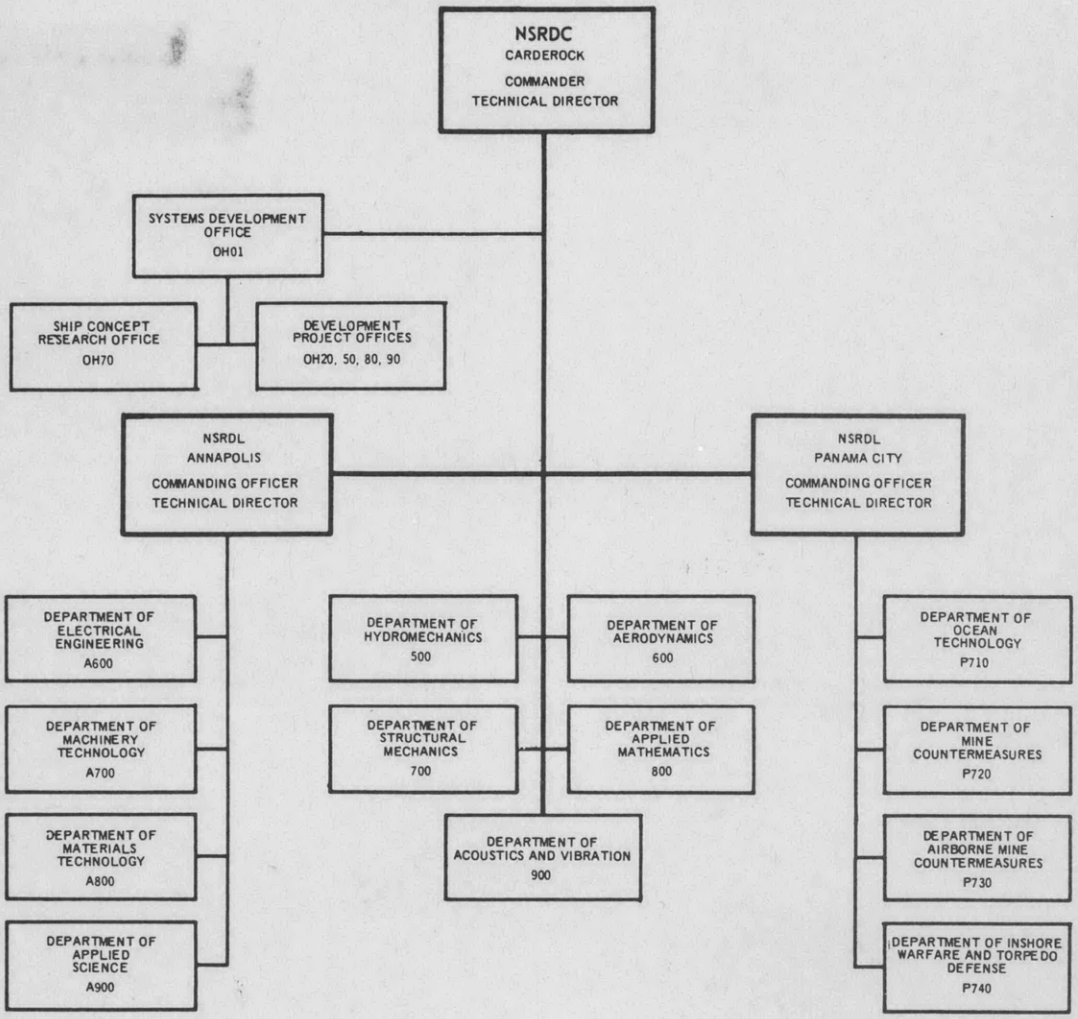

CENTER REPORT COVER
NDW-NSRDL(A) 3960/172 (9/70)

TURBULENT FLOW DRAG-REDUCTION BY DILUTE POLY(ETHYLENE OXIDE) SOLUTIONS IN CAPILLARY TUBES

By
Ira Michael Felsen

March 1971 8-717 Report 3240

ABSTRACT

Title of Thesis: TURBULENT FLOW DRAG-REDUCTION BY DILUTE POLY(ETHYLENE OXIDE) SOLUTIONS IN CAPILLARY TUBES

Ira Michael Felsen, Doctor of Philosophy, 1970

Thesis directed by: Associate Professor Theodore G. Smith

An experimental investigation of turbulent flow drag-reduction was conducted using dilute solutions of poly(ethylene oxide) flowing in capillary tubes.

This study was initiated to investigate turbulent flow drag-reduction by dilute poly(ethylene oxide) solutions in capillary tubes and thereby elucidate the mechanism of drag-reduction through interpretation of the experimental results.

Flow through capillary tubes was chosen as a means to (1) obtain a large ratio of solid surface area to fluid volume, and (2) obtain high shear stresses at low Reynolds numbers. This allowed investigation of surface effects and polymer degradation as a function of a number of variables which are known to influence drag-reduction.

Small bore capillary tubes were coated with monomolecular layers having various surface free energies. Use of these tubes offered a method of distinguishing whether drag-reduction is due in part or wholly to some property(ies) or configuration of the macromolecule in solution, or to the properties and configuration of the polymer adsorbed on the solid surface and interacting with the

solution flowing through and around the adsorbed polymer film.

In the small-bore uncoated-glass capillary tubes used, a 1 ppm poly(ethylene oxide) Coagulant solution gives drag-reduction as high as 56%. In addition, the Virk maximum drag-reduction asymptote is obtained, even at concentrations as low as 1 ppm for poly(ethylene oxide) Coagulant,and 10 ppm for poly(ethylene oxide) WSR-N-3000. Drag-reduction increases systematically with decreasing concentration, at constant Reynolds number, prior to the onset of degradation. The effect of increasing concentration is to allow intersection with the maximum drag-reduction asymptote at a higher percent drag-reduction. Upon reaching the asymptote, degradation begins and proceeds rapidly with increasing pressure driving force, or, for higher concentrations, the curves intersect and then run along the asymptote until degradation begins. Virk's asymptote is verified as being diameter and molecular weight independent. At equal Reynolds numbers, drag-reduction is independent of tube diameter until polymer degradation begins in the smaller diameter tube. At Reynolds numbers corresponding to equal wall shear stresses, drag-reduction decreases with increasing tube diameter.

In a series of 0.016 inch diameter capillary tubes of surfaces fluorocarbon, hydrocarbon, silicone, and glass, a 1/2 ppm poly(ethylene oxide) Coagulant solution gives drag-reduction as high as 59% in the glass tube. All tubes give equal drag-reduction until the onset of degradation

is approached. The maximum Reynolds number, or stability before the onset of degradation, is obtained in the uncoated glass tube. The experimental evidence shows an increase in the maximum Reynolds number at the onset of degradation with increasing surface free energy of the tube coatings. Consequently, drag-reduction increases with increasing surface free energy, at equal Reynolds numbers, at the onset of degradation.

A semi-flexible film hypothesis is presented. Emphasis is placed on the importance of surface viscosity and Gibbs elasticity of an adsorbed or hydrogen bond associated polymer film, and not on turbulence suppression by individual polymer molecules. A wall associated polymer film, exhibiting optimum surface rheology characteristics, may act to inhibit turbulence in the wall region, and thus stabilize flow and retard the onset of degradation.

ADMINISTRATIVE INFORMATION

This study was funded by the In-House Independent Research Program under Work Unit 1-821-135A and completed under Task Area Z-R011 01 01, Task 05600.

This report was originally published as a doctoral thesis for the University of Maryland.

ACKNOWLEDGMENTS

The author wishes to thank Professor T. G. Smith for the guidance and encouragement given during this study.

This work would not have been possible without financial assistance from the Naval Ship Research and Development Laboratory, Annapolis, Maryland. Funds were provided by the In-House Independent Research Program, Assignment 81-135. Special gratitude is extended to Paul Schatzberg, Nathan Glassmann, Bob Belt and the procurements and publication staffs of NSRDL and the University of Maryland Chemical Engineering Department.

Computer time was provided by the Computer Science Center at the University of Maryland under Grant 302/01/141.

The author appreciates the help of Dr. Lloyd Robeson of Union Carbide for donating the poly(ethylene oxide) used in this study.

TABLE OF CONTENTS

LIST OF TABLES

Chapter Page

LIST OF FIGURES

CHAPTER I

INTRODUCTION

The pioneering paper in the field of drag-reduction by dilute polymer solutions in turbulent flow was presented by B. A. Toms (1). He showed, for conditions of turbulent flow and constant pressure gradient, that the average velocity of a solvent fluid increased markedly upon the addition of minute amounts of a certain polymer. Consequently, the presence of the polymer results in a lower pressure gradient, at the same average velocity, than would be obtained for the solvent in turbulent flow. Hoyt (2, 3) and Fabula (4) demonstrated that minute quantities of the water soluble polymer poly(ethylene oxide) reduces drag as much as 80%, and that as little as 0.001% poly(ethylene oxide) dissolved in distilled or sea water reduces drag by as much as 60%. Their experiments with a wide variety of natural and synthetic polymers indicate three major physical characteristics that the polymer must exhibit in order to reduce drag. These are (1) an essentially linear (unbranched) molecular structure, (2) a high molecular weight, and (3) good solubility in the liquid solvent.

The object of this thesis is to investigate turbulent flow drag-reduction by dilute poly(ethylene oxide) solutions in capillary tubes and thereby elucidate the mechanism of drag-reduction through interpretation of the experimental results.

Flow in capillary tubes is chosen as a means to:

1. Obtain a large ratio of solid surface area to fluid volume: If the surface area of the capillary tube is as large as possible in comparison to the volume of fluid flowing through the capillary tube, the influence of the wall and buffer transition boundary regions in comparison to the remainder of the tube is enhanced. The surface area to volume ratio in a circular tube is $4/D$, where D is the inside diameter of the tube. Smaller diameter capillary tubes, therefore, give larger surface area to volume ratios. The shear stress at the wall, or the pressure drop across the capillary, however, becomes exceedingly high with increasing D. The capillary tubes used are chosen as a compromise between the increasing surface area to volume ratio and the mechanical and thermal limitations placed on the polymer molecules by the increasing wall shear stress.

In order to establish the relative importance of surface effects in understanding the mechanism of drag-reduction, the effect of adsorption (of polymer molecules from solution onto the solid surface) is investigated by changing the variables which are known to influence adsorption. These variables include (a) coating the inside surface of glass capillary tubes in order to obtain a spectrum of surface free energies, (b) polymer concentration, (c) polymer molecular weight, (d) hysteresis effects, (e) solution pH, and (f) surface

area to volume ratio (i.e. by changing tube diameter). Using capillary tubes with various surface coatings offers a method of distinguishing whether the Toms phenomenon is due in part or wholly to some property(ies) or configuration of the macromolecule in solution, or to the properties and configuration of the polymer adsorbed to the solid surface and interacting with the solution flowing through and around the adsorbed polymer film. Parameters b through e above, change the properties or configuration of the molecules in solution in addition to the polymer adsorption characteristics, and are therefore less discriminating than changing the surface of the capillary tubes by coating with monomolecular layers having various surface free energies.

2. Obtain high shear stresses at low Reynolds number: In the capillary tubes chosen, the wall shear stress is always greater than the onset shear stress needed to initiate drag-reduction. Consequently, the normal laminar-to-turbulent transition Reynolds number is bypassed, and an extension of the laminar flow region into the turbulent flow region is observed until degradation of the polymer occurs. In the high shear stress field, the macromolecules are mechanically degraded at low Reynolds numbers. The onset of polymer degradation and the relationship of this onset to surface effects is investigated.

Poly(ethylene oxide) is selected because of its ready availability in several molecular weights, its excellent drag-reduction properties

in water, its use and characterization by other investigators, and its relatively well defined physical properties.

CHAPTER II

LITERATURE SURVEY

II-A. Fluid Dynamic Equations

II-A-1. Laminar Flow of Newtonian Fluids in Smooth, Circular Tubes:

The simplest rheological equation for a viscous fluid is given, in cylindrical coordinates, by Newton's law of viscosity, Equation (II-1).

$$\tau = -\mu \frac{dv_z}{dr} = \mu\dot{\gamma} \qquad \text{(II-1)}$$

This states that the shear force per unit area (defined as the shear stress), τ, is proportional to the negative of the local velocity gradient (defined as the shear rate), $\dot{\gamma}$. z is the flow direction and r is the radial direction along which the velocity and shear stress are changing. The classical definition of a Newtonian fluid is one for which Equation (II-1) is valid where the Newtonian viscosity, μ, is independent of shear stress and shear rate. For flow in circular tubes, the maximum velocity is obtained at the center of the tube. The velocity gradient, therefore, vanishes at the tube center. The shear stress increases with distance from the tube center and reaches a maximum in the last molecular layer of fluid at the wall. Hence, assuming that the no-slip-at-the-wall boundary condition is realized, both the shear stress and

shear rate vanish at the center of the tube, and are at a maximum at the interface between the solid surface and the layer of fluid adjacent to the solid surface.

A summary of equations for laminar isothermal flow of Newtonian liquids through long, smooth, circular tubes is presented below.

Shear Stress at Tube Wall, τ_w:

$$\tau_w = \frac{R\Delta P_c}{2L} \tag{II-2}$$

where R is the tube radius, ΔP_c is the pressure drop across the tube, and L is the tube length.

Shear Stress, τ:

$$\tau = \tau_w (r/R) \tag{II-3}$$

where r is distance from the center of the tube.

Volumetric Flow Rate, Q:

$$Q = \frac{\pi D^4 \Delta P_c}{128 \mu L} \tag{II-4}$$

Equation (II-4) is the well known Hagen-Poiseuille law.

Average Velocity, $\overline{V}$:

$$\overline{V} = \frac{Q}{\pi R^2} \tag{II-5}$$

Velocity at Tube Center (maximum velocity), V_m:

$$V_m = 2\overline{V} = \frac{R^2 \Delta P_c}{4\mu L} \tag{II-6}$$

Point Velocity, v_z:

$$v_z = V_m \left[1 - (r/R)^2\right] \tag{II-7}$$

Shear Rate at Tube Wall, $\dot{\gamma}_w$:

$$\dot{\gamma}_w = \frac{1}{\pi R^3} \left[3Q + \Delta P_c \frac{dQ}{d\Delta P_c}\right] \tag{II-8}$$

Equation (II-8) is the well known Rabinowitsch law. This law is a general relationship independent of the nature of the fluid. For Newtonian fluids, Equation (II-8) reduces to:

$$\dot{\gamma}_w = \frac{4Q}{\pi R^3} = \frac{8\overline{V}}{D} \tag{II-9}$$

The Rabinowitsch Equation (II-8) is often used to define an average wall shear rate for pipe flow experiments when the flowing fluid does not obey Newton's law of viscosity, Equation (II-1). In general, dilute polymer solutions of poly(ethylene oxide), less than 50 parts per million by weight (<50 ppm), obey Equation (II-1) for the high shear rates which exist at the wall region in capillary tubes. Equation (II-9) can be used to calculate the wall shear rate.

II-A-2. Turbulent Flow of Newtonian Fluids in Smooth, Round Tubes:

Two dimensionless numbers which are used to describe the flow of fluids are the Reynolds number and the Fanning friction factor.

The Reynolds number, Re, is used as a criterion to describe the nature of flow of a fluid around a solid object or in a conduit. The Reynolds number is the dimensionless ratio of momentum transferred by inertial transport to momentum transferred by molecular transport, and is defined for pipe flow as:

$$Re = \frac{D\overline{V}}{\nu_o} = \frac{DV\rho_o}{\mu_o} \qquad \text{(II-10)}$$

where D is the inner diameter of the pipe, $\overline{V}$ is the average velocity of the fluid, and ν_o is the kinematic viscosity equal to μ_o/ρ_o where ρ_o is the solvent density and μ_o is the solvent viscosity. Flow in pipes is laminar for Reynolds numbers less than 2100, is in transition from laminar to turbulent for Reynolds numbers between 2100 and 3000, and is turbulent for Reynolds numbers greater than 3000.

For flow in smooth circular tubes, the Fanning friction factor (f), as defined in several standard engineering texts (5, 6) is the dimensionless coefficient of resistance to

flow and is defined by the relationship between the pressure gradient and flow kinetic energy.

$$f = \left[\frac{D}{4}\right]\left[\frac{\Delta P_c}{L}\right]\left[\frac{1}{\frac{1}{2}\rho_o \overline{V}^2}\right] \qquad \text{(II-11)}$$

where $\Delta P_c/L$ is the pressure gradient per unit length of pipe.

Combining the Hagen-Poiseuille law, Equation (II-4) with the definition of friction factor gives, for laminar flow,

$$f = 16/Re \qquad Re \leq 2100 \qquad \text{(II-12)}$$

The turbulent curve on the f versus Re plot was established experimentally by Nikuradse. Blausius derived a relationship between the friction factor and Reynolds number for Reynolds numbers between 3,000 and 100,000 which assumes a 1/7th power-law turbulent velocity-distribution. His results are expressed as:

$$f = .0791/Re^{.25} \qquad \text{(II-13)}$$

The nature of the velocity profile in turbulent flow is quite different from that obtained in laminar or streamline flow. At equal average velocities, the velocity profile in laminar flow is parabolic, as can be surmised from the Hagen-Poiseuille Equation (II-4), while the turbulent velocity profile is blunted.

The point of maximum velocity, Vm, for both laminar and turbulent flow occurs at the tube centerline. In laminar flow, the average velocity is about .5 Vm, while in turbulent flow, the average velocity is .75-.85 Vm.

Prandtl was the first to succeed in predicting turbulent velocity profiles. He postulated that during turbulent flow the velocity of the fluid adjacent to the wall was zero and that in the close vicinity of the wall there remained a layer of fluid which was in laminar motion. This is the famous "no slip at the wall" boundary condition which has proved so successful in correlations of momentum, heat, and mass transfer. The existence of a laminar boundary is, in general, widely accepted. Sherwood, Smith, and Fowles (7) review some of the current work in velocity profile measurements while presenting experimental verification of the existence of a slightly deviant laminar boundary layer. Prandtl suggested that the velocity gradient of a fluid near the wall should be dependent only on the kinematic wall shear stress (τ_w/ρ_o), the distance from the wall (y), and the kinematic viscosity (ν_o) and independent of the flow in the central portion of the pipe. Prandtl derived the linear relation for the velocity at any point (v) in the laminar sublayer of a micromolecular fluid in turbulent flow. Equation (II-14) is often called the inner law or the law of the wall.

$$\frac{v}{v_\tau} = \frac{yv_\tau}{\nu_o} \tag{II-14}$$

and

$$v_\tau = (\tau_w/\rho_o)^{1/2} \tag{II-15}$$

where v_τ is the friction or shear velocity.

The dimensionless terms v/v_τ and yv_τ/ν_o are often written as:

$$u+ = v/v_\tau \tag{II-16}$$

$$y+ = yv_\tau/\nu_o \tag{II-17}$$

Sherwood, Smith and Fowles (7) have shown the laminar sublayer velocity profile is close to, but not exactly, described by Equation (II-14) to a distance of $y+ \sim 0.2$ for water flowing in glass pipes. Granville (8) has discussed the various sublayers that exist within circular tubes as distinguished according to the behavior of their velocity profiles. These are:

1. Laminar sublayer - Turbulent fluctuations are effectively damped out.

2. Transitional sublayer - Shear stresses are influenced by both laminar and turbulent conditions.

3. Inner turbulent sublayer - Inner and outer laws apply.

4. Outer turbulent sublayer - Turbulent core.

The outer turbulent region can be described by a logarithmic velocity distribution equation, or velocity - defect equation, of the form:

$$\frac{Vm - v}{v_\tau} = F\ (y/R) \tag{II-18}$$

where R is the tube radius and F (y/R) is some function of (y/R). Prandtl obtained a velocity distribution equation derived from his mixing length theory which yields:

$$\frac{Vm - v}{v_\tau} = F\ (y/R) = -\frac{1}{\varkappa}\ell n\ (y/R) \tag{II-19}$$

where $\varkappa$ is von Kármán's constant; $\varkappa = 0.4$.

Von Kármán obtained, from his similarity theory:

$$\frac{Vm - v}{v_\tau} = F\ (y/R) = -\frac{1}{\varkappa}\left[\ell n\ (1 - \sqrt{1 - y/R} + \sqrt{1 - y/R}\right] \tag{II-20}$$

The velocity in the central portion of the pipe (turbulent core) is independent of viscous behavior for fully developed turbulent flow. The difference between the maximum velocity at the center of the pipe (Vm), and the point velocity (v) is a function of the kinematic wall shear stress, the distance from the wall, and the

pipe radius, R. Equation (II-18) is often called the outer law or velocity-defect law. A universal logarithmic velocity distribution equation can be obtained by equating the velocity gradient for the laminar region expressed as Equation (II-14) and the turbulent core region, Equation (II-18). This yields:

$$v/v_\tau = A \ln (yv_\tau/\nu_o) + B_2 \qquad \text{(II-21)}$$

or

$$u+ = A \ln y^+ + B_2 \qquad \text{(II-22)}$$

A = 2.5 and is the reciprocal of von Kármán's constant. B_2 is an empirically determined constant for a micromolecular fluid and can be used as a measure of the thickness of the laminar sublayer.

Von Kármán treated the transitional sublayer and the inner turbulent sublayer as a single "buffer" region in analyzing the velocity distribution data of Reichardt (9). The results of his analysis are presented in three relationships which are used to estimate the complete velocity profile for micromolecular fluids in turbulent flow in smooth pipes.

Laminar layer:

$$u^+ = y^+ \qquad y^+ < 5 \qquad \text{(II-14)}$$

Buffer layer:

$$u^+ = -3.05 + 5.0 \ln y^+ \qquad 5 \leq y^+ \leq 30 \qquad \text{(II-23)}$$

Turbulent core:

$$u^+ = 5.5 + 2.5 \ln y^+ \qquad y^+ > 30 \qquad \text{(II-24)}$$

The average velocity ($\overline{V}$) is obtained by integrating the point velocity (Equations II-14, II-23, II-24) over the entire cross sectional area of the pipe. Coupling the result of this integration with the definition of friction factor (Equation II-11) yields Prandtl's "Universal Law of Friction" for long, smooth, circular tubes.

$$\frac{1}{\sqrt{f}} = A \log_{10} (Re\sqrt{f}) - B \qquad \text{(II-25)}$$

where A = 4.0 and B = 0.4 for $3000 \leq Re \leq 3,250,000$.

II-A-3. Flow of Newtonian Fluids in Smooth, Circular Capillary Tubes:

Latzko (10) predicts the entrance length, Le, required for the friction factor to become equal to the fully developed turbulent friction factor is:

$$Le/D = .623 (Re)^{.25} \qquad \text{(II-26)}$$

for D = .016 inch, and for Re = 10^4, the entrance length is approximately .01 inch or 1/4 of a millimeter. It is therefore assumed that no entrance or exit corrections are necessary for large (>50) L/D ratios when using the capillary tube and Reynolds number referred to above.

The primary correction which must be applied to the total pressure in order to obtain the pressure held in equilibrium inside a capillary tube is a kinetic energy correction:

$$\Delta P_c = \Delta P_t - m \rho_o \overline{V}^2 \qquad \text{(II-27)}$$

ΔP_c is the corrected pressure drop across the capillary tube and represents the pressure held in equilibrium inside the capillary if entrance and exit effects are neglected. ΔP_t is the total pressure drop across the ends of the capillary tube. The last term in Equation (II-27) represents the Hagenback "kinetic energy correction" and represents that part of the energy which is imparted to the liquid leaving the capillary and destroyed outside the capillary by conversion into heat. ρ_o is the density of the liquid and m is a constant coefficient. m = 1.12 for a parabolic velocity distribution and 1/2 for the case of a uniform velocity across the capillary tube. Since neither of these cases applies to this work, a value of m = 1.0 was chosen (11).

II-B. Poly(ethylene oxide) Properties

II-B-1. Poly(ethylene oxide) Solid:

Poly(ethylene oxide) meets all the requirements of a good drag reducer. It is a water soluble linear polymer having a repeating unit of:

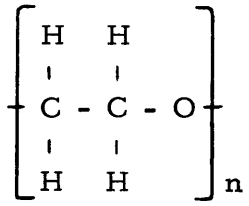

C is carbon, O is oxygen, H is hydrogen, and n is the number of repeating units in the polymer chain. Poly(ethylene oxide) is commercially available from Union Carbide Corporation under the trade name Polyox. Blends with uncharacterized molecular weight distributions are available in grades of average molecular weights from approximately one hundred thousand to ten million.

For a polymer molecule of molecular weight 4.27×10^6, Patterson (11) calculates that the strung-out length, based on bond distances, is 369,000 A°, and that the diameter is about 4 A°. Also, a molecule which assumes a compact ball configuration, having the same density as the dry state, would have a radius of 110 A°.

II-B-2. Poly(ethylene oxide) in Dilute Solution:

The radius of gyration of a 4.27×10^6 weight average molecular weight poly(ethylene oxide), as calculated from the light scattering data of Merrill et al (12), is 2300 A°. Not surprisingly, the evidence points toward the conclusion that the configuration of the molecule in solution is intermediate between a strung-out and a compacted ball.

Filisko (13) has indicated that the configuration of poly(ethylene oxide) in concentrated solution is that of a helical coil and that the coil stability is obtained through hydrogen bonding in the neighboring polymer molecules. Hand and Williams (14) show that the system poly(acrylic acid) - water abruptly becomes a good drag-reducer when the pH of the solution is lowered between pH 3 and pH 2.8. As evidence of the helical coil configuration, Hand and Williams cite the work of Mathieson and McLaren (15) who have shown that near this pH poly(acrylic acid) undergoes a second-order phase transition from extended rod to a more compact structure, suspected to be helical. From the above evidence, one can speculate that there is a relationship between the polymer molecule having a helical configuration in solution and the good drag-reducing characteristic of the solution. Mathieson and McLaren also suggest that poly(acrylic acid) precipitates in the region of pH 2, while Hand and Williams find no

evidence of precipitation and are able to achieve an even higher drag-reduction at pH 2. This is contrary to the well documented evidence that drag-reducers are more effective in a good solvent and, therefore, lose much of their effectiveness near the point of precipitation of the polymer from solution.

Polymer elongation and orientation in the flow field is of considerable interest. Little (16) has shown that poly-(ethylene oxide) solution of MW 200,000 and 600,000 continues to deform with increasing shear rate or velocity gradient even after alignment with the flow field is essentially completed. The concentrations used were high (2-4% and .12-.5% for the low and high polymers, respectively). Alignment with the flow field is well established for a large number of polymer molecules, and is, in fact, the basis of several of the proposed mechanisms of viscous drag-reduction. Cottrell (17) has shown that in a couette shear field the actual elongation fell short of the 10 fold elongation predicted, and that the deformation of the polymer molecule was in agreement with theories developed for nonfree-draining coils which exhibit a finite internal viscosity.

II-C. Adsorption of Polymer Molecules

Polymer adsorption is a complicated process which involves competing interactions between the polymer and the solid surface, and the polymer and the solvent. In addition, an

attempt to elucidate the conformation of an adsorbed molecule involves predictions of the number of polymer segments attached at the surface, the strength of those attachments, the thickness of the adsorbed layer, the percent surface coverage, and the availability of the unattached portions of the polymer to interact with the polymer solution. Stromberg (18) summarizes the major advances in polymer adsorption theories and experimental methods.

II-C-1. Theories of Adsorption of Polymers from Solution onto a Solid Surface:

Jenckel and Rumback (19) proposed a model of polymer adsorption where the polymer adsorbed segments (trains) are separated by bridges (loops) extending into the solution. Frisch, Simha, and Eirich (20) used this model in their statistical-mechanical treatment of equilibrium polymer adsorption. The adsorbed polymer molecule was assumed to be characterized by a Gaussian distribution of end-to-end distances. One end of the molecule is attached to the origin of a coordinate system while the other end takes a random walk until it hits a solid surface which acts as a reflecting wall. The probability, averaged over all polymer segments, that an arbitrary segment of the polymer molecule is trapped on the surface, is a function of the number of polymer segments, the probability that a segment is adsorbed

upon contacting the surface, and the bond angles and flexibility of the polymer chain. When one segment of the polymer chain is adsorbed, a new distribution of end-to-end distance is determined. This treatment was extended by Frisch and Simha to treat solvent adsorption, chain interference near the surface, and multilayer adsorption. In addition, Frisch treated the limiting cases of very weak and very strong attractive forces. One fundamental weakness in the above theory is that the shape of a molecule having zero attractive energy was determined, and this shape was not considered a variable in treating the thermodynamic equilibrium between the surface phase and the solution. This treatment led to the conclusion that the fraction of polymer segments on the surface (p) is proportional to the square root of the total number of segments (t) and that relatively few segments are actually on the surface unless the attractive forces are very high. At low attractive energies, therefore, a low value of p is predicted requiring large loops to extend into the solution. In addition, the size of these loops is predicted to be proportional to the square root of the molecular weight. The above is in disagreement with a few of the more recent theories and experiments. Other conclusions from the Frisch-Simha-Eirich theory, in agreement with more recent theories, predict a flat molecule with a large value of p at large attractive energies, preferential

adsorption of high-molecular-weight factions (if chain interference at the surface is not a controlling factor), and a positive or negative effect of temperature on the amount of adsorption which depends on solid-solvent-polymer interaction factors.

A thermodynamic approach to polymer adsorption was proposed by Forsman and Hughes (21) for very dilute solutions with slight surface coverage and small polymer-surface interactions. The actual fraction of the surface covered by the polymer segments (θ) is proportional to the square root of the molecular weight. Forsman and Hughes also predicted that the adsorption isotherm has an initial slope which increases rapidly with increasing molecular weight and levels off more rapidly as the molecular weight increases. For low surface coverage and low concentrations, and for small surface-interaction energies, Langmuir type adsorption prevails. The Langmuir region associates increased adsorption with increasing molecular weight, and decreasing adsorption with increasing temperature.

Silberberg (22) attempted to overcome the weakness of the Simha-Firsch-Eirich theory by considering the effect of the surface-polymer interaction energy for the cases of (a) the ends of the adsorption loop at a minimum distance apart, (b) not all surface layer sites adsorbing, and (c) not all polymer segments adsorbable. Basic conclusions from Silberberg's treatment of

the isolated adsorbed polymer molecule are (a) the sizes of the loops and the trains along the surface are independent of the molecular weight, (b) for a flexible molecule, the loops are small, and the molecule is close to the surface if all surface sites and polymer segments are adsorbing, (c) structural restrictions increase the size of the loops and increase the energy requirements for adsorption, and (d) even for sterically unfavorable cases, the energy requirements for adsorption are not very large.

Silberberg (22) extended his model to include solvent effects and equilibrium with polymer molecules in solution. For dilute solutions and high molecular weight ($>10^4$) the amount of polymer adsorbed is independent of both molecular weight and the equilibrium volume fraction of polymer molecules in the solution adjacent to the adsorbed layer. The layer is, in general, thin for high attractive energy. The value of p is high at low adsorption energy, showing that an appreciable amount of adsorption will occur even under unfavorable conditions.

Hoeve, DiMarzio, and Peyser (23), and Roe (24) have shown that Silberberg's assumption of uniform-size loops and trains was too restrictive. For an isolated molecule, in disagreement with Silberberg, they predict a distribution of loop sizes, and for flexible molecules, very large loops and few

adsorbed units for very small adsorption energies, and small loops and larger values of p as the energy increases. In agreement with Silberberg, and in disagreement with Simha-Frisch-Eirich, they stated that large energies are not required for large values of p and small loop sizes.

Prediction of the theoretical configuration of polymer molecules rests, in part, on experimental results which will report values of the adsorption energy for adsorption of a polymer segment at a solvated surface. Experimentally, however, one usually measures the thickness of the adsorbed layer and the fraction, p, of chain segments attached to the surface.

II-C-2. Experimental Techniques:

Several experimental techniques have proved useful in elucidating the conformation of adsorbed polymers. These are:

1. Viscosity Measurements
2. Infrared Spectroscopy Measurements
3. Ellipsometry Measurements.

These experimental techniques will be discussed in Sections II-C-3 to II-C-6.

II-C-3. Viscosity Measurements:

Adsorbed film thicknesses from precision viscosity measurements, using capillary type viscometers, appear to give anomalous results for polymer solutions of very dilute

concentrations. Curves of η_{sp}/c versus c yield linear plots down to low concentrations. At some low concentration, dependent on molecular weight, the curve deviates from a straight line and begins to bend upward, or downward. This effect has been reviewed by Öhrn (25) and interpreted as being caused by a failure to account for adsorption effects in the capillary viscometer. Öhrn calculates the thickness of the adsorbed layer using the relation:

$$\eta_{sp}^*/c = \eta_{sp}/c + 4a\,(\eta_{sp}/c + 1/c)(1/R) \qquad \text{(II-28)}$$

where η_{sp}^*/c is the apparent reduced viscosity, η_{sp}/c is the true reduced viscosity $\left(\eta_{sp} = \frac{\eta-\eta_o}{\eta_o}\right)$, η is the solution viscosity, η_o is the solvent viscosity, a is the thickness of the adsorbed polymer layer, and R is the capillary radius. In order to calculate the "hydrodynamic" average thickness of an adsorbed polymer film, it is necessary to assume that the thickness is constant for a given concentration, and to measure the solution viscosity with various diameters of capillary tubes.

The actual relationship of an average "hydrodynamic" thickness to the molecular dimensions and conformation of the adsorbed molecule is not clear. Complicating factors are: (1) the unknown concentration distribution of the adsorbed layer, with the concentration decreasing from the surface, and (2) the

effect of shear rate on the concentration distribution and layer thickness. For these reasons, and others, measurement of the extension of the adsorbed polymer molecule from the solid surface is difficult with ordinary viscometer techniques. A great deal of information, however, has been obtained by Rowland et al (26) using variations of the viscometry technique. In a most absorbing series of experiments, Rowland (27) calculated the reduction in effective cross section of sintered glass capillary tubes to obtain an average hydrodynamic thickness of several adsorbed polymer films. In general, Rowland concludes that under many conditions polymers adsorb onto solids from dilute solution in the form of monolayers of molecular coils whose dimensions are proportional to those of the free coils in that particular solution.

II-C-4. Infrared Spectroscopy Measurements:

Fontana and Thomas (28) reported the only direct experimental method for determining the fraction, p, of available polymer segments that are attached to the surface. This method is based upon a shift in the wavelength of one or more infrared absorption peaks for the polymer molecule when the polymer is adsorbed (attached) to the solid surface. In general, for strongly adsorbed molecules (high attraction energy) there is little or no dependence of p on adsorbance (weight of polymer

adsorbed/weight of adsorbent) or concentration. The number of adsorbed segments, p, although high at low concentrations, decreases with an increase in adsorbance or concentration although p is high at low concentrations. This behavior is consistent with the concept of an increasing loop size as the concentration increases. These results are in agreement with the latest theories which propose a flat conformation, independent of concentration for high interaction energies and the possibility of large or small loops at lower attractive energies.

II-C-5. Ellipsometry Measurements:

The method of ellipsometry is based on measuring the changes in state of polarization of light upon reflection from a surface. The measurements are performed in situ with the adsorbed polymer in contact with the solution under quiescent conditions. Using this technique, the thickness and refractive index of the adsorbed film can be measured. Since the adsorbed film is a mixture of polymer and solvent, the refractive index can be used to determine the composition of the adsorbed layer and together with the measured thickness, the amount of polymer adsorbed per unit area.

Stromberg's (29) work is illustrative of polymer adsorption experiments and analysis of the conformation of adsorbed polymer molecules.

Ellipsometric measurements were made on the system polystyrene (MW ~ 1,370,000) in cyclohexane adsorbing onto chrome and mercury, and poly(ethylene o-phthalate) in methylacetate adsorbing onto chrome.

i. Polystyrene-cyclohexane-chrome: The time necessary to attain an "equilibrium" value of adsorbance is found to be dependent on the solution concentration and molecular weight of the polymer. For the system described, the adsorbance was approximately 3 mg/cm^2 after a few minutes, 5 mg/cm^2 after 50 minutes, and reached a plateau of about 7 mg/cm^2 after 24 hours. This time effect is interpreted to indicate an initially flat conformation, with subsequent desorption of some of the original segments and adsorption of additional polymer molecules, resulting in larger loops and increased thickness of the film. At low concentrations, the polymer molecule appears to be in a flat configuration. The thickness rises rapidly with a small increase in concentration while the adsorbance rises less rapidly but peaks at about the same concentration as the thickness. In general, the fraction of segments adsorbed per polymer chain, p, decreases as the concentration increases in order to allow more segments to loop into the solution. At low molecular weights, the thickness of the film is proportional to the square

root of the molecular weight. At a MW ~ 3,300,000, the curve reaches a plateau.

ii. Polystyrene-cyclohexane-mercury: Adsorption onto mercury was markedly different. The film thickness reached a value in the first few minutes and remained constant over a 24-hour period while the adsorbance increased. Also, the thickness of the adsorbed layer was independent of molecular weight. Therefore, a flat configuration is rapidly assumed, and this configuration is maintained as the empty surface sites are filled by additional adsorbing molecules. Therefore, the value of p, the fraction of chain segments on the surface, is independent of time, molecular weight, and surface population.

A measure of the attractive energy between polystyrene and the metallic surfaces is the London dispersion force, γ^d. γ^d is approximately 100 dynes/cm for chrome, and 200 dynes/cm for mercury. Thus, adsorption in a flattened configuration is attributed, by Stromberg, to the higher interaction energy in the polystyrene-mercury system. For high attractive energies, as espoused by Silberberg's theory, it is reasonable to expect a high value of p, and a small loop size independent of the coil dimensions in the solution. In addition, any change in the film thickness during the adsorption period would be small.

Stromberg qualifies the above analysis by stating that a fundamental difference may exist between liquid and solid adsorbing surfaces, but this factor is presently unresolved.

iii. Poly(ethylene o-phthalate)-ethylacetate-chrome: The same results were obtained for the polar polyester adsorbing on chrome as was obtained for the system polystyrene-cyclohexane-mercury. The primary difference between this system and polystyrene-cyclohexane-chrome system is the increased attractive energy due to the polar polyester molecule.

II-C-6. Adsorption of Poly(ethylene oxide) - Experimental Results:

Ellipsometric studies under quiescent conditions of dilute solutions of PEO have recently been performed by Peyser (34). His in situ measurements of a 400 and a 1300 ppm coagulant solution show no measurable adsorption after four days onto quartz slides. Peyser states, however, that a finite adsorption does take place (as determined qualitatively from studies of adsorption onto pyrex powder). If adsorption does take place, the macromolecule must assume an extremely flat configuration and/or not adsorb as a very concentrated film. In line with this reasoning, Peyser places an upper limit on the amount adsorbed as a function of the film thickness and the concentration or adsorbance. If an adsorbed film of 50 A^{o} was present, the film would have been observed if the film adsorbance was 1 mg/m^2.

Conversely, if the film adsorbance was as high as 1 mg/m^2, then the film thickness could not be greater than 50 A°.

Howard & McConnell (35) studied the adsorption of PEO of molecular weight $<10^4$ onto porous nylon. Their results show a negative adsorption of PEO from water onto nylon. Their results, however, are suspect due to their use of a porous adsorbent. For example, the surface area of the nylon when calculated from a methanol isotherm was 100 m^2/g, approximately 30 times higher than that measured from a BET nitrogen isotherm (3.41 m^2/g). The authors attribute this to penetration of the nylon by small molecules of suitable polarity. On this basis, the absorption of water, a very small, very polar molecule, is even more likely. Since the adsorption of polymer molecules onto internal adsorption sites is limited by pore size and diffusion effects, and since the specific amount of adsorbent swelling is unknown, and since the amount of polar solvent absorbed by the porous nylon is extremely large in comparison with the amount of polymer expected to adsorb, the adsorption of PEO onto low energy surfaces remains experimentally unresolved.

II-C-7. Summary, Adsorption:

Under quiescent equilibrium conditions, adsorption of poly(ethylene oxide) on very high energy surfaces (e.g., quartz)

is expected to be in a flat configuration, less than 50 A° and having a high value of p, and held tightly to the surface because of the high attractive energy. For tubes with lower surface free energy, the adsorbed polymer, if any, is expected to be in a less flat configuration, having a lower value of p than the quartz surface, and in general, held less tightly to the surface.

The effects of the shear field imposed by the flowing fluid on the adsorbance and adsorption configuration is unknown, as are the dynamic interactions between the adsorbed layer and the polymer molecules in solution.

II-D. Characterization of Capillary Tubes by Capillary Rise Experiments

Zisman (36) offers an excellent review of the thermodynamic wetting properties of solids and adsorbed films. The Dupré equation defines the reversible work of adhesion of liquid and solid, W_A.

$$W_A = \gamma_{S^{\circ}} + \gamma_{LV^{\circ}} - \gamma_{SL} \qquad \text{(II-29)}$$

where $\gamma_{S^{\circ}}$ = free energy at interface of solid and vacuum; $\gamma_{LV^{\circ}}$ = free energy at interface of liquid and saturated vapor (surface tension); γ_{SL} = free energy at interface between solid and liquid. Young's equation treats the contact angle of a liquid as the result of the mechanical equilibrium of a drop resting on a plane solid

surface under the action of three surface tensions.

$$\gamma_{SV^o} - \gamma_{SL} = \gamma_{LV^o} \cos\theta \qquad \text{(II-30)}$$

where γ_{SV^o} = free energy at interface of solid and saturated vapor; θ = contact angle. Wettability is usually defined in terms of the contact angle. When a liquid is nonspreading, $\theta \neq 0^o$; when the liquid wets the solid completely and spreads freely over the surface at a rate depending on the liquid viscosity and solid surface roughness, $\theta = 0^o$. Therefore, the contact angle is an inverse measure of wettability. Combining the Young and Dupré equation and eliminating γ_{SL} results in the most commonly used definition of the reversible work of adhesion.

$$W_A = (\gamma_{S^o} - \gamma_{SV^o}) + \gamma_{LV^o} (1 + \cos\theta) \qquad \text{(II-31)}$$

$$W_A = fsv^o + W_A^* \qquad \text{(II-32)}$$

$$fsv^o = (\gamma_{S^o} - \gamma_{SV^o}) \qquad \text{(II-33)}$$

where fsv^o = immersion free energy of solid in vapor phase (sometimes called "equilibrium spreading pressure" with symbol π); W_A^* = reversible work of adhesion of liquid to solid when coated with a film of the saturated vapor. For low energy surfaces (e.g., polymers), it is generally agreed that fsv^o $<<< W_A^*$ or the difference between the vacuum state and the

saturated vapor state is negligible. For high energy surfaces (e. g., metals), fsv^{o} is important.

Theoretical work by Good (37) relates γ_{S}^{o} to equilibrium contact angle data, with the result:

$$\gamma_{S}^{o} = \frac{[\gamma_{LV}^{o} (1 + \cos\theta) + fsv^{o}]^{2}}{4 \Phi^{2} \gamma_{LV}^{o}} \qquad \text{(II-34)}$$

where Φ is a function of the molecular properties of the liquid-solid system (dipole moment, ionization energy, and molecular radius). In many situations, Φ has a numerical value close to unity. Since $fsv^{o} <<< W_{A}^{*}$ for low energy surfaces, Good's equation can be reduced to the more useful form:

$$\gamma_{S}^{o} = \frac{\gamma_{LV}^{o} (1 - \cos\theta)^{2}}{4} \qquad \text{(II-35)}$$

combining with $W_{A} = \gamma_{LV}^{o} (1 + \cos\theta)$, Equation (II-31), and assuming $fsv^{o} <<< W_{A}^{*}$:

$$\gamma_{S}^{o} = (W_{A}/2)^{2}/\gamma_{LV}^{o} \qquad \text{(II-36)}$$

$$W_{A} = 2 (\gamma_{S}^{o} \gamma_{LV}^{o})^{1/2} \qquad \text{(II-37)}$$

A well known method of determining the surface tension of a liquid, γ_{LV}^{o}, is to place a clean glass capillary tube into the liquid of interest. The liquid will rise above or fall

below the reservoir liquid level. The surface tension of the liquid can be obtained from a force balance, with the result:

$$\gamma_{LV}^{o} = \frac{r\rho_o gh}{2\cos\theta} \qquad \text{(II-38)}$$

where r = inside radius of the capillary tube; ρ_o = density of the liquid; g = 981 cm/sec^2, h = capillary rise; θ = contact angle.

Combining the capillary rise Equation (II-38) with the work of adhesion Equation (II-31), and neglecting fsv^{o} results in the relation:

$$W_A = \gamma_{LV}^{o} + r\rho_o gh/2 \qquad \text{(II-39)}$$

The surface free energy is calculated from the work of adhesion through Good's Equation (II-36).

CHAPTER III

THEORIES OF DRAG-REDUCTION

Virk (38) has shown that there exists a maximum drag reduction asymptote beyond which no further reduction of viscous drag has been found experimentally. This asymptote is expressed as

$$f = 0.42\ (Re^{-0.55}) \qquad \text{(III-1)}$$

as compared to

$$f = 16.0\ (Re^{-1.0}) \quad \text{Poiseuille} \qquad \text{(III-2)}$$

$$f = 0.0791\ (Re^{-0.25}) \quad \text{Blasius} \qquad \text{(III-3)}$$

For turbulent flow drag-reduction ($Re > 3000$), the region of the f versus Re plot is, therefore, presently confined to that portion between the Blasuis line and the Virk maximum drag-reduction asymptote. At a constant Reynolds number, the friction factor (coefficient of resistance to flow) is lower for the polymer solution than for the pure solvent. Since von Kármán's constant, κ, remains unchanged (39) Prandtl's "Universal Law of Friction" needs to be modified in order to indicate the presence of the macromolecule (polymer) in the micromolecular solvent.

The universal logarithmic velocity law for polymer solutions, analogous to Equation (II-22) becomes:

$$u^+ = A \ln y^+ + B_1 \qquad \text{(III-4)}$$

where B_1 is an unknown function of the polymer concentration, polymer physical and chemical characteristics, the kinematic wall shear stress, the distance from the wall, and the solvent kinematic viscosity. Important polymer characteristics are molecular weight, solubility, adsorptivity, radius of gyration, rigidity, elasticity, and viscoelasticity, among others.

Understandably, then, a comprehensive correlation based on all known properties of macromolecules in solution is forthcoming.

Several empirical relationships have been proposed to describe the flow behavior of dilute polymer solutions in pipes and to correlate this flow behavior with the physical and chemical properties of the solutions. Meyer (42) analyzed the velocity profiles measured by Ernst (39) and suggested the following correlation:

$$\frac{1}{\sqrt{f}} = \left(4 + \frac{\alpha}{\sqrt{2}}\right) \log_{10} Re\sqrt{f} - \frac{\alpha}{2} \log_{10} \left(\frac{\sqrt{2}\, U^* D}{\nu_o}\right) - 0.4 \qquad \text{(III-5)}$$

where α is Meyer's adjustable fluid property parameter; U^* is the critical friction velocity for drag reduction.

Elata, Lehrer, and Kahanovitz (53) proposed a similar equation which predicts the critical value of $Re\sqrt{f}$ at which drag-reduction is initiated if the relaxation time (λ) of the polymer molecule is known.

$$\frac{1}{\sqrt{f}} = \left(4 + \frac{\alpha}{\sqrt{2}}\right)\log_{10} Re\sqrt{f} - \frac{\alpha}{\sqrt{2}}\log_{10}\frac{\lambda\nu_o}{D^2} - 0.4 \qquad \text{(III-6)}$$

The relaxation time developed by Rouse (54) can be expressed as

$$\lambda = \left(\frac{6\,\rho_p\nu_o}{\pi^2 kTN}\right)\left(\frac{\nu_p - \nu_o}{\nu_o C}\right)M \qquad \text{(III-7)}$$

where ρ_p is the polymer density; k is the Boltzmann constant; T is the temperature; N is Avagadro's number; M is the molecular weight of the polymer; C is the concentration of the polymer solution.

Oldroyd (41) proposed that the interaction between rotating polymer chains and pipe wall increases the dimensional thickness of the laminar boundary layer. Photographic evidence, by Shaver and Merrill (40), shows a suppression of vortices near the wall for turbulent flow of weakly viscoelastic solutions. The decreased turbulence in the boundary layer reduces momentum transfer in the radial direction, thus effectively increasing the axial flow velocity. Oldroyd (41) defines this average velocity change in the axial direction as a "slip" velocity, $\overline{V}_s$, which is

superimposed on the average solvent velocity, $\overline{V}_o$, to give the average polymer solution velocity, $\overline{V}_p$.

Oldroyd's slip at the wall theory will remain an engineering correlation method, rather than a fundamental answer to the mechanism of drag-reduction, until an order of magnitude improvement in the measurement of velocity profiles near the wall is obtained. Another possibility, although unlikely, is that the mobile adsorbed layer of long chain polymer molecules at the wall aligns itself with the shear field in a configuration such that the frictional resistance in the wall area is reduced. Oldroyd's concept of boundary layer thickening, however, is an established phenomenon, which seems to correlate drag-reduction data (42). Boundary layer thickening, however, appears to be a consequence of the mechanism, rather than the mechanism, of drag-reduction. The laminar boundary layer has been shown to have a thickness, in dimensionless units, of $y^+ \sim 10$ (38), in comparison with $y^+ \sim 5$ in the pure solvent.

The value $y^+ \sim 10$ is quite interesting, since Laufer (43) has shown that all turbulent energy rates reach a sharp maxima, "near the pipe wall," at $y^+ \sim 10$. Virk (38) chose to characterize the small scale turbulence with a "dissipation wave number," k_d, of dimensions $(\text{length})^{-1}$, which was derived

from the turbulent energy spectrum near the wall. This lead to Virk's "onset hypothesis" which is summarized as

$$2R_g (v_T/\nu_o) = 0.015 \pm 0.005 \qquad \text{(III-8)}$$

where R_g is the rms radius of gyration of a random coiling molecule in dilute solution. Virk showed that Equation (III-8) is relatively independent of concentration and pipe diameter. Further study of the onset of drag-reduction by Hanson (44) and Patterson (11) have shown Virk's onset hypothesis to be partially incorrect as both workers obtained an earlier onset with increasing concentrations. However, Patterson's work shows a "general agreement" with the Virk onset hypothesis.

ν_o/v_T is a measure of the smallest turbulent eddies present in the flow field. Virk's calculations indicate that the macromolecule is about two orders of magnitude smaller than the size of the dissipative eddies at the onset of drag reduction. This led Virk to analyze an analogous "time" based hypothesis, substituting macromolecular relaxation time, λ, for $2R_g$ and a dissipation frequency, W_d, for k_d. The time onset product (λW_d) yields a 100 fold variation over the same experimental data where the length onset product, Equation (III-8), is constant within $\pm 30\%$. These results suggest, with respect to mechanism analysis, the following three conclusions. First, the time based

hypothesis, which shows the influence of viscoelasticity in drag-reduction, may not play as large a role as length scale phenomena. Secondly, since the size of the eddy at onset is two orders of magnitude larger than the isolated polymer molecule, and the onset "constant" is a function of concentration anyway, that the length based scale needs improvement in order to predict the mechanism of drag-reduction. Finally, the physical ability of the macromolecule to suppress turbulence in the formative stages, at wall distances $<y^+ = 10$, appears important. In addition, it appears that the rate of change of shear rate, and solvent particle acceleration, may be important. The final mechanism should predict the onset of drag-reduction, eventual saturation to Virk's asymptote and the onset of degradation.

The existence of clumps or clusters of polymer molecules was established by Fabula (45). The aggregation theory proposed by Fabula, Lumley and Taylor (46) suggests that the migration of stretched aggregates away from the center of intense shearing retards the intensification of shear layers. In a later paper, Lumley (47) concludes that the agglomerates are formed, and broken up, as a consequence of the fluctuating strain rate of the turbulence. In addition, the agglomerates formed are probably not dynamically important at the low volume concentrations important in drag-reduction since the time scale for the

formation of an agglomerate is about an order of magnitude longer than the relevant time scale of the strain rate.

Merrill (12) suggested that as macromolecules elongate, the local viscosity perpendicular to the direction of shear might be orders of magnitude greater than the viscosity parallel to the direction of shear. The presence of elongated macromolecules in the high shear region near the wall suppresses turbulent fluctuations in the radial direction due to a local anisotropic viscosity. Since the turbulent eddies at drag-reduction onset are two orders of magnitude larger than the molecules, and since the macromolecules should see turbulent eddies as a laminar flow (11), direct interaction of macromolecules with existing turbulence as the mechanism of drag-reduction is unlikely.

The addition of long chain polymers to a solvent in quantities defined in parts per million results in a solution which theoretically exhibits viscoelastic behavior. Under the influence of a change in shear rate, or a transient shear, a dissolved polymer molecule is assumed to act as an elastic body, absorbing the energy imparted to it by the accelerated solvent molecules. The relaxation time of the molecule, λ, is the time required for the disturbed molecule to release the adsorbed energy and return to its equilibrium configuration in the steady

shear field. According to the viscoelastic theories, the polymer molecule suppresses turbulent eddies by absorbing the turbulent kinetic energy in the form of potential or configurational energy, and then being transported from the wall region to the turbulent core where the molecule relaxes and releases the stored energy (48-50). Adsorption of a small amount of energy in the buffer region is assumed to substantially change the velocity profile in the wall region, and release of this energy is assumed to negligibly affect the turbulence within the turbulent core. Walsh (51) predicts that as the ratio of energy storage in the molecule to the turbulent energy diffusion becomes unity, drag-reduction should begin. This ratio is given as

$$\frac{8CM[\eta]^2 \tau_w}{R_c T} \qquad \text{(III-9)}$$

Verification of this equation remains unestablished pending investigation with a homologous series of fractionated polymers. A major uncertainty of the viscoelastic theory is that explicit in the theory is the transport of the molecule from the wall region to the turbulent core, thus causing drag-reduction to be a function of competition between the molecule transport time and the molecule relaxation time. Patterson (11) states that it has not been demonstrated that the relaxation time is longer than the transport time.

A turbulent flow experiment with a coiled tube might give some clue to the applicability of the viscoelastic theory. The coil will induce a secondary flow in the pipe and the velocity profile will vary in the angular direction as well as the radial direction. The result of this internal circulation is to cause the transport of polymer molecules through a decreasing shear field toward the tube axis and then back through an increasing shear field toward the pipe wall. If the decreased transport time due to secondary flow is significant with respect to the transport time in a straight tube, and is also significant with respect to the polymer relaxation time, an increase in drag-reduction should be observed if viscoelasticity is important.

The single, most striking, property of poly(ethylene oxide) solutions is their ability to be drawn out into a "string" or "fiber." Filament formation in uniaxial tension, or thread flow, is usually exhibited by solvent solutions whose bulk viscosity is some 1000 times greater than the viscosity of effective poly(ethylene oxide) drag-reducing solutions. Droplet formation along the extending fiber indicates that the solvent is being squeezed out of the fiber, resulting in a fiber exhibiting a high viscoelasticity. Birefringent studies between crossed polarizers by Pruitt, Rosen, and Crawford (52) indicate that the solute molecules are perpendicular to the direction of the fiber, and

that as the solvent is "sweated" out, the fiber packs in a helical configuration.

Extension under uniaxial tension results in "stretching" the polymer molecule into a long ellipsoid, allowing no freedom of rotation. This inability to rotate causes large rates of deformation along the principal axis resulting in a high effective viscosity. Lumley (47) calculates that the relative viscosity in the thread configuration is about four orders of magnitude greater than in simple shear. The presence of an irrotational flow field near the wall region could oppose intensification of turbulence in the axial direction through damping by polymers exhibiting an extremely high uniaxial, or elastic, viscosity. Solution elasticity is ascribed to the surface tension gradient between thickened and thinned areas of film. Patterson (11) follows this line of reasoning and proposes, through a liquid drop analogy, that the general form of the parameter upon which the extent of deformation is expected to depend, for a uni-directional strain field, is:

$$\tau_w \, Re^3 / R_c T \qquad \text{(III-10)}$$

Correlation of drag-reduction parameters with Equation (III-10) has not yet been attempted.

Pruitt, Rosen, and Crawford (52) observed, qualitatively, the effects of adsorption onto glass container walls. They observed a thin film of adhered polymer, which upon shaking would detach itself from the wall in the form of coherent clumps. Other qualitative experiments were performed, such as showing a spontaneous decrease in relative viscosity upon the addition of a small amount of activated charcoal, and the decreased rate of viscosity losses upon storage in glass jars previously coated with an adsorbed polymer film. These experiments, although extremely qualitative, confirmed that polymer adsorption on glass surfaces does take place under quiescent conditions. Adsorption under flow conditions, however, was not investigated. The view was brought forth that adsorption of polymer molecules at surfaces implies some type of ordered, possibly anisotropic, packing that would be able to generate an unusual elastic contribution in a turbulent flow field. Therefore, a link may exist between the tendency of macromolecules to associate on or near a suitable surface, such as a liquid or solid surface, and hence influence or alter the flow field by its presence.

A fundamental link between adsorption and drag-reduction has never been shown experimentally. Early attempts (30-31) at explaining a "persistance" effect by postulating a

slowly desorbing polymer film was investigated by Little (32) and found to have little substance. The persistance of drag-reduction when the polymer solution was displaced by the base solvent was attributed to differences in viscosity and slow migration of drag-reducing fluid out of pressure tap connections. Little (33) himself fell victim to the complexities of polymer adsorption experiments in an attempt to measure an adsorption isotherm for PEO coagulant adsorbing onto 30μ glass beads. The reduction in concentration of the liquid above the beads was measured by means of a viscosity experiment. The problems that arose were apparently due to preferential adsorption of high molecular weight factions by the glass beads, and degradation of the polymer solution with time.

Measurements of drag-reduction with a rotating disk apparatus by Peyser (34) showed no significant difference between a Teflon, nylon, pyrex, and 18-8 stainless steel surface although significant drag-reduction was obtained for all surfaces. Results with the pyrex disk indicated no difference in drag-reduction if (a) the disk was clean or unclean at the time of running the experiment, (b) the disk was allowed to stand for several hours before running, and (c) rinsed just prior to use after standing in solution for several hours. In one experiment, rotation of the disk was stopped when degradation began (as

indicated by a drop in torque reduction) and started up again with the same solution. Drag-reduction continued from the point where it left off, thereby showing that no rejuvenation of the system occurred due to unsheared polymer molecules adsorbing from the bulk fluid.

CHAPTER IV

APPARATUS

IV-A. General Description

Nitrogen gas is used to pressurize a stainless steel, one gallon, reservoir. Please refer to Figure IV-1. The fluid in the tank is expelled, under constant pressure, through smooth, precision-bored capillary tubes. Precision pressure gauges indicate the uncorrected pressure difference between the entrance to the capillary tube and the exit where explusion to atmospheric pressure occurs. The exiting fluid is collected in a beaker and transferred to a graduated cylinder. The efflux time is obtained from an electric timer which is activated by a mercury switch. The accuracy of the pressure gauges, and measurement of the volumetric flow rate, is approximately 1/2%.

IV-B. Detailed Description

Detailed descriptions of the following system sub-units are presented under the headings.

IV-B-1. Capillary Tubes

IV-B-2. Pressure Regulation

IV-B-3. Pressure Gauges

IV-B-4. Stainless Steel Reservoir

IV-B-5. Flowmeter

IV-B-6. Timer

IV-B-7. Fittings, Connectors, Valves

IV-B-8. Water Filter

IV-B-9. Capillary Rise Equipment

IV-B-10. Solution Make-up Equipment

IV-B-11. Viscometers

IV-B-1. Capillary Tubes:

Inside diameter tolerances of the Truebore precision glass capillary tubes are $\pm$ 0.0010 cm. The glass tubes are cut to length by the manufacturer and used as received. The glass tubes are mounted as follows: (Please refer to Figure IV-2.) The outside diameter of the glass tube is measured with a micrometer. The standard drill size chosen has a diameter 5 to 15 mils larger than the tube diameter. A 1/4 NPT stainless steel 316 plug is bored with the proper drill in order to allow insertion of the tube through the plug. Coarse emery cloth is used to roughen the outside of the portion of the glass tube which is covered by the plug. Epoxy (Hysol epoxi-patch kit 1c) is prepared and smoothed on both the inside of the plug and the roughened portion of the capillary tube. The opening of the capillary tube is protected with a tiny piece of pressure sensitive teflon tape, and then inserted through the plug. This leaves a film of epoxy between the tube and plug. The tube is then rotated several times within the plug until a continuous film is obtained as observed by visual inspection through the glass. The excess epoxy is wiped off,

the teflon adhesive removed, and a tube number is written with marking pen on the stainless steel plug. The epoxy hardens within one hour and is ready for use after a twenty four hour curing period.

This mounting procedure is carefully tested using a reservoir pressure of 1500 psi.

Table IV-1 shows the capillary tube designation, length, diameter (obtained by calibration with mercury), and length to diameter ratio for each tube.

TABLE IV-1: DIMENSIONS OF CAPILLARY TUBES

Capillary Number	Length (cm)	Diameter (cm)	L/D
G12	20.32	.03074	661
G16B	30.48	.04084	746
G16C	30.48	.04089	746
G16E	30.48	.04087	746
G16F	30.48	.04086	746
G20A	30.48	.05121	595
G20B	30.48	.05118	595
G20C	30.48	.05119	595
G31	60.96	.07882	773

IV-B-2. Pressure Regulation:

Three nitrogen cylinders are used in order to allow convenient use of three two-stage regulators having control ranges of 0-60, 60-180, and 180-2000 psi.

IV-B-3. Pressure Gauges:

Four precision pressure gauges and a mercury manometer are used to measure gauge pressure. Exit pressure is always atmospheric. The gauges are calibrated with a dead weight tester using water as the hydraulic fluid. All readings are within $\pm$ 1/2%. The manometer is used from 0-8 psi, and the four pressure gauges are used in the ranges 8-20, 20-200, 200-600, and 600-2000 psi. The manometer is also used to measure the head in the reservoir to prevent overfilling.

IV-B-4. Stainless Steel Reservoir:

The 304 stainless steel cylindrical blowdown tank has a capacity of one gallon, stands 24-1/2 inches vertically, has a 4 inch O.D., weighs 16-1/2 pounds, is pressure rated at 1800 psi, and is tapped 1/2 inch female NPT at both ends. The cylinder, and all the auxiliary stainless steel fittings are pressure tested at 2000 psi for one hour before experimentation began. The cylinder collar screws into a small cylinder inverter which affords a convenient method of holding the cylinder firmly.

IV-B-5. Flowmeter:

The liquid ejected from the capillary tubes enters a three dimensional glass tee (shaped somewhat like the three dimensional XYZ axis). Please refer to Figure IV-3. The glass tee is held in a rubber stopper. The rubber stopper is held by a clamp which is

inserted in a pivot block. The pivot block is held by a clamp to a ring stand. A mercury switch was taken from a pressure controller and fastened with teflon adhesive tape to one leg of the glass tee, and is wired to a timer. Consequently, rotating the clamp which is holding the glass tee ninety degrees results in simultaneously collecting the effluent liquid and starting the timer. At the end of collection, the reverse process results in diversion of the liquid stream to the sink and stops the timer. The liquid is collected in 400 milliliter beakers and is transferred to an appropriate graduated cylinder. All turbulent flow runs continue until either one hundred milliliters is collected or 100 seconds of time elapses. In most cases, both of these conditions are fulfilled. Repeat runs with the same dilution of polymer solution at the previous pressure setting or with water invariably coincide to within ± 0.5 cc of liquid collected. The minimum estimated run to run accuracy of this procedure is, therefore, 1/2%.

IV-B-6. Timer:

The electric timer is activated by the mercury switch. One full sweep is ten seconds, with one second divisions and one tenth second subdivisions. A second inside scale reads one thousand seconds, with 100-second divisions and ten-second sub-divisions. Pressing the reset levers brings both hands to zero after each collection.

IV-B-7. Fittings, Connectors, Valves:

All fittings and connecting lines are made of 316 or 304

stainless steel except in the low pressure gas line where brass fittings and copper tubing are used.

Stainless steel, high pressure, braided hose are used to connect the gas system to the cross on the reservoir, and to connect the one inch stainless steel outlet line to the pressure-gauge board. The stainless steel screwed bonnet valve upstream of the capillary tube is rated at 3000 psi, has 1/2 inch tube connections, and a 0.312 inch orifice opening. The 1/2 inch stainless steel tubing and large orifice valve offer negligible pressure drop as compared to the capillary tube. All other valves shown are 3000 psi rated brass forged body valves having a 0.172 inch orifice. The nominal burst pressure of the rupture disc is 2200 psi. The manometer is connected or disconnected with flexible PVC tubing.

IV-B-8. Water System:

Tap water is passed through a line filter into an ion-exchange bed. The water then passes through an activated carbon bed and finally into the central demineralized water system. Prior to use, the demineralized water is passed through a 0.8 micron Millipore filter (142 mm diameter).

IV-B-9. Capillary Rise Equipment:

The capillary rise equipment consists of a large glass jar (12 inches high, 6 inches diameter), two 6 inch diameter plexiglass discs, five wooden blocks (1-1/2 inches thick), a rubber stopper, a

12 inch plastic ruler having 1 mm divisions, and a rubber band. Please refer to Figure IV-4. The rubber stopper is split in half, the ruler inserted, and the rubber band wound tightly around the stopper. The top of the ruler is adjusted so that when the first Plexiglas disc is placed on top of the jar, the ruler is held in place by the weight of the Plexiglas. A 1/2 inch hole is drilled in the center of the lower Plexiglas piece to allow free passage to the capillary tubes. A large "V" is cut into each of the wooden blocks to allow free passage to the capillary tubes and to afford convenience in removal. The upper Plexiglas disc is drilled and tapped 1/4 male NPT to take the stainless steel plugs that are epoxied to the glass capillary tubes. When the capillary tube is inserted, the tube is in close proximity to the ruler, thus allowing a reading of the capillary rise or depression. Readings coincided to within $\pm$ 0.2 mm of cathetometer readings. For checking, this is adequate.

IV-B-10. Solution Make-up Equipment:

This consists of 4000 ml beakers, glass stirring rods, 5 gallon battery jars (12 inch diameter), magnetic stirrers and glass encased stirring bars, Plexiglas covers for the battery jars, aluminum foil covers for the 4000 ml beakers, graduated cylinders, weighing bottles, and a single pan balance.

IV-B-11. Viscometer:

Routine type Cannon-Fenske viscometers are used to obtain viscosity. The viscometers were calibrated by the Cannon Instrument Company. The procedure used is described by the standard methods of the ASTM D 445. Solution densities were obtained with a 0.900 - 1.100 g/cc range hydrometer.

CHAPTER V

PROCEDURE AND CHEMICALS

V-A. General Procedure

Most runs include preparation of a 1000 ppm master solution, dilution to the desired concentration, a series of runs with various capillary tubes, and reduction of experimental data by computer. No attempt is made to control the solution temperature. Solution temperature varies less than .5°C during runs taken on any one day. Solution temperature is taken normally at the start of each run and used as data to calculate the water viscosity. The water temperature for most experiments was 22 $\pm$ 3°C.

V-B. Detailed Procedure

V-B-1. Master Solution Preparation:

1500 ml of water are placed in a 4000 ml beaker. A weighing bottle containing 2-3 grams of poly(ethylene oxide) is weighed on a single pan balance. A 10 inch glass stirring rod is used to manually stir the 1500 ml of water in the beaker. A spatula is used to carefully sprinkle the polymer on to the moving surface of water. The gentle agitation of the surface prevents clumping of the polymer and assures consistent mixing from solution to solution. The amount of polymer sprinkled on the surface is obtained by weighing the empty bottle by difference. Water is added to obtain the desired concentration.

One day of quiescent standing was required for preparation. The solution is gently stirred before dilution.

V-B-2. Dilution Procedure:

A glass battery jar is filled with 15,000 ml of water. Concentrated polymer solution, from the master solution is measured in a graduated cylinder and added. Makeup water brought the total volume to 16,000 ml. The solution is gently stirred overnight by means of two glass coated stirring rods (1-1/2 inches). The stirring rods rest on the bottom of the battery jar and are driven by one or two water powered magnetic stirrers. This assures continuous yet gentle movement of the solution until use. The battery jar is covered with a solid plexiglass cover.

V-B-3. General Test Procedure:

Please refer to the system schematic diagram, Figure IV-1, in following the procedure outlined in Appendix B.

V-B-4. Capillary Rise Procedure:

After coating, the capillary rise is taken at several equidistant levels along the tube. Variation in capillary rise at the different positions was less than $\pm$ 2 mm. After each run, the capillary rise is taken at one point; the point where the water meniscus on the outside of the tube is at the tube midpoint. The procedure for the one point capillary rise is presented in Appendix C.

V-B-5. Preparation of Tubes for Coating:

The potassium dichromate - concentrated sulfuric cleaning solution is drawn up through the capillary tube by vacuum. The solution is allowed to remain in the tube for 1-2 hours. The tube is rinsed thoroughly with water. A 5% sodium hydroxide solution is drawn up through the tube and immediately rinsed thoroughly. The tube is dried for 5-10 minutes in a nitrogen stream.

V-B-6. Capillary Tube Coating:

The freshly prepared solution is drawn up through the clean, dry, capillary tube by a vacuum. The vacuum is released and the tube removed from the solution. Several inches of fluid are allowed to escape from the exit end of the tube. The capillary tube is then gently rolled and the tilted to allow complete wetting of the tube for a period of five minutes. The tube is dried for thirty minutes in a nitrogen stream. The silicone coated tube is rinsed thoroughly with water before drying.

V-B-7. Calibration of Capillary Tubes with Mercury:

A small piece of adhesive tape is placed on the bottom of the vertical capillary tube. A two inch piece of flexible tubing is fit onto the top of the tube and filled with mercury. The adhesive tape is partically removed and the mercury forced into the tube by pressing on the top of the mercury meniscus in the flexible tubing. Once the flow isstarted, the syphoning action proceeds spontaneously.

When the tube is filled, the tape is pressed to shut off the mercury flow. The remaining mercury is skimmed off by removing the flexible tubing while keeping the capillary tube in a vertical position.

The mercury is then transferred to a weighing bottle that has been previously weighed. The tube is turned over and the tape removed. The mercury that remains in the tube is blown out by a rubber bulb. The diameter of the capillary tube is calculated by knowing the length of the tube, and the weight and density of the mercury. The temperature of the mercury was 25°C $\pm$ 1°C for all calibrations. The density of mercury is obtained from the Handbook of Physics and Chemistry.

V-C. Chemicals

V-C-1. Poly(ethylene oxide) polymers were obtained from Union Carbide and used as received. The two grades used were WSR-N-3000 (Blend 63) of nominal MW $\sim$ 600,000 and Coagulant (Blend 1472-4) of nominal MW $\sim$ 6,000,000.

V-C-2. Demineralized filtered water is used. The preparation has been described previously.

V-C-3. A silicone surface is obtained by using a water soluble silicone concentrate, Siliclad. One part Siliclad to 100 parts water is mixed just prior to coating.

V-C-4. A hydrocarbon surface is obtained with high purity hexatriacontane $[(CH_3[CH_2]_{34}CH_3)$, FW = 506.99] or 99.8% pure stearic

acid $\left[(CH_3\left[CH_2\right]_{16}\ COOH,\ FW = 284.49\right]$. Stearic acid is preferred because of its polar acid group which bonds to the glass surface. Hexatriacontane is dissolved in ACS certified cyclohexane $\left[(CH_2(CH_4)CH_2,\right.$ $\left.FW = 84.16\right]$ to a molar concentration of 4.3×10^{-4}. Stearic acid is dissolved in cis-decahydronapthalene (i.e. decalin, $C_{10}H_{18}$, FW = 138.25) to a molar concentration of 1.0×10^{-3}. The decalin is percolated through a one foot column of 28-200 mesh silica gel just prior to use.

V-C-5. A fluorocarbon surface is obtained by using Nyebar barrier film type C. This barrier film is a 2% solution of 1H, 1H - pentadecafluorooctyl methacrylate $\left[C_7F_{15}CH_2OCOC(CH_3) = CH_2\right]$ dissolved in xylene hexafluoride.

V-C-6. Acid cleaning solution is prepared by mixing 20 grams of potassium dichromate crystals in 1000 ml of concentrated sulfuric acid.

V-C-7. Alkaline cleaning solution is prepared by mixing 5 grams of sodium hydroxide pellets in 100 ml of water.

CHAPTER VI

RESULTS AND DISCUSSION

VI-A. Characterization of Capillary Tubes by Capillary Rise Experiments

Table VI-1 is a summary of tube designation, general surface type, work of adhesion, and surface free energy. In all cases, the liquid used for capillary rise determinations was water and the tubes used to obtain these numbers were the same tubes used in the drag-reduction experiments. Please refer to Appendix A for sample calculations of the work of adhesion and the surface free energy.

TABLE VI-1: Characterization of Inside Surface of Capillary Tubes

Surface Type	Capillary Number	Work of Adhesion (dynes/cm)	Surface Free Energy (dynes/cm)
Silicone	G16B	90.5	26.5
Fluorocarbon	G16C	51.0	9.03
Hydrocarbon	G16E	84.6	24.8
Glass	G16F	144.0	72.0
Glass	620A	140.4	70.2
Stearic Acid	620B	78.9	21.6
Fluorocarbon	620C	50.7	8.93

VI-B. Characterization of Capillary Tubes with Water

Figure VI-1, in Appendix B, shows the results of friction factor versus Reynolds number for water in G16 series capillary tubes. The representative surfaces are fluorocarbon, hydrocarbon, silicone, and glass. In all cases, the diameter obtained from calibration with mercury is used to calculate the Reynolds number and friction factor.

In laminar flow, comparison to Poiseuille's law was excellent. In turbulent flow (Re >3000) the friction factor in all tubes was uniformly 3 to 4% too low. A similar observation was made by Virk (38), p 121, in a 0.292 cm capillary tube. A least squares fit of the solvent data yields a solvent reference line for each capillary tube for $3000 \leq Re \leq 10,000$. This allows a direct comparison between solvent and polymer solution friction factors when calculating drag-reduction.

It can be observed from Figure VI-1 that the transition region is different for each of the tubes used. The transition to turbulence for the four tubes yields no evident correlation with the surface chemistry parameters of the capillary surfaces. Also, there is no obvious dependence on tube surface roughness, as the turbulent region points are all uniformly lower than the turbulent flow line as given by the Blausius equation. This emphasizes, once again, the importance of flow geometry in turbulent flow experiments. Even tubes matched by

visual inspection, and having equal diameters, length, and flow geometry, appear different in the turbulent flow transition region. The experiments reported here with polymer solutions by-passed the transition region since the critical shear stress for the onset of drag-reduction is lower than the shear stresses attained in the capillary tubes used. The question of the effect of different transition regions profiles on polymer solution dynamic properties is unresolved.

VI-C. Drag-Reduction and Degradation as a Function of Surface Free Energy

Figures VI-2 to VI-11 are double logarithmic plots of the friction factor as a function of Reynolds number obtained by using the G16 series of capillary tubes for concentrations of 1/2 to 50 parts per million (ppm) PEO grade Coagulant. Each plot represents a direct comparison between capillary tubes where the primary difference is the nature of the surface in contact with the flowing fluid. Each set of experiments (data on one plot) is performed with the same master batch and dilution of polymer solution on the same day. In all experiments, a random order of tube usage was maintained. This direct comparison method is chosen in order to eliminate polymer solution variables in an attempt to isolate the effect of surface coating. In each case, the wall shear stress is higher than that needed for the onset of drag reduction. Consequently, drag-reduction begins immediately, and continues until degration of the polymer occurs.

Upon degradation, the friction factor rises towards the friction factor for the solvent.

In Figures VI-2 and VI-3 a distinct pattern is evident. The points for each tube closely follow the laminar flow line through the transition region. At some specific Reynolds number, onset of degradation, not transition, occurs in the fluorocarbon tube. At this Reynolds number, the other tubes maintain stability of drag-reduction and are continuing to proceed down the path of increasing drag-reduction or decreasing friction factor. One by one, onset of degradation begins at a later Reynolds number until all the tubes exhibit degradation. The maximum Reynolds number, or stability before the onset of degradation is obtained in the uncoated glass tube. These results are replotted in the form of semi-log plots of drag-reduction versus Reynolds number of Figures VI-12 and VI-14. Percent drag-reduction, DR, is defined as:

$$DR = 100\left[1 - fp/f\right]_{Re} \qquad \text{(VI-1)}$$

where f_p is the polymer friction factor, and f is the friction factor calculated from the least squares line obtained from fitting the turbulent flow data, for water, in Figure VI-1.

The effect of surface coatings on drag-reduction is evident; the onset of degradation is shown to be a function of Reynolds number for each of the different surfaces at poly(ethylene oxide) concentrations of 1/2 and 1 ppm.

At this point, several clarifying facts should be kept in mind. First, drag-reduction is shown to decrease with Reynolds number because the curves of Figures VI-12 and VI-14 emphasize the onset of the degradation region. Second, the close proximity of the points before degradation and the coming together of points after degradation strongly indicate that surface roughness is not a factor, although this is not a completely resolved question. Third, the maximum experimental error, upon repetition of experiments, is about .5% of the volume of fluid collected, or $\pm$ 15 Reynolds number units and about $\pm$ 1 percent drag-reduction unit. The error in repetition measurements is, therefore, approximately the size of the symbols used to represent the data points. Fourth, the effect of degradation on the friction factor of recycled poly(ethylene oxide) solutions is shown in Figure VI-16. Figure VI-16 is a plot of f versus Re for a fresh 4 ppm coagulant solution flowing in glass capillary tube G16F, and for two recycled solutions. One gallon of 4 ppm solution was allowed to pass through tube G16F at each of the two Reynolds numbers 3650 and 9500. These two Reynolds numbers are on opposite sides of the Reynolds number at which the maximum drag-reduction for the onset of degradation is achieved. Recycling of the solution, run previously at Re = 3650 resulted in approximately the same f versus Re curve. Recycling of the solution run previously at Re = 9500, resulted in almost complete loss of drag reduction effectiveness. This loss of effectiveness is

attributed to mechanical degradation of the polymer. Referring again to Figures VI-12 and VI-14, it is apparent that at a constant Reynolds number, a correlation exists between drag-reduction and some measure of the nature of the capillary tube.

The results of Lyman et al (57), and Bischoff (58) on the coagulation time of blood as a function of surface free energy and work of adhesion appears to be apropos. The mechanism of blood coagulation appears to be intimately connected to the adsorption of high molecular weight species such as platelets or to the denaturing of a plasma protein (the Hageman factor) by adsorbed colloidal silica. Figures VI-13 and VI-15 are semi-log plots of drag-reduction as a function of surface free energy and work of adhesion for the 1/2 ppm and 1 ppm solutions, respectively. The data for these plots are taken from Figure VI-12 and VI-14 at the Reynolds number, Re_{max}, where maximum drag-reduction occurs in the uncoated glass tube. Obviously, the exact shape of Figures VI-12 and VI-14 depends on the Reynolds number chosen for cross-plotting. The trend, however, is the same; drag-reduction increases with surface free energy and work of adhesion for the results as presented.

As discussed in Chapter II, the configuration of the adsorbed molecule is influenced by the attractive energy of the surface, and that a high energy surface tends to hold the polymer molecule tightly and in a flat configuration. On the other hand, a very low energy surface,

fluorocarbon, tends to hold the adsorbed molecule less tightly and in a somewhat less flattened configuration. Also, the highest shear stress region is at the interface between the wall and the last layer of fluid, which in this case might be a layer of polymer molecules interdispersed with solvent molecules. It appears likely, therefore, that an adsorbed polymer film may give some degree of stability to the process of mechanical degradation in a shear field.

It should be noted, at this point, that the fundamental mechanism of drag-reduction, as pertains to an adsorbed film, is still unresolved experimentally. At best, the influence of an adsorbed polymer film on the stability of the onset of drag-reduction is indicated, and the direct relationship in Figures VI-13 and VI-15 between surface free energy and drag-reduction comes about through the imposed definition of drag-reduction and the nature of the degradation curve on the f versus Re plot.

The effect of surface on drag-reduction as a function of concentration is shown in Figures VI-4 to VI-11. Figures VI-4 to VI-6 are replotted as drag-reduction versus Reynolds number in Figures VI-17 to VI-19. Figure VI-6 is included to show the degree of variability that can be expected when using solutions prepared from different master batches for a 2 ppm solution. For 3/2 and 2 ppm PEO coagulant solutions, the surface effect appears to be diminishing. Further increases in concentration bring all the curves together and little

or no effect is observed, as shown in Figures VI-7 to VI-11.

In general, the fluorocarbon degradation sequence lies to the left of the other data. The reason for this is unknown, but may be due to surface roughness or waviness or possibly to a continuing surface effect. However, the point at which the onset of degradation begins is the same as the other tubes for concentrations above 2 ppm.

The data in Figure VI-7 was taken in tubes that were immersed for 24 hours in a 1500 ppm coagulant solution. The standard run procedure was followed with a 3 ppm solution. The resultant data points for the two tubes are virtually superimposed.

Hysteresis experiments were performed on 1, 3, and 10 ppm coagulant solutions flowing in glass capillary tubes G16C (fluorocarbon surface) and G16F (glass). Figure VI-20 is an example of the results obtained from this series of experiments. In all cases, a return along the curve in the direction of decreasing Reynolds number coincided exactly, within experimental error, to the curve obtained with increasing Reynolds number. No hysteresis loop was observed.

Figures VI-21 to VI-23 are plots of f versus Re for a 3 ppm coagulant solution flowing in glass capillary tubes G12, G16F, and G31. Dilute sulfuric acid and sodium hydroxide were added immediately prior to running to obtain the acidic and basic solutions. In all cases, the effect of pH on drag-reduction and the onset of degradation is small

Figures VI-24 to VI-27 are plots of the friction factor as a function of Reynolds number obtained by using the G16 series of capillary tubes for concentrations of 10 to 60 ppm poly(ethylene oxide) grade WSR-N-3000. Figure VI-28 is a plot of drag-reduction as a function of Reynolds number for the data in Figure VI-24. Figure VI-29 is a plot of drag reduction as a function of surface free energy and work of adhesion for the 10 ppm solution.

Figure VI-24, for a 10 ppm solution of low MW (MW$\backsim$600,000) WSR-N-3000, shows the same trend as observed for a 1 ppm solution of higher MW (MW$\backsim$ 6,000,000) coagulant. The order of magnitude difference in concentration and molecular weight to achieve basically the same effect is interesting. Little (16) shows that for a homologous series of PEO, the concentration for a 40% DR, C_{40}, divided by the critical concentration for the touching of random coils, Cc, from Shin (59), is a constant ratio, equal to .01, regardless of molecular weight. In analogy to C_{40}, let C_d be the concentration at which the onset of degradation is distinguishable in tubes of different surface free energy. Table VI-2 shows about a tenfold increase in C_{40} for about a tenfold change in molecular weight. In comparison, a tenfold change in C_d occurs when changing the molecular weight about tenfold. Small bore capillary tube data appear to yield a constant slope, on an f versus Re plot, until degradation occurs. The question of a single slope on "saturation" in small bore capillary tubes will be considered in a later section.

TABLE VI-2: Analogy between C_{40} (16) and C_d

MW	C_{40} (ppm)	C_d (ppm)
6×10^6	3	1
5×10^6 (a)	25	10

[a]The nominal MW$\sim$ 600,000 for WSR-N-3000 used in this study.

Figures VI-30 to VI-32 are plots of the friction factor as a function of Reynolds number obtained by using the G20 series of capillary tubes for concentrations of 1 to 10 ppm of poly(ethylene oxide) grade coagulant. The G20 series of capillary tubes, therefore, shows no onset degradation effect and there is essentially no separation of curves for the highMW coagulant solution.

The onset degradation effect, therefore, disappears at tube diameters above approximately .016 inches, and above either a 2 ppm PEO coagulant solution or a 10 ppm WSR-N-3000 solution.

VI-D. Drag-Reduction and Degradation for Flow in Uncoated Glass Capillary Tubes

Figures VI-33 to VI-35 are semi-log plots of drag-reduction as a function of Reynolds number with concentration as a parameter for flow in uncoated glass capillary tubes. The G16 series shows the results for PEO grade WSR-N-3000 at concentrations of 10, 20, 30, 60 ppm, and for poly(ethylene oxide) grade coagulant, at concentrations 1/2, 1, 2, 4, 7, 10, 50 ppm. The G20 series shows the results for poly(ethylene oxide) grade coagulant at concentrations of 1, 5, 10 ppm.

Also shown in Figures VI-33 to VI-35 is the Virk maximum drag-reduction asymptote as calculated from the ratio of polymer friction factor, $f_p = .042/Re^{.55}$ to the friction factor obtained from the Blausius equation, $f = .0791/Re^{.25}$, at equal Reynolds numbers.

VI-D-1. Dependence of Drag-Reduction on Concentration and Molecular Weight:

For flow in small bore capillary tubes, where high wall shear stresses prevail, a number of observations are evident.

(1) A 1 ppm poly(ethylene oxide) coagulant solution gives drag-reduction as high as 56%.

(2) Drag-reduction increases systematically with decreasing concentration prior to the onset of degradation. For example at Re = 4000 (please refer to Figure VI-33), DR$\sim$44% at 50 ppm, DR$\sim$47.5% at 10 ppm, DR$\sim$48% at 7ppm, DR$\sim$51% at 4 ppm, DR$\sim$52.5% at 2 ppm, and DR$\sim$55% at 1 ppm. This effect is too large in magnitude to be due to Einsteinian viscosity effects and, therefore, is attributed to "structural" turbulence. Structural turbulence as referred to in this study is used to describe an increase in turbulence due to the presence of a higher concentration of polymer. An example of increased turbulence due to a higher polymer concentration is the earlier onset of drag-reduction with increasing polymer concentration as observed by Paterson (11) and Hanson (44). Interestingly, the curves of higher concentration approach the asymptote at approximately the same angle.

(3) Consequently, the effect of increasing concentration is to allow intersection with the maximum drag-reduction asymptote at a higher percent drag-reduction.

(4) Upon reaching the asymptote, degradation begins and proceeds rapidly with increasing pressure driving force.

(5) For the higher concentrations (> 10 ppm), the curves intersect and then run along the asymptote until degradation begins.

(6) Virk's asymptote is verified as being molecular weight independent for PEO grades Coagulant and WSR-N-3000. The shear stresses used in this study are an order of magnitude larger than those reported previously (11, 38) yet, a striking feature of the data in Figures VI-33-35 is the remarkable adherence to the asymptote, even for WSR-N-3000 whose nominal MR$\sim$ 600,000. The theoretically, and possibly philosophically, stimulating aspect of these graphs is the polymer's ability to just attain the zenith of drag-reduction, expressed mathematically as the maximum drag-reduction asymptote, and then give up, or degrade.

Poly(ethylene oxide) grade WSR-N-3000 (MW$\sim$600,000) is, at higher concentrations, as efficient a drag-reducer as the higher molecular weight (MW$\sim$ 6,000,000) PEO grade Coagulant. This implies, but does prove, that although the long chain PEO molecules are more effective drag-reducers, the higher molecular weight factions may not be overly important.

VI-D-2. Dependence of Drag-Reduction on Pipe Diameter:

Flow in capillary tubes offers a convenient means of eliminating variation in the onset of drag-reduction. The wall shear stress for the G12, G16F, G20, and G31 glass capillary tubes is always greater than the onset shear stress needed to initiate drag-reduction. Consequently, the friction factor - Reynolds number curve appears to extend directly from the laminar flow region through the usual transition region ($2100 \leq Re \leq 3000$). The f_p-Re curve continues until it approaches the Virk maximum drag-reduction asymptote, and then either falls short or continues along the asymptote until degradation of the polymer occurs.

A relationship between shear stress, Reynolds number, friction factor, tube diameter, and solution viscosity and density can be obtained by combining the equations

$$f = \frac{1}{4}\frac{D}{L}\frac{\Delta P}{\frac{1}{2}\rho\bar{v}^2}, \quad Re = \frac{D\bar{v}\rho}{u} \quad \text{and} \quad \tau_w = \frac{R}{2}\frac{\Delta P}{L}.$$

Thus,

$$\tau_w = \frac{f(uRe)^2}{2\rho D^2} \qquad \text{(VI-2)}$$

where u is in poise, ρ is in gm/cm^3, D is in cm, and τ_w is in $dynes/cm^2$.

Figure VI-36 is a plot of Reynolds number versus friction factor in capillary tubes of diameters .03074 (G12), .04084 (G16F), and .07882 (G31) cm. The L/D ratios are 661 (G12), 746 (G16F), and 773 (G31). All three tests were performed on the same day with the same dilution of

3 ppm Coagulant (MW$\sim$6,000,000) polymer solution. Therefore, the parameters that are constant, or nearly constant, for this set of experiments are (1) solution viscosity density, (2) polymer concentration and molecular weight, and (3) tube characteristics such as surface free energy, roughness, and entrance and exit conditions.

If this discussion is limited to the portion of the fp-Re curves before the onset of degradation, several conclusions can be drawn.

(1) Virk's asymptote is verified as being diameter independent for flow in capillary tubes of the sizes stated.

(2) At equal Reynolds numbers, drag-reduction is independent of pipe diameter until polymer degradation begins in the smaller diameter tubes. Consequently, the maximum drag-reduction possible increases with increasing pipe diameter and is a consequence of the decreasing shear field.

(3) Comparisons of drag-reduction at equal shear stress are difficult to interpret clearly. The comparison must be made at Reynolds numbers which yield equal wall shear stresses. Comparisons of drag-reduction as a function of Reynolds number for a 10 ppm Coagulant polymer solution in capillary tubes of diameters .04084 (G16F) and .05121 (G20A) cm, can be made from the curves in Figures VI-10 and VI-32. At equal solvent wall shear stress, application of equation VI-2 to both tubes yields the relation:

$$(\mathrm{Re}\sqrt{f}/D)_{G16F} = (\mathrm{Re}\sqrt{f}/D)_{G20A} \qquad \text{(VI-3)}$$

For $(Re)_{G20A} = 5000$, $(f)_{G20A} = .0041$, and $(Re\sqrt{f})_{G16F} = 403$. By fitting the fp-Re curve to a straight line, or by trial and error, $(Re)_{G16F} = 7400$. At Re = 5000, $(DR)_{G16F} \sim 63\%$, and at Re = 7400 $(DR)_{G20A} \sim 54\%$. Therefore, at Reynolds numbers corresponding to equal wall shear stresses, drag-reduction decreases with increasing tube diameter.

VI-E. Interpretation of Results: Semiflexible Film Hypothesis.

The quest for uncovering the mechanism of drag-reduction has brought investigators along the path of ever decreasing circles. Of all the mechanisms proposed, viscoelasticity (relaxation and time scale hypothesis), and filament formation (high effective viscosity in axial extension), remain as the least unlikely candidates. Virk (38) and Paterson (11) both question the validity of the relaxation time hypothesis through experimental and theoretical reasoning while the recent work of Poreh et al (60) conclude that there is no influence of shear rate on the dynamic viscosity of polymer solutions and hence the elasticity of the polymer molecule plays no fundamental role in drag-reduction. It appears that a dead end is approaching in trying to understand the mechanisms of drag-reduction as a function of the properties or configuration of non-associated macromolecules in solution.

The possible role of surface rheology in understanding the mechanism of drag-reduction and in explaining the difference in onset of degradation with different surface free energy materials is presented

below. Emphasis is placed on the importance of surface viscosity and Gibbs elasticity of an adsorbed or hydrogen bond associated polymer film, and not on turbulence suppression by individual polymer molecules.

Paterson (11) calculated the volume fraction of a 0.05 ppm solution (polymer MW$\sim$ 6,000,000) to be 0.00006. Hence, a 1 ppm solution has a volume fraction of polymer molecules to solvent of 0.0012. In addition, Lumley (47) has shown that few agglomerates are formed and that interparticle effects are small at the low concentrations significant to the drag-reduction phenomenon. Consequently, since the polymer volume fraction is low, and since interparticle solution effects are negligible, it is difficult, at least, to conceptually understand the role of the individual molecule in suppressing turbulence within the laminar sublayer. As infinite dilution is approached, fewer and fewer molecules are in solution. Yet, the maximum drag-reduction asymptote can still be obtained, or approached. Interparticle effects in solution are virtually impossible, but interparticle effects at the adsorbing surface are far from impossible. A hypothesis of a semi-flexible surface film of adsorbed or associated polymer molecules is presented to explain the mechanism of drag-reduction.

It is well known that a film of surface active molecules on a liquid surface will tend to lower the liquid surface tension and markedly increase the stability of the surface film (55). An example is damping

of water waves with a monomolecular film of a surface active agent. The ability of an absorbed film composed of surface active molecules or polymer macromolecules to play a role in wave damping, foam stabilization, emulsion stability, and suspension polymerization is ascribed to changes in surface film viscosity, surface film elasticity and, for ionic species, electrostatic repulsion (61).

In general, determination of surface viscosity or elasticity entails measurement of a resistance to shear in the plane of an interface. For films, the surface viscosity, u_s, is equal to the sum of the shear surface viscosity coefficient, ϵ (dyne-sec/cm), and the dilational surface viscosity coefficient, $\bar{\kappa}$ (dyne-sec/cm). The dilational surface viscosity coefficient, $\bar{\kappa}$, is expressed as

$$\frac{1}{\bar{\kappa}} = \frac{1}{\Delta\gamma} \frac{d\ell nA}{dt} \qquad \text{(VI-4)}$$

where $\frac{1}{\bar{\kappa}}$ is the fractional change in area per unit time per unit applied surface pressure; $\Delta\gamma$ is the film pressure; A = total surface area of the film; t = time.

The dilational deformation gradient induces surface movement characterized by a surface resilience or elasticity. The equilibrium quantity corresponding to the dilational parameter, $\bar{\kappa}$, is the Gibbs modulus of surface elasticity, E_s.

$$E_s = \frac{-2\, d\gamma}{d\ell nA} \qquad \text{(VI-5)}$$

The reciprocal of E_s is the film compressibility, β.

A surfactant tends to reduce the surface tension of the solvent by adsorbing at a high energy surface, and the adsorption of surfactant is controlled by Gibbs adsorption law, Equation VI-6. This law is derived by defining the interfacial boundary between a solid surface and a binary solution such that the Gibbs excess concentration of the solvent is zero (55).

$$-\Delta\gamma = \gamma_{LV}{}^{o} - \gamma = R_c T \int_{o}^{a_2} 2\, d\ell n\, a_2 \qquad \text{(VI-6)}$$

where $\gamma_{LV}{}^{o}$ =the interfacial tension between pure solvent and solid (surface tension of solvent); γ = the interfacial tension between solution and solid; Γ_2 = the Gibbs excess surface concentration of the solute, and a_2 is the activity of the solute. For dilute solutions, concentration or mole fraction can be substituted for activities, and Γ_2 is usually determined by measuring adsorption through the exchange in concentration of the solution in contact with the solid. Cotton (56) uses the method of Adams and Guggenheim to solve for the surface excess value, Γ_2. This entails an nth order polynomial fit of the adsorption data, where n = the number of data points. The Gibbs equation describes the adsorption of idealized adsorbates. This condition is not met in describing the adsorption of drag-reducing polymer macromolecules, and the Lilberberg (22) or Hoeve, DiMarzio and Peyser (23) models must be used in lieu of equation VI-6.

Kanner and Glass (61) list several generalizations of adsorbed surfactant monolayer behavior. These are: (1) Surface viscosity and elasticity characteristics are markedly influenced by a high molecular

weight analog of the surfactant being studied; (2) An increase in temperature or solution pH affects a decrease in the surface viscosity and elasticity characteristics; (3) Surface parameters are concentration and time dependent; (4) Interfacial viscosity is normally increased by the formation of interfacial complexes by van der Waals, ionic or hydrogen bonding between dissimilar adsorbates.

Adsorbed polymer monolayer behavior is usually extracted from surfactant behavior. However, some examples of adsorbed polymer monolayer behavior are: (1) investigations of protein films have shown that interfacial hydrogen bonding increases film surface viscosity and elasticity (62-64); (2) The surface viscosity parameter depends upon the degree of polymerization and monomer structure; (3) At low polyester concentrations, Hookian elasticity is observed; at high concentrations, where a closely packed monolayer is assumed to exist, viscoelastic behavior prevails (65); and (4) Increases in surface viscosities and elasticities can occur before segments of the polymeric surface film become close-packed.

The effects of surface viscosity and elasticity on foam stability (66) showed that foams of greater stability were produced from solutions having high surface viscosity. However, foam stability is also achieved with materials of low surface viscosity (67). In general, the mechanism of foam stabilization appears to be an optimization of a number of parameters. These are : (1) surface viscosity; (2) film elasticity;

(3) electrostatic repulsions; and (4) complexing due to van der Waals, ionic, and hydrogen bonding molecular forces.

An analysis of gravitational laminar thinning of a soap film, including surface viscosity and elasticity effects, has been reported by Whitaker (68). Two dimensionless parameters which affect the analysis are α_E, a ratio of bulk to surface viscosity, and β_E, an elasticity parameter.

$$\alpha_E = \frac{\mu L_f^2}{\mu_s d} \tag{VI-7}$$

where μ = bulk viscosity (dyne-sec/cm^2); L_f = film length (cm); μ_s = surface viscosity = $\bar{\kappa} + \epsilon$, where $\bar{\kappa}$ = dilational surface viscosity coefficient (dyne-sec/cm) and ϵ = shear surface viscosity coefficient (dyne-sec/cm); and d = half thickness of film (cm).

$$\beta_E = \frac{C^o \frac{\partial \gamma}{\partial C}}{\rho g \quad L_f d} \tag{VI-8}$$

where C^o is the equilibrium surface film mass density (gm/sq cm); C is the surface film mass density (gm/sq cm).

For surface rheology to be important with respect to a mechanism of drag-reduction, an adsorbed or hydrogen bond associated film of poly(ethylene oxide) must be present regardless of the nature of the tube surface. As discussed in Chapter II, the literature is practically devoid of quantitative adsorption studies of very high ($>10^6$) molecular weight polymers. The presence of an adsorbed

film on lower surface free energy materials, or in the presence of a shear field, cannot be established without further polymer adsorption studies. Perhaps, an adsorption study utilizing polymers tagged with radioactive tracers would yield more quantitative results.

Assume, then, that the theoretical adsorption model of Hoeve, DiMarzio, and Peyser (23) is applicable to the system poly(ethylene oxide)-water-solid surface, and that an adsorbed film is present on all surfaces. For very high attractive energy surfaces, such as quartz, an adsorbed film of poly(ethylene oxide) is expected to have the following configuration: (1) a flat configuration, of thickness and/or adsorbance less than 50 Å and/or 1 mg/m^2; (2) a large number of attached polymer segments (trains); (3) a small number of solvated loops. For low surface energy materials, such as a fluorocarbon surface, the adsorption of poly(ethylene oxide) is predicted to have the following configuration: (1) a broad distribution of loop sizes; (2) the looped segments may be large; (3) the concentration of loops is low; (4) the number of trains are small, and (5) the trains are held less tightly to the surface. For a logarithmically intermediate surface energy material, such as glass, some combination of the above cases is expected. Hypothetically, an optimum film stability might be obtained by a semi-flexible film exhibiting optimum surface viscosity and elasticity characteristics. The poly(ethylene oxide) film which adsorbs onto the glass tube from solution or which associates due to hydrogen bonding

might be such a film. A semiflexible adsorbed film, such as that predicted to be found on glass, would be most likely to repair and sustain itself. Repair of the film entails the relieving the surface tension gradient $d\gamma / \partial A$ through film surface movement, or through surface adsorption from the bulk or subsurface phase. For high deformation rates, adsorption is thought to be the faster step in surface equilibrium (61).

The density and "configuration" of the adsorbed polymer film is sufficient, for all surface free energy tubes, to produce maximum drag-reduction. Adsorption onto active sites, and hydrogen bonding between water and various molecular-weight poly(ethylene oxide) fractions may be responsible for high enough level of film surface viscosity and elasticity to inhibit wall turbulence. The connection between drag-reduction and the elastic behavior of polymer molecules has been previously pointed out by Paterson (11). Paterson states that such "an irrotational flow field may be present in the immediate wall region. By opposing the intensification of axially oriented wall vortices, the rate of "busting" (ejection of slow moving fluid near the wall into the outer flow) would be expected to decrease. Although the structure of the turbulence in the wall region is not presently well understood, the process of ejection of low momentum fluid from the wall appears to be an important aspect of the wall turbulence problem." The adsorbed semiflexible film, therefore, acts to effectively damp out wall ejections, or, possibly,

to partially suppress, on a molecular scale, the initiation of turbulence. The net effect of turbulence suppression in the wall region is to increase the thickness of the laminar boundary layer and, consequently, to allow the system to exhibit the phenomenon of drag-reduction.

An adsorbed film acts as a large unified film through hydrogen bonding between polymer molecules, water and the solid surface, and hence is associated with surface viscosity and elastic characteristics. As molecules are pulled away due to the shear field, other molecules are adsorbed from the bulk solution in order to repair the film and maintain its surface characteristics. Degradation occurs when the film is no longer able to maintain its stability. The stability depends on the viscous, elastic, and ionic properties of the film which in turn are a function of the thickness, density, and adherence of the film to the solid surface. The adsorbed polymer film stability, therefore, increases with increasing surface free energy of the solid surface until the optimum combination of surface viscosity and elasticity is reached. For the experimental results obtained in this investigation, maximum film stability hence higher drag-reduction was obtained with the highest surface free energy tube used (i.e. glass).

No effect of time on drag-reduction is observed by either starting an experiment with a clean tube or starting with a tube soaked overnight in a concentrated solution. Surface viscosity is known to be a

function of time. The time scale, however, may be extremely short and surface parameter adjustments are likely to be made before the 100 seconds needed for a significant amount of fluid to be collected experimentally. The same reasoning applies to hysteresis experiments which cycle through the stress at which degradation begins. Consequently, system time scales are most likely shorter than experimental measurement time scales.

CHAPTER VII

CONCLUSIONS

Turbulent flow drag-reduction by dilute poly(ethylene oxide) solutions was investigated utilizing small bore capillary tubes. Glass capillary tubes were coated with monomolecular layers having various surface free energies. In a series of 0.016 inch diameter capillary tubes of surfaces fluorocarbon, hydrocarbon, silicone, and glass,

1. A 1/2 ppm poly(ethylene oxide) Coagulant solution gives drag-reduction as high as 59% in the glass tube.

2. All tubes give equal drag-reduction until the onset of degradation is approached.

3. The maximum Reynolds number, or stability before the onset of degradation, is obtained in the uncoated glass tube.

4. The experimental evidence shows an increase in the maximum Reynolds number at the onset of degradation with increasing surface free energy of the tube coatings. Consequently, drag-reduction increases with increasing surface free energy, at equal Reynolds numbers, at the onset of degradation with a 1 ppm Coagulant solution (Coagulant MW ~ 6,000,000), and a 10 ppm WSR-N-3000 solution (WSR-N-3000 MW ~ 600,000).

5. The onset degradation effect disappears at tube diameters above 0.016 inches, and above a 2 ppm poly(ethylene

oxide) Coagulant solution and a 10 ppm WSR-N-3000 solution.

In the uncoated glass capillary tubes used,

1. A 1 ppm poly(ethylene oxide) Coagulant solution gives drag-reduction as high as 56%.

2. The Virk maximum drag-reduction asymptote is obtained, even at concentrations as low as 1 ppm for poly (ethylene oxide) Coagulant and 10 ppm for poly (ethylene oxide) WSR-N-3000.

3. Drag-reduction increases systematically with decreasing concentration prior to the onset of degradation.

4. The effect of increasing concentration is to allow intersection with the maximum drag-reduction asymptote at a higher percent drag-reduction.

5. Upon reaching the asymptote, degradation begins and proceeds rapidly with increasing pressure driving force.

6. At higher concentrations, the curves intersect, and then run along, the asymptote until degradation begins.

7. Virks asymptote is verified as being diameter and molecular weight independent.

8. At equal Reynolds numbers, drag-reduction is independent of tube diameter until polymer degradation begins in the smaller diameter tube.

9. At Reynolds numbers corresponding to equal wall shear stresses, drag-reduction decreases with increasing tube diameter.

A semiflexible film hypothesis is presented. Emphasis

is placed on the importance of surface viscosity and Gibbs elasticity of an adsorbed or hydrogen bond associated polymer film, and not on turbulence suppression by individual polymer molecules. A wall associated polymer film, exhibiting optimum surface rheology characteristics, may act to inhibit turbulence in the wall region, and thus stabilize flow and retard the onset of degradation. The net effect of turbulence suppression in the wall region is to increase the thickness of the laminar boundary layer and/or the buffer region, and consequently, allow the system to exhibit the phenomenon of drag-reduction. For the experimental results obtained in this investigation, maximum film stability, hence higher drag-reduction, was obtained with the capillary tube having the highest surface free energy (i.e. glass).

APPENDIX A

CALCULATION OF SURFACE TENSION OF WATER FROM A GLASS CAPILLARY TUBE

$$\gamma_{LV}^{o} = r\rho_{o}gh/2\cos\theta$$

For glass, $\cos\theta = 1.0$, Tube G16F, $T = 22^{o}C$

$$r = .02043 \text{ cm}$$

$$h = 7.20 \text{ cm}$$

$$\rho_{o} = .998 \text{ gm/cm}^3$$

$$g = 981 \text{ cm/sec}^2$$

$$\gamma_{LV}^{o} = (.02043)(.998)(981)(7.20)/2(1.0) \text{ dynes/cm}$$

$$\gamma_{LV}^{o} = 72.0 \text{ dynes/cm}$$

CALCULATION OF WORK OF ADHESION BETWEEN WATER AND GLASS

$$W_A = \gamma_{LV}^{o} + \gamma_{LV}^{o}\cos\theta$$

For glass, $W_A = 2\gamma_{LV}^{o} = 144.0$ dynes/cm

CALCULATION OF WORK OF ADHESION BETWEEN WATER AND COATED TUBES

$$W_A = \gamma_{LV}^{o} + \gamma_{LV}^{o}\cos\theta$$

$$W_A = (\gamma_{LV}^{o})_{water} + r\rho gh/2$$

For fluorocarbon coated tube G16C:

$$W_A = 72.0 + (.2045)(.998)(981)(-2.10)/2$$

$$W_A = 51.0 \text{ dynes/cm}$$

CALCULATION OF SURFACE FREE ENERGY FROM WORK OF ADHESION USING GOOD'S EQUATION

$$W_A = 2\,\Phi\,(\gamma_{so}\,\gamma_{LV}{}^{o})^{1/2}$$

$$\Phi = 1.0$$

$$\gamma_{LV}{}^{o} = 72.0$$

For G16C, fluorocarbon coated

$$\gamma_{so} = (W_A/2)^2/\gamma_{LV}{}^{o}$$

$$\gamma_{so} = (51.0/2)^2/72.0$$

$$\gamma_{so} = 9.03 \text{ dynes/cm}$$

APPENDIX B

GENERAL TEST PROCEDURE

1. Open valve BVI, thus releasing the water in the reservoir. At this time the plug and capillary tube is not yet screwed into the 1/4 inch female NPT fitting. The one gallon of water is collected in a plastic container and discarded.

2. BVI is closed.

3. FV5, FV6, FV7, FV8, FV9 are opened.

4. The flexible PVC tube is connected to the manometer, and the solid stainless steel plug is removed from the top of the reservoir.

5. Transfer of the solution to the reservoir is accomplished manually. A 600 ml polypropylene beaker is used to transfer the liquid to a funnel which has been placed in the top of the reservoir. 200 ml are poured in and then removed by opening BVI. BVI is closed and filling begins again. Filling ends when the mercury in the manometer rises to the appropriate position.

6. For turbulent flow tests. FV7 is closed and the flexible tubing is removed from the manometer. For calibration runs, the manometer is needed and FV7 remains open.

7. Teflon tape is wrapped around the plug and the plug is inserted in the top of the reservoir.

8. Teflon tape is wrapped around the plug containing the capillary tube and inserted into the female fitting.

9. BVI is opened and the solution is allowed to drop into a small beaker for ten minutes before a run is started.

10. FV9 is closed.

11. The main valves of the nitrogen cylinders are opened. FV1, FV2, and FV3 are open. FV4 is closed.

12. The first few points of each run are designed to fall within the laminar range. For most of the tubes used, the diaphragm valve on the 0-60 psi two stage regulator is opened slowly until the pressure gauge reads 20 psi. At this point, the solution leaving the capillary tube enters the glass tee and is directed to the sink.

13. The electric timer is reset.

14. A beaker is placed under the glass tee.

15. The tee and attached mercury switch are flipped 90° and simultaneous collection of the liquid and activation of the timer occurs.

16. When 100 ml or 100 seconds, or both, have elapsed, the glass tee is flipped to the original position, thus stopping collection of the solution and simultaneously deactivating the timer.

17. The gauge pressure, time, and liquid volume collected are recorded as data.

18. The diaphragm valve on the pressure regulator is closed further, thus increasing the pressure, and steps 13 through 17 are repeated.

19. When the required pressure exceeds 60 psi, FV3 is shut and the 60-180 psi pressure regulator is used.

20. Steps 13 through 17 continue, with the appropriate pressure gauge and pressure regulator valves being opened and closed, until a predetermined pressure is reached.

21. At the end of a run, the diaphragm valves on the pressure regulators are closed, and the pressure throughout the system is released by slowly opening FV9.

22. For runs where three of four tubes of different surface free energy are used, the capillary tube is removed and the reservoir is refilled starting with step 4 .

23. At the end of the series of runs, the reservoir is flushed with water by inserting the rubber tubing and opening FV10.

24. After flushing, the reservoir is filled with water, and the capillary tubes reinserted. The tubes are flushed with water for ten minutes and then dried for five minutes by insertion into the female fitting and opening FV4.

25. The reservoir is refilled with water.

26. The regulators are depressurized.

APPENDIX C

CAPILLARY RISE PROCEDURE

1. The glass jar containing the stopper and plastic ruler is filled to the appropriate level with water. Water temperature was 24° C $\pm$ 2° C.

2. The ruler is moved to the center of the jar and the lower Plexiglas disc is placed on the jar and the ruler in such a position as to "lock" the ruler in place directly behind the hole in the Plexiglas disc. The water level is read on the ruler.

3. The appropriate number of blocks are placed on the Plexiglas disc.

4. The capillary tube is screwed into the upper Plexiglas disc, and the disc is placed on the blocks with the exit end of the capillary tube being inserted through the lower Plexiglas disc and into the water. Care is taken to avoid entrapped gas bubbles on the bottom of the glass capillary tube, and establish proper alignment with the scale on the ruler.

5. For uncoated tubes, a rubber bulb (open on both ends) is temporarily connected to the capillary tube by means of flexible PVC tubing. The water is sucked up to 3 or 4 cm above the final reading and made to fall from 5 to 8 cm below. After sucking the liquid up three times, it is allowed to fall to an equilibrium height. The height assumed by the lower edge of the meniscus is read after one minute of elapsed time.

6. For coated tubes, the meniscus is allowed to rise, and the height read after one to three minutes of elapsed time. For multi-point readings, one block at a time is removed. Again, the meniscus is allowed to rise, and the height read after one to three minutes.

7. The capillary tube is removed and dried.

APPENDIX D

FIGURES

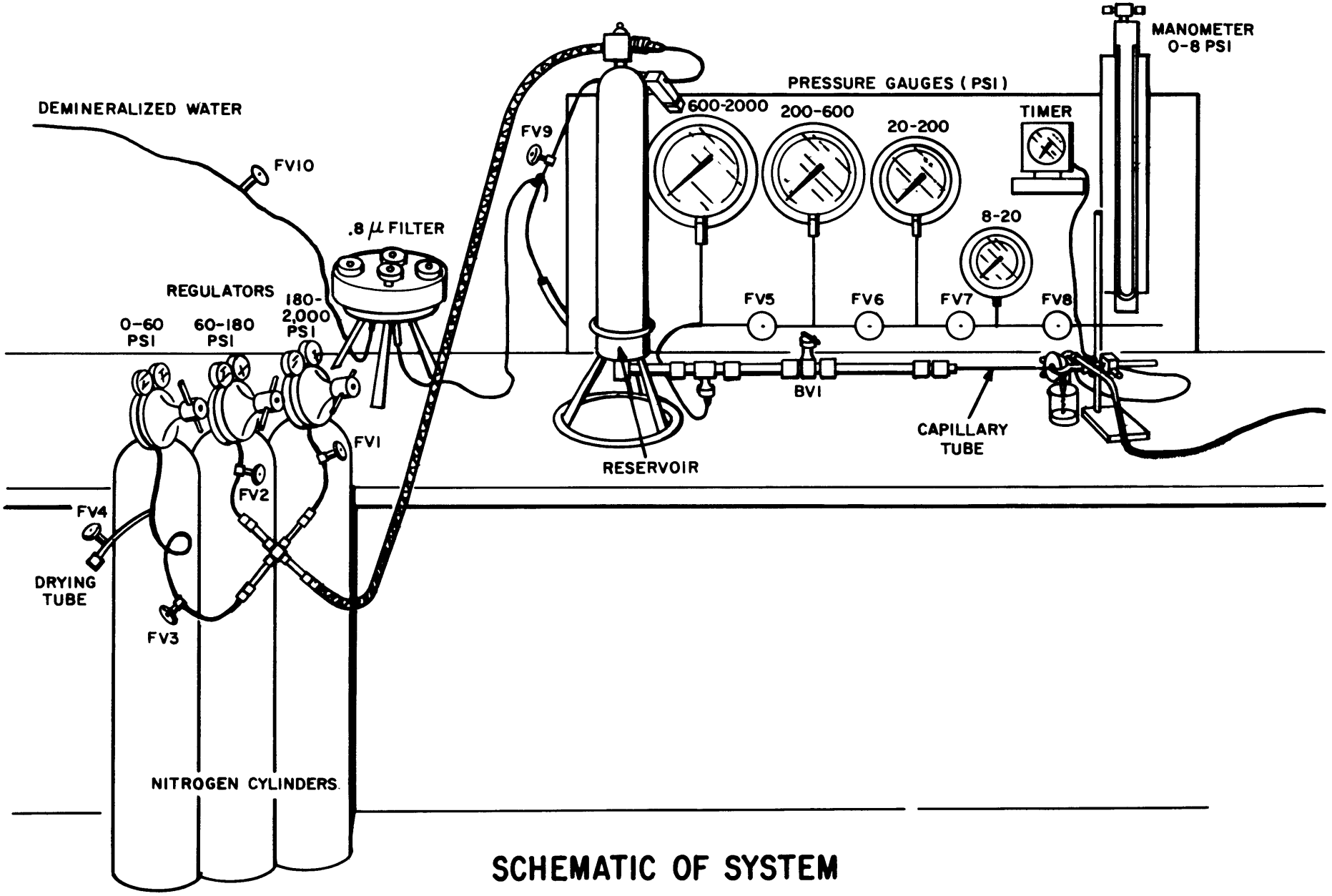

SCHEMATIC OF SYSTEM

Figure IV-1

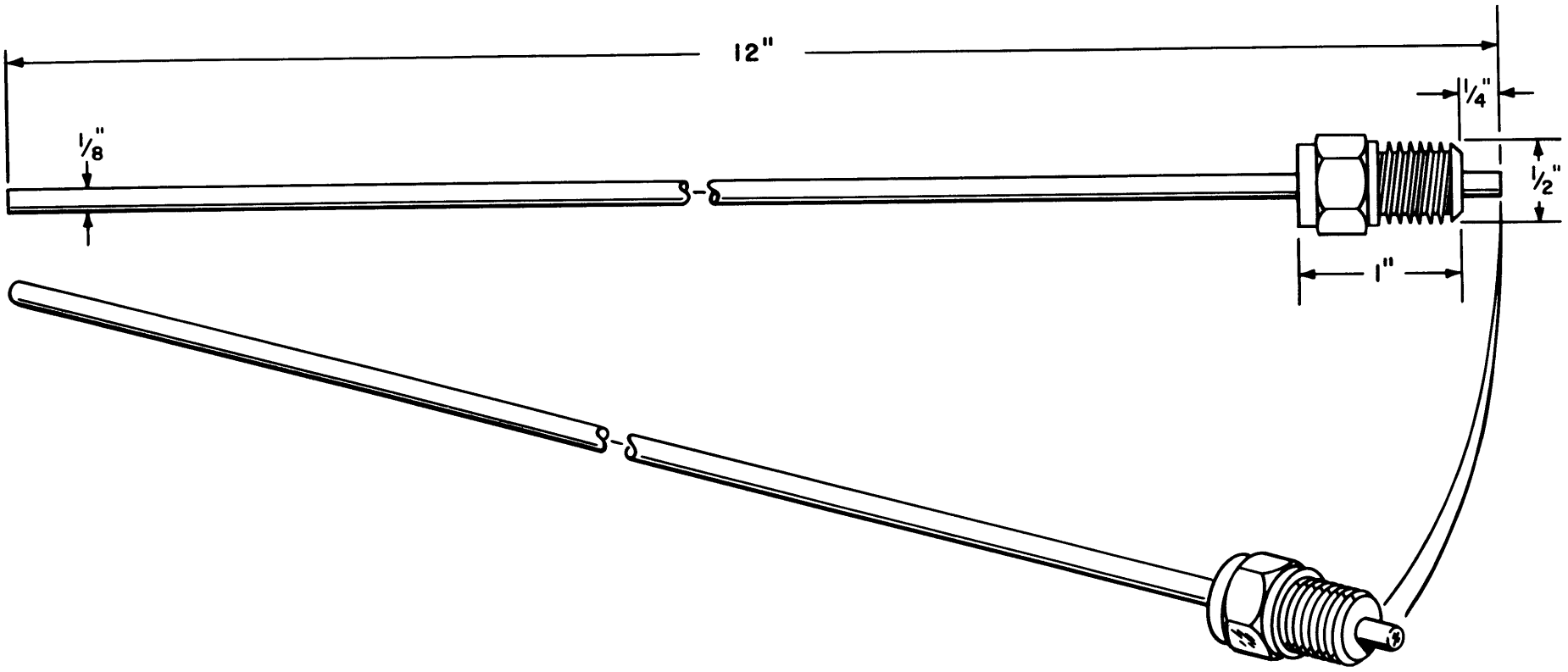

CAPILLARY TUBE

Figure IV-2

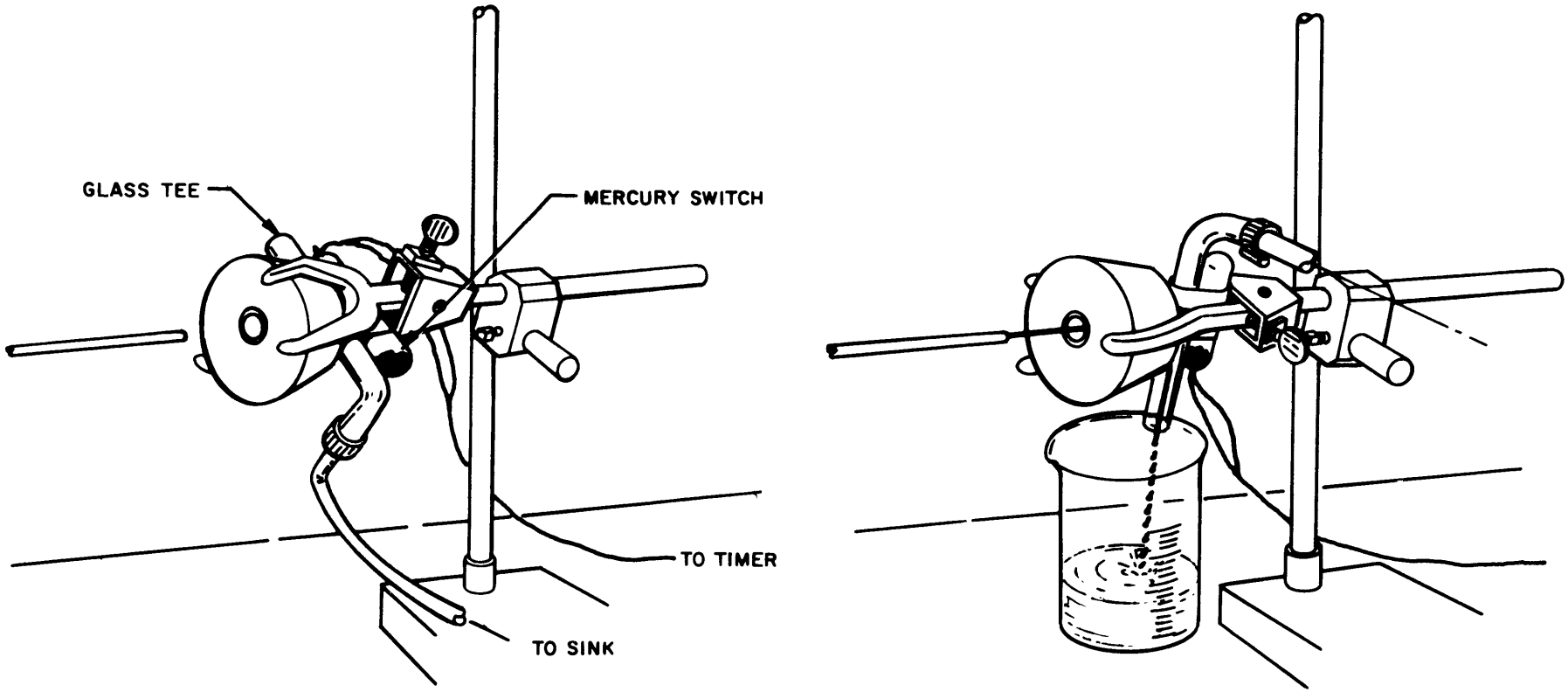

SCHEMATIC OF COLLECTION SYSTEM

Figure IV-3

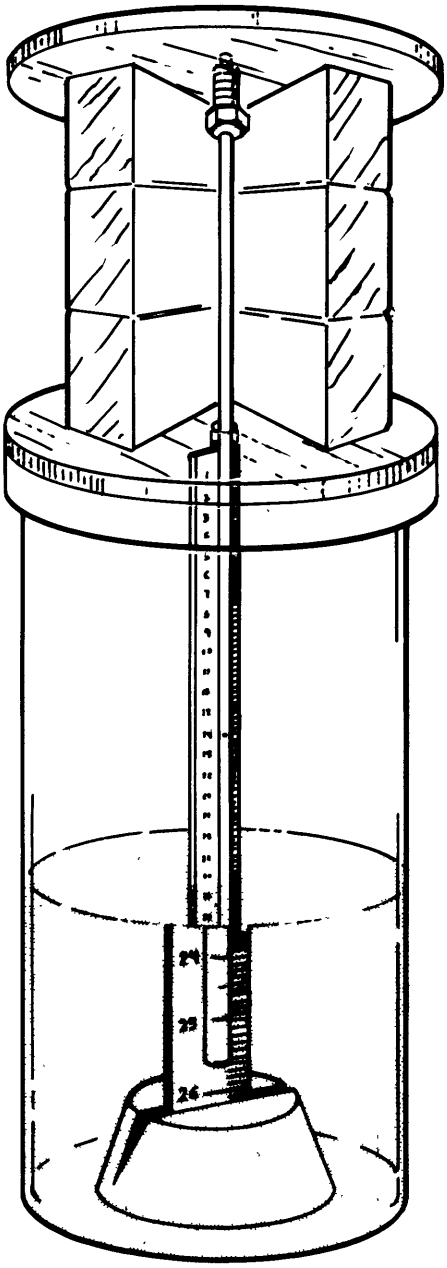

CAPILLARY RISE

Figure IV-4

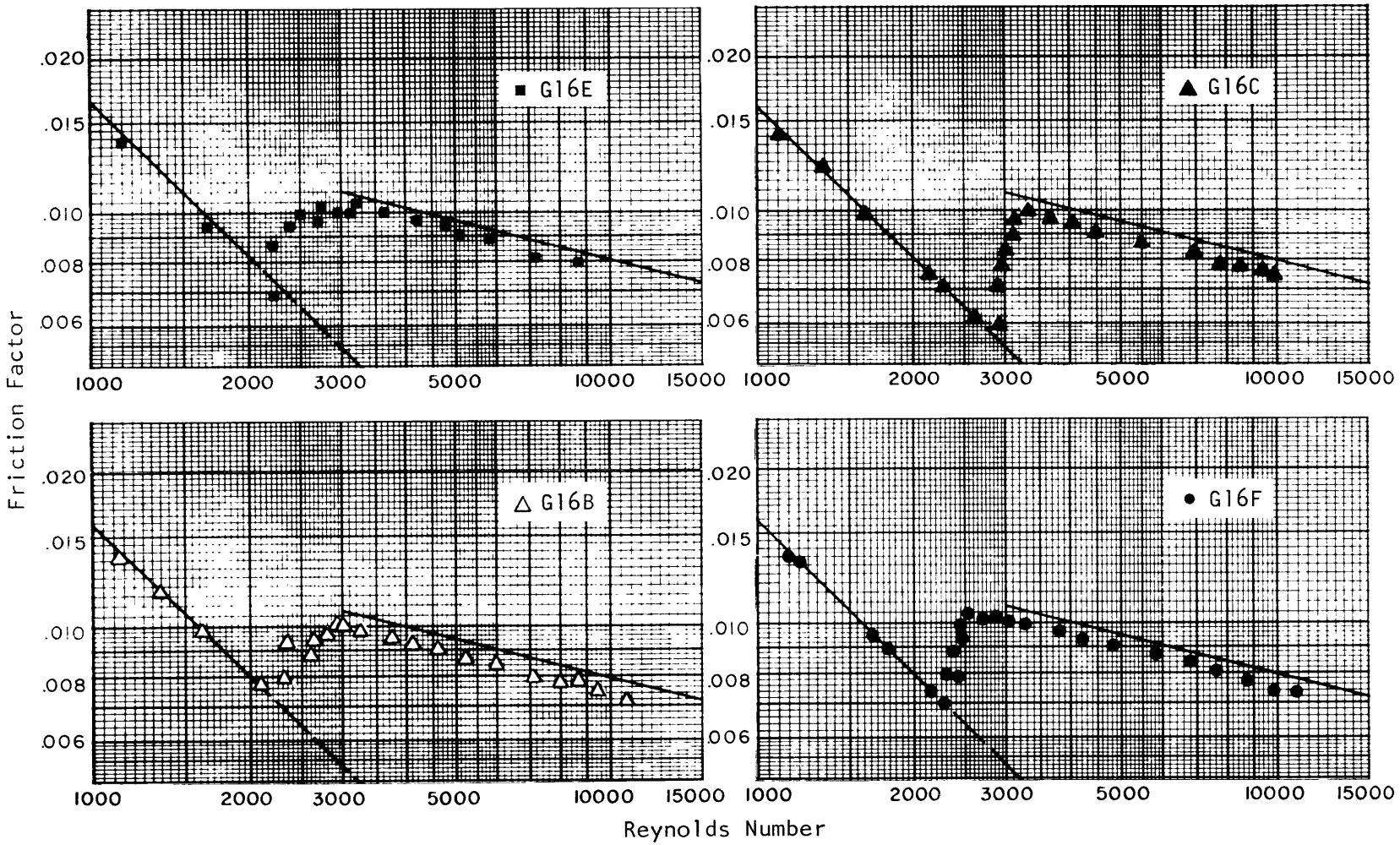

Friction Factor versus Reynolds Number for water in G16 Series capillary tubes. G16F is uncoated glass; G16C has a fluorocarbon surface coating; G16B has a silicone surface coating; G16E has a stearic acid (hydrocarbon) surface coating.

Figure VI-1

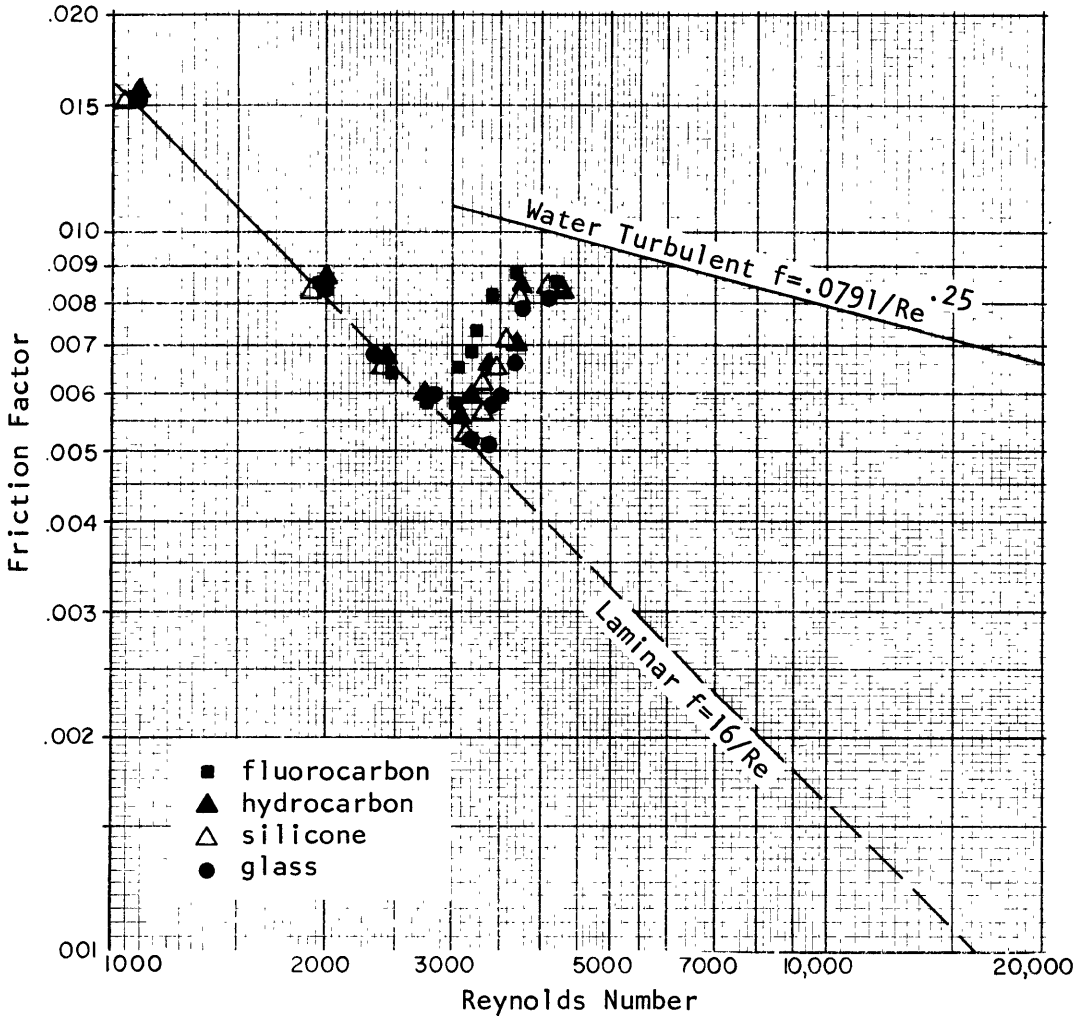

Friction Factor versus Reynolds Number for a 1/2 ppm "coagulant" solution in G16 Series capillary tubes.

Figure VI-2

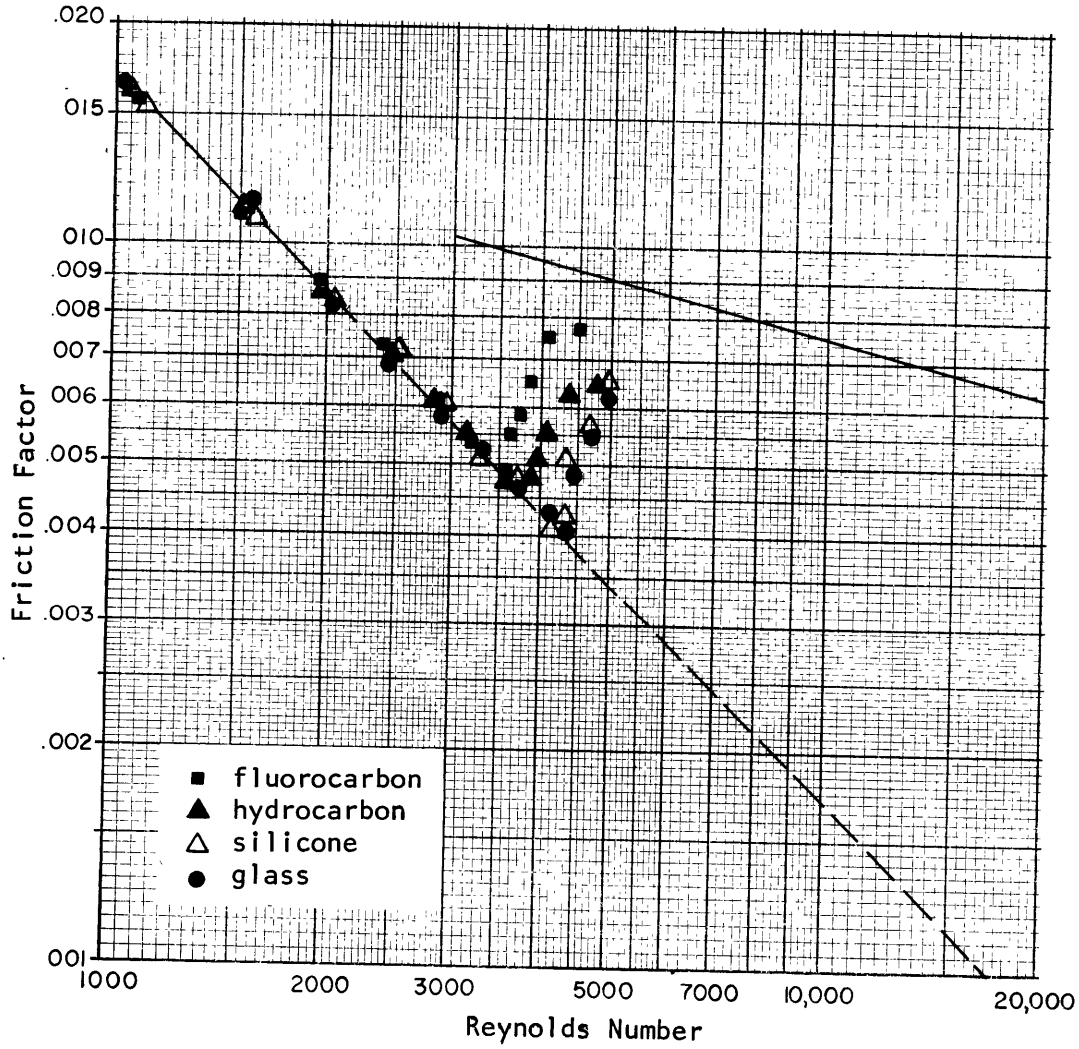

Friction Factor versus Reynolds Number for a 1 ppm "coagulant" solution in G16 Series capillary tubes.

Figure VI-3

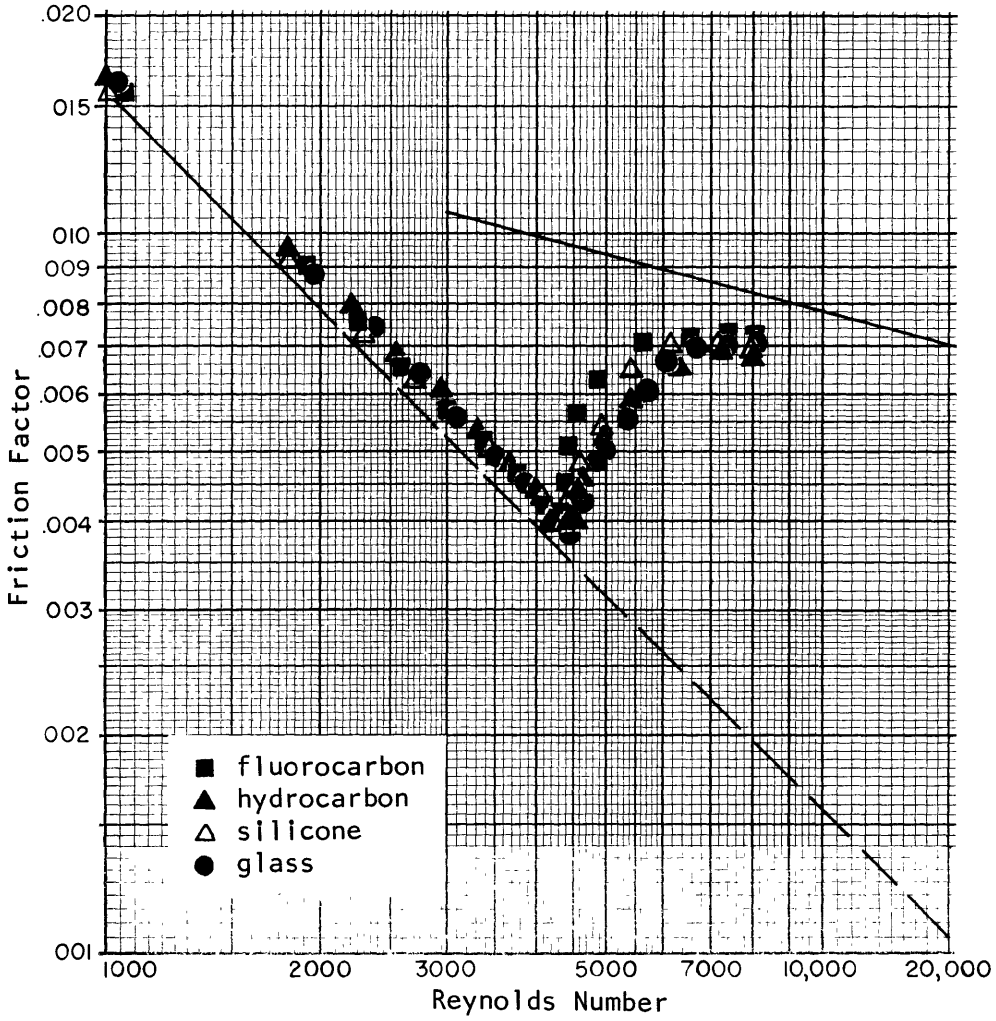

Friction Factor versus Reynolds Number for a 3/2 ppm "coagulant" solution in G16 series capillary tubes.

Figure VI-4

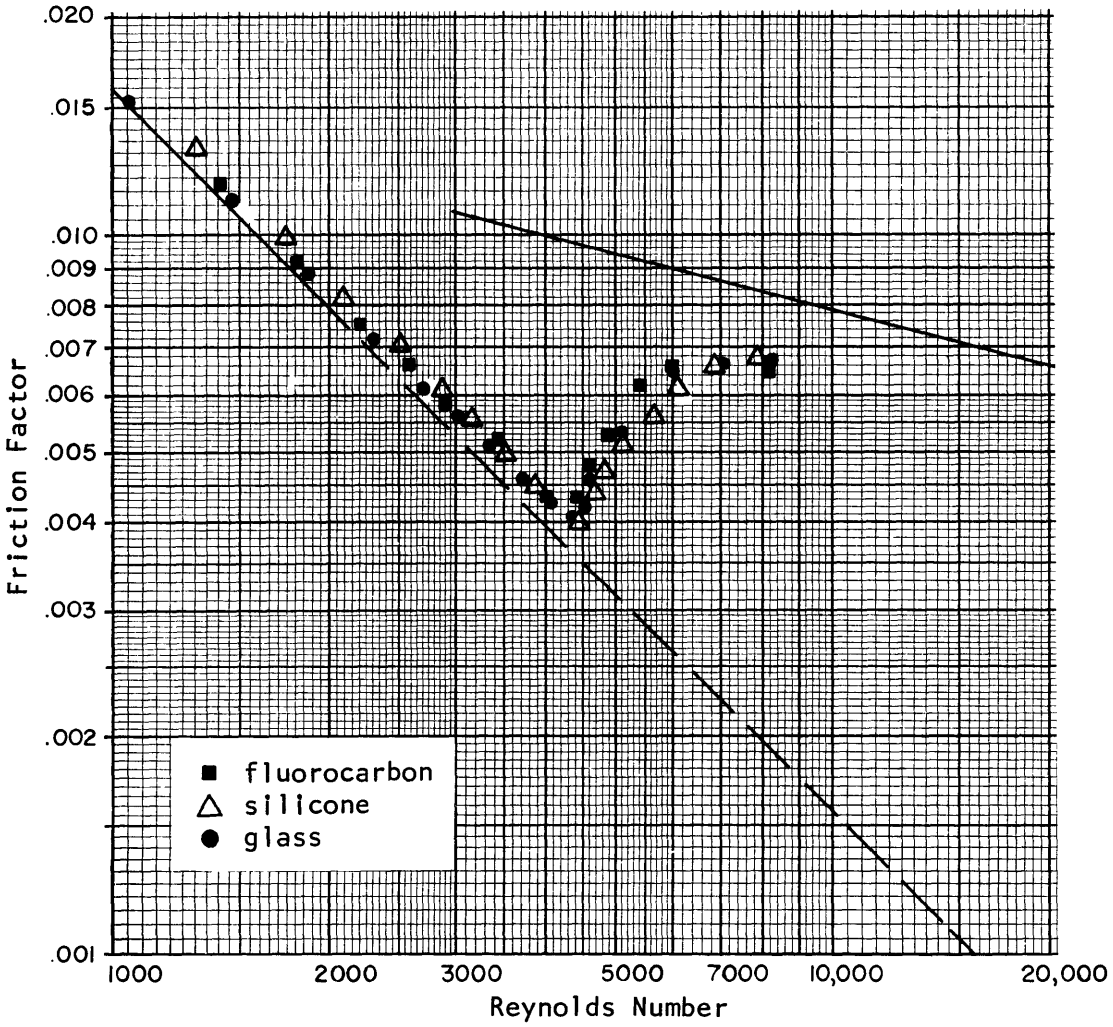

Friction Factor versus Reynolds Number for a 2 ppm "coagulant" solution in G16 series capillary tubes.

Figure VI-5

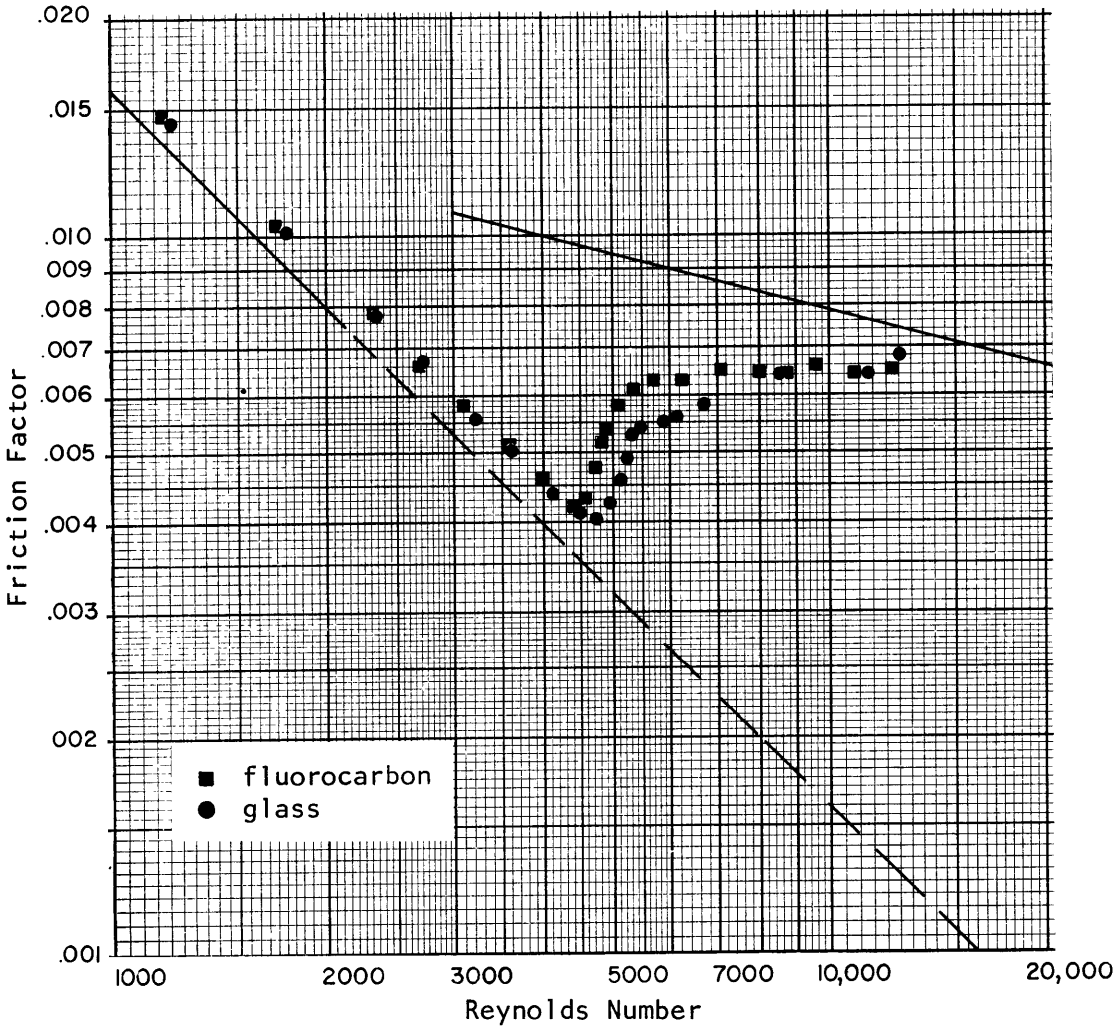

Friction Factor versus Reynolds Number for a 2 ppm "coagulant" solution in G16 series capillary tubes.

Figure VI-6

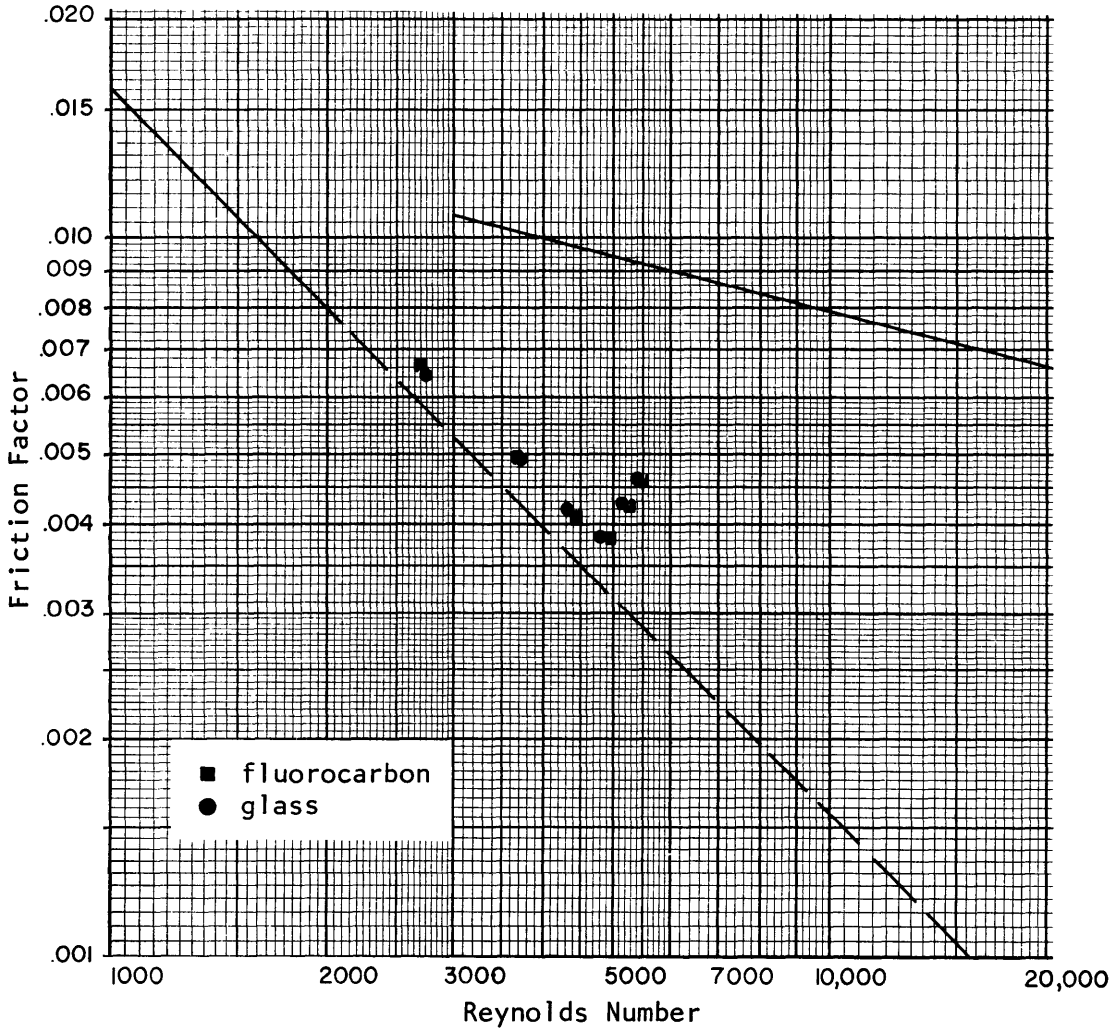

Friction Factor versus Reynolds Number for a 3 ppm "coagulant" solution in G16 series capillary tubes.

Figure VI-7

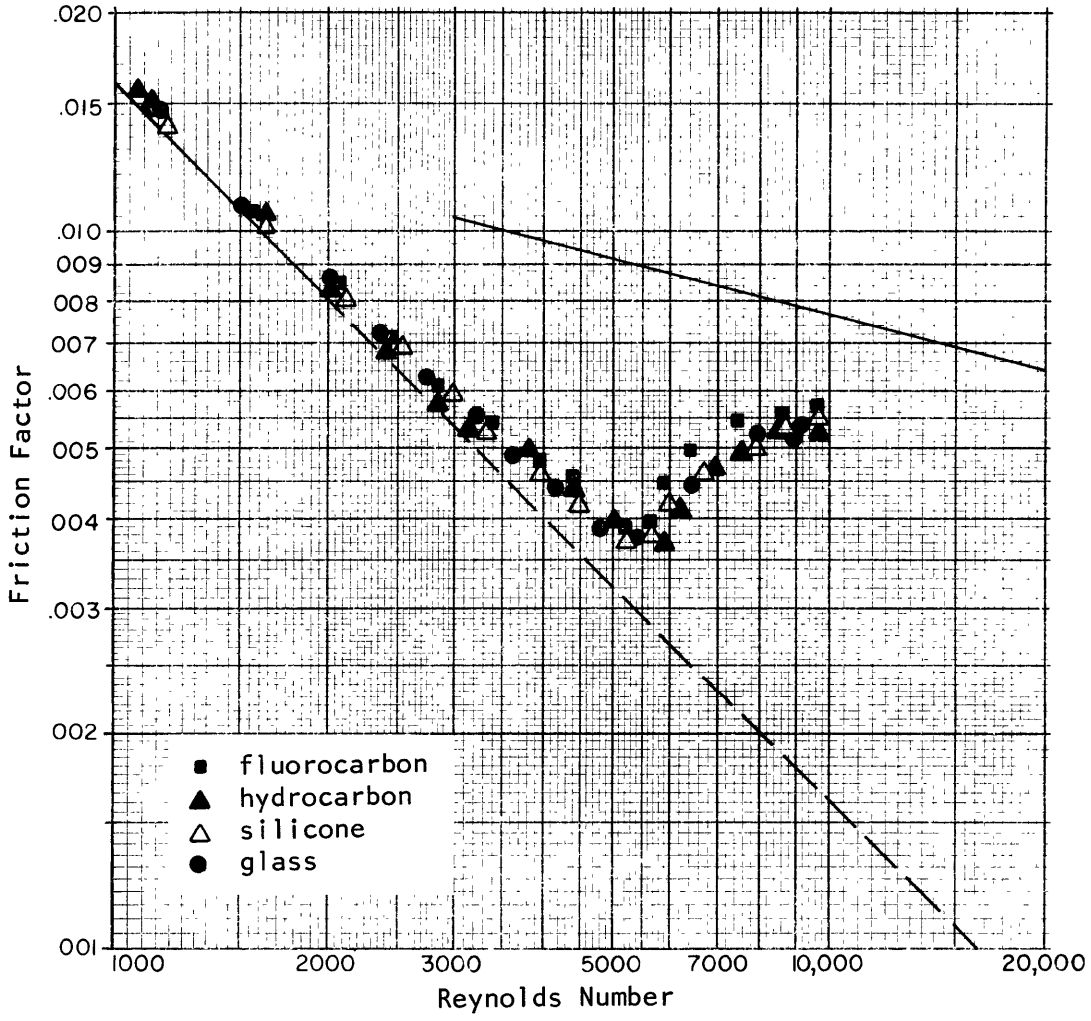

Friction Factor versus Reynolds Number for a 4 ppm "coagulant" solution in G16 series capillary tubes.

Figure VI-8

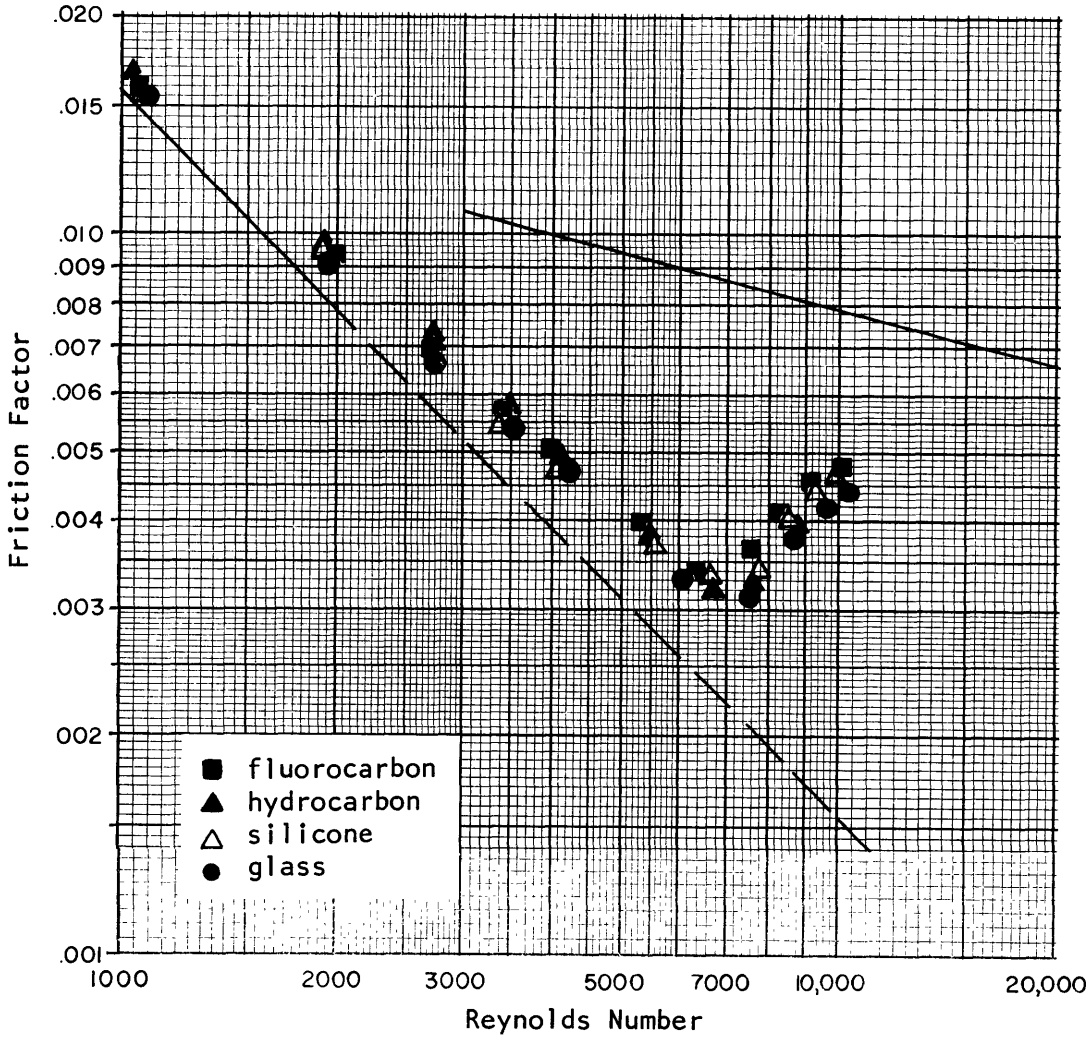

Friction Factor versus Reynolds Number for a 7 ppm "coagulant" solution in G16 series capillary tubes.

Figure VI-9

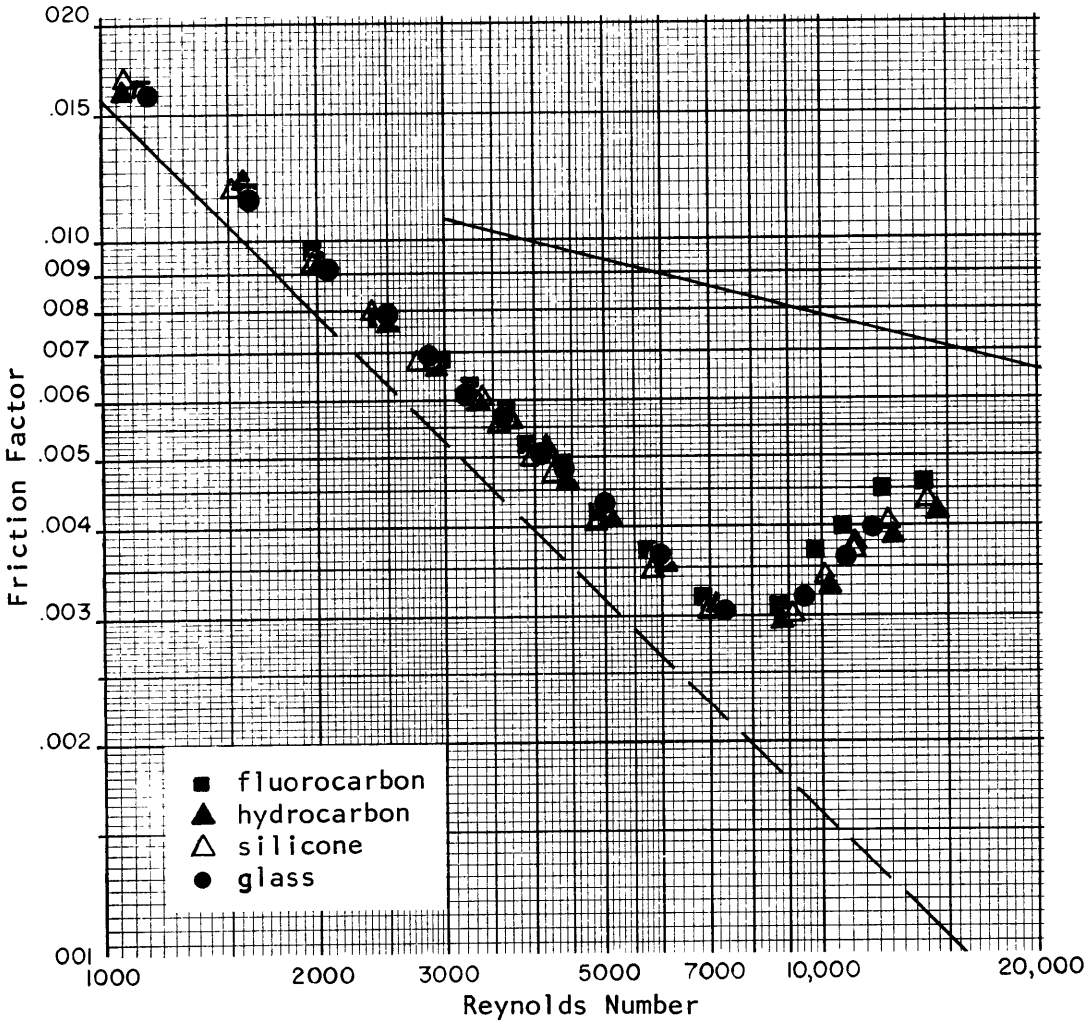

Friction Factor versus Reynolds Number for a 10 ppm "coagulant" solution in G16 series capillary tubes.

Figure VI-10

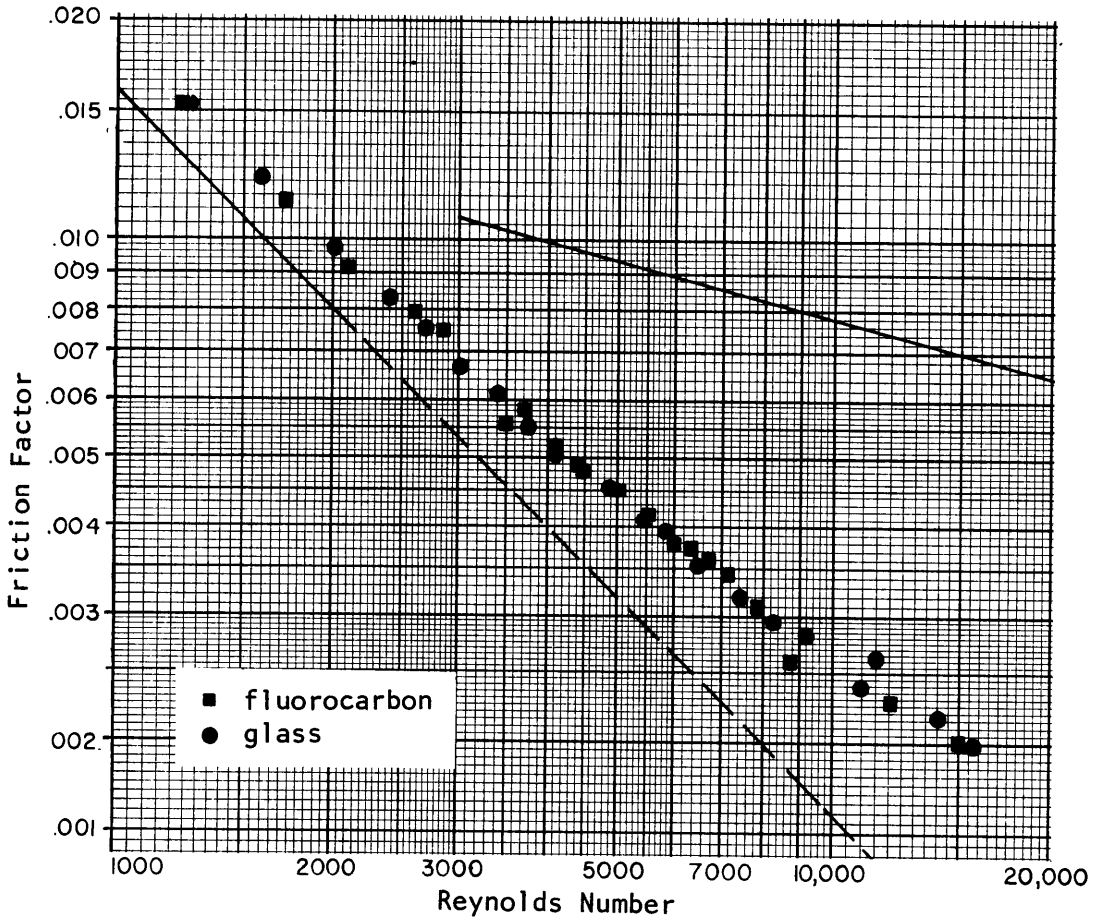

Friction Factor versus Reynolds Number for a 50 ppm "coagulant" solution in G16 series capillary tubes.

Figure VI-11

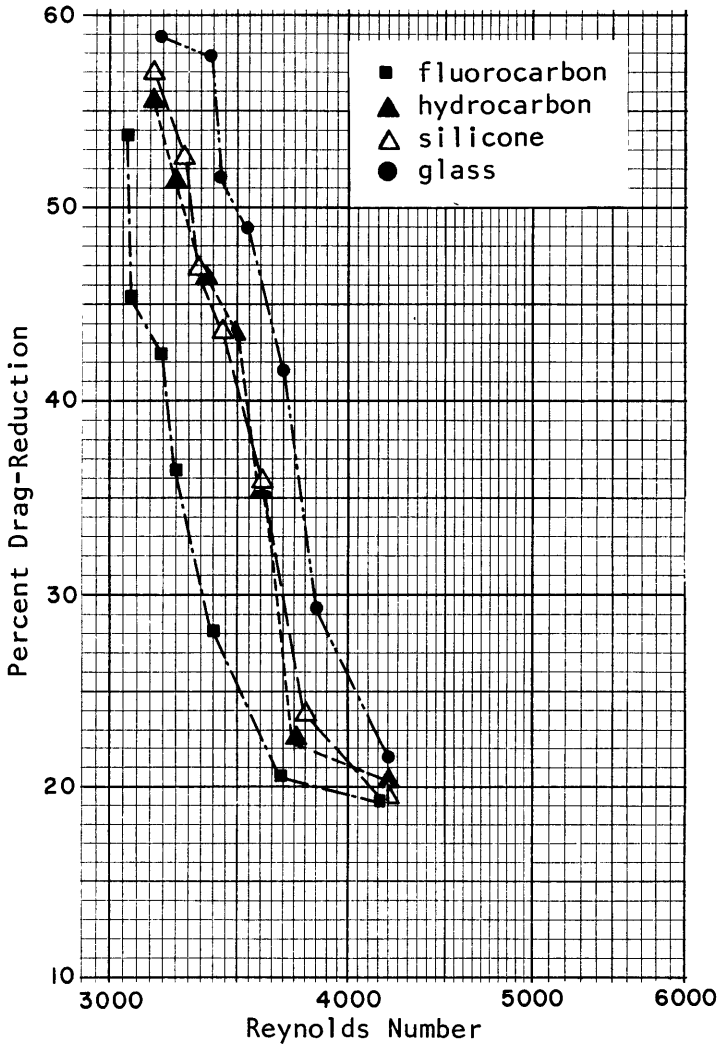

Drag-Reduction versus Reynolds Number for a 1/2 ppm "coagulant" solution in G16 series capillary tubes; replotted from Figure VI-2 with % DR=100(1-fp/f) Re.

Figure VI-12

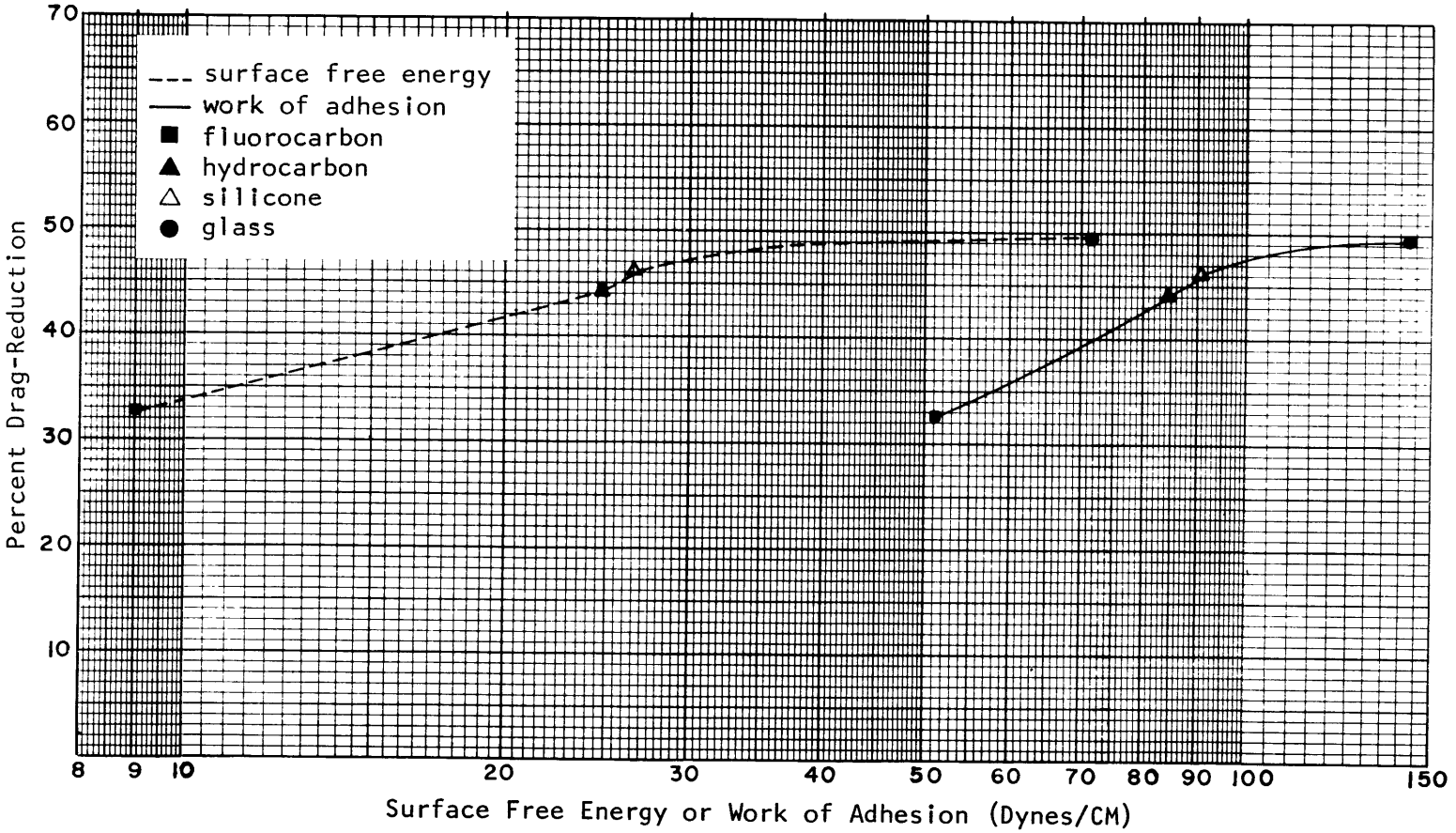

Drag-Reduction as a function of surface free energy and work of adhesion for a 1/2 ppm poly (ethylene oxide) "coagulant" solution in G16 series capillary tubes; Re_{max} = 3200.

Figure VI-13

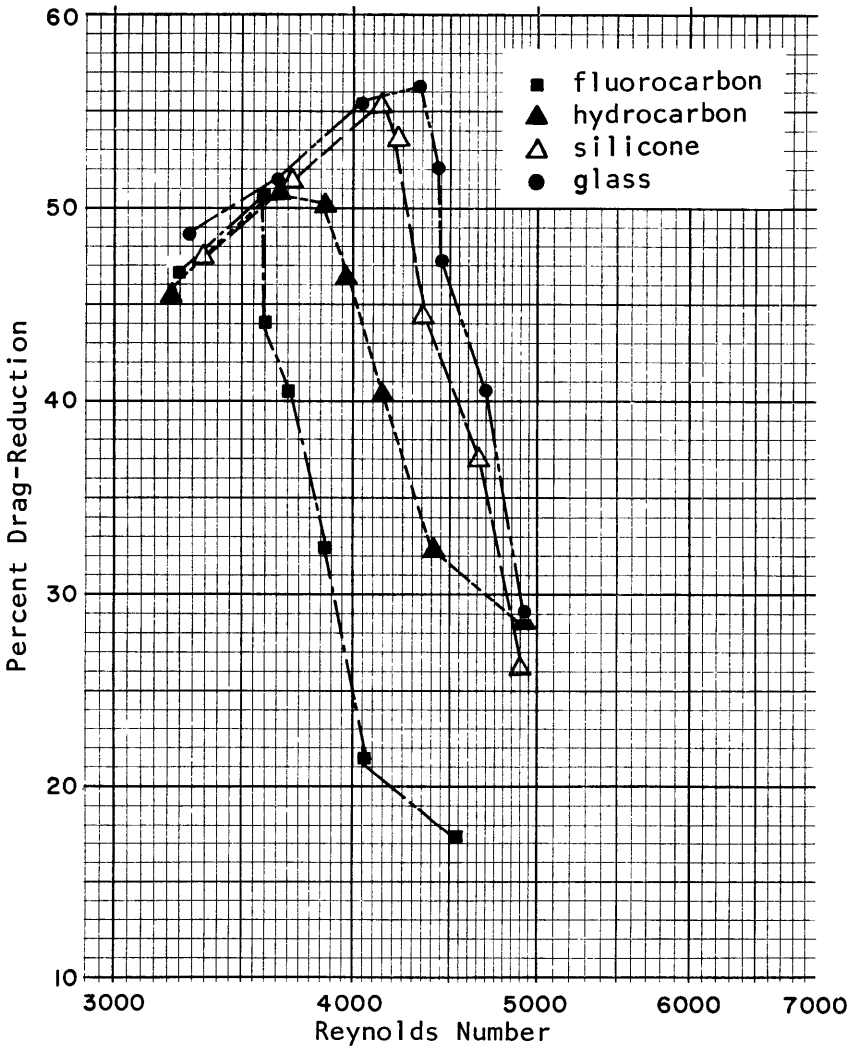

Drag-Reduction versus Reynolds Number for a 1 ppm "coagulant" solution in G16 series capillary tubes; replotted from Figure VI-3 with % DR=100(1-fp/f) Re.

Figure VI-14

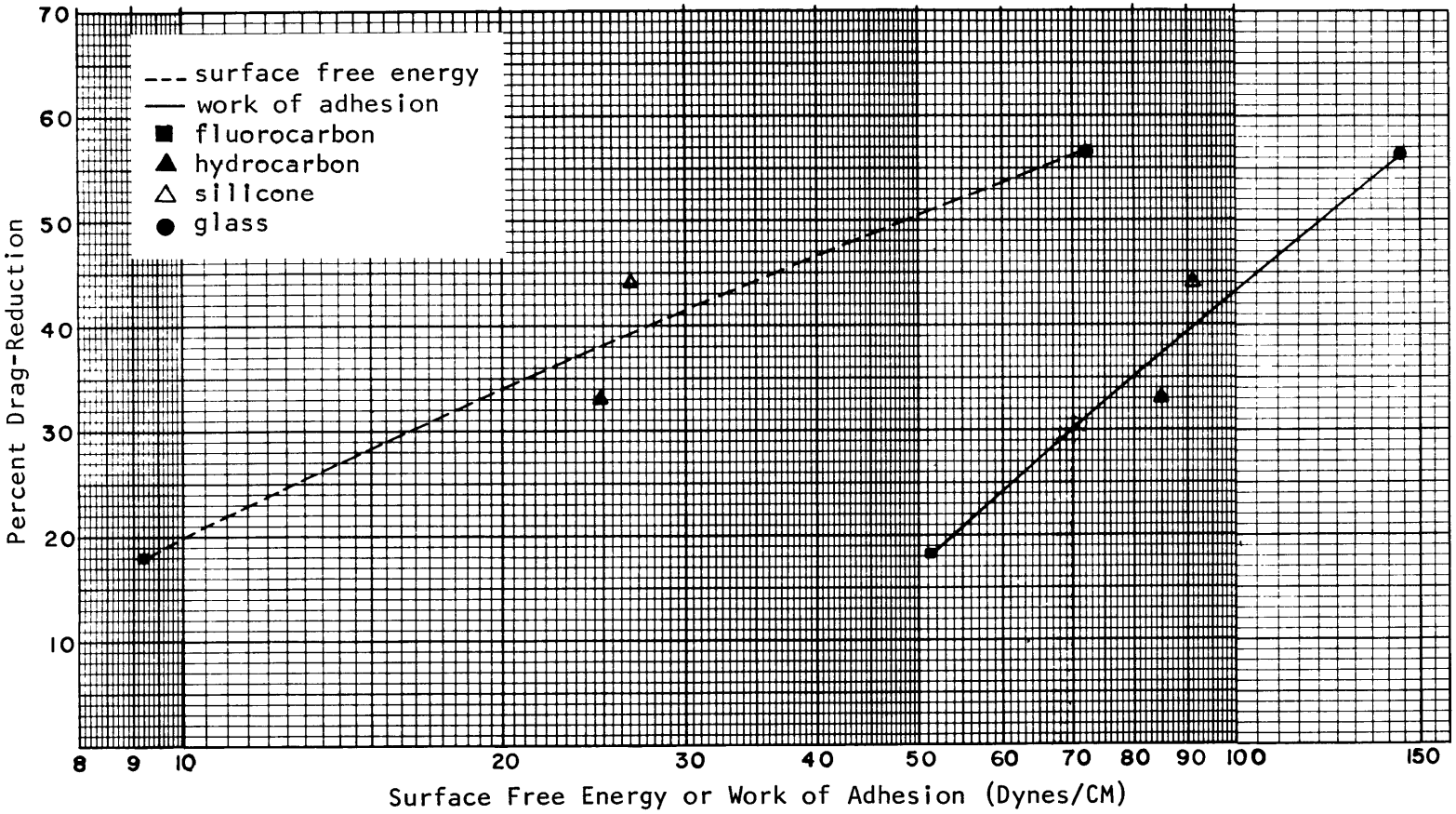

Drag-Reduction as a function of surface free energy and work of adhesion for a 1 ppm poly(ethylene oxide) "coagulant" solution in small bore capillary tubes; Re_{max} = 4350.

Figure VI-15

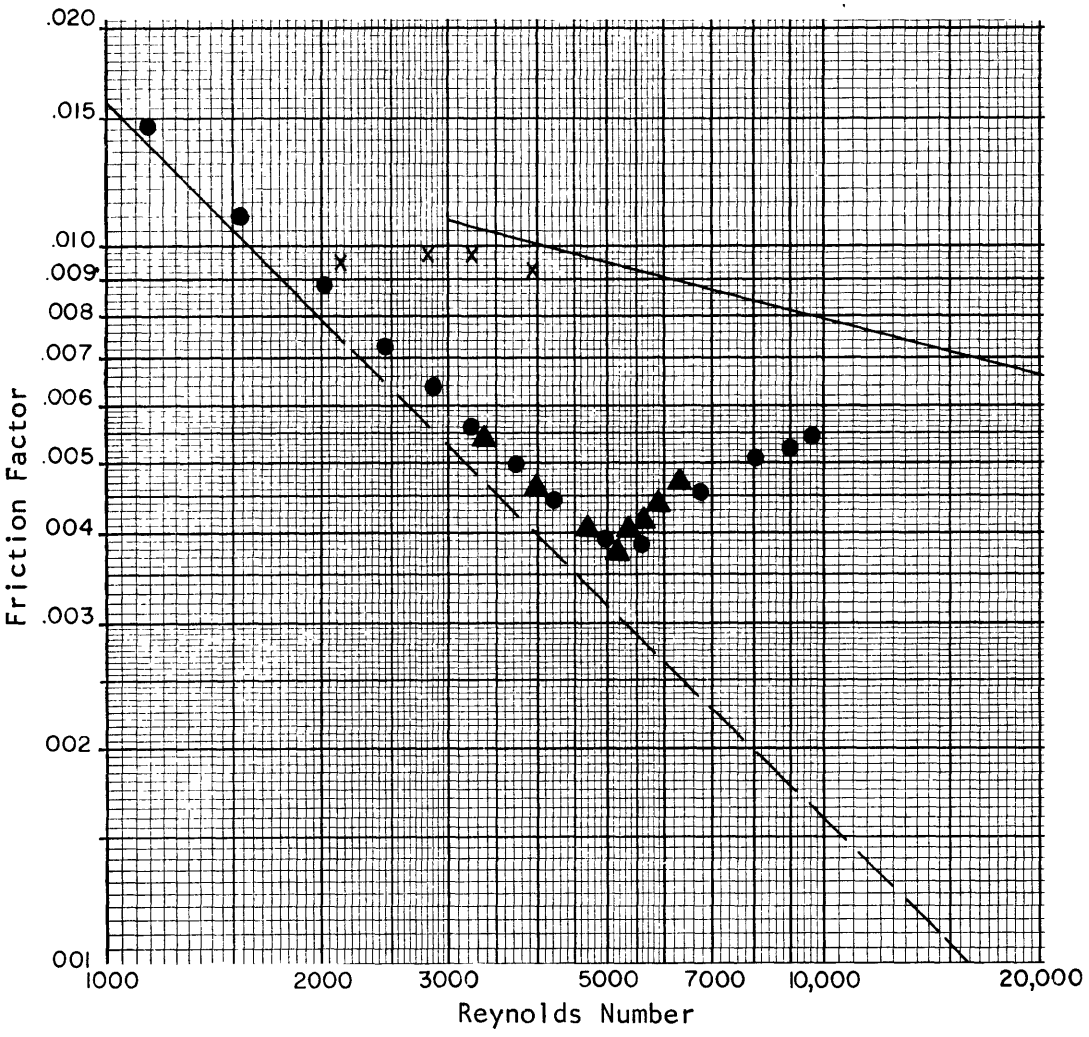

Friction Factor versus Reynolds Number for a 4 ppm "coagulant" solution in glass capillary tube G16F; degradation runs; ● once through, ▲ second time through after being passed through the first time at Re = 3650, X second time through after being passed through the first time at Re = 9500.

Figure VI-16

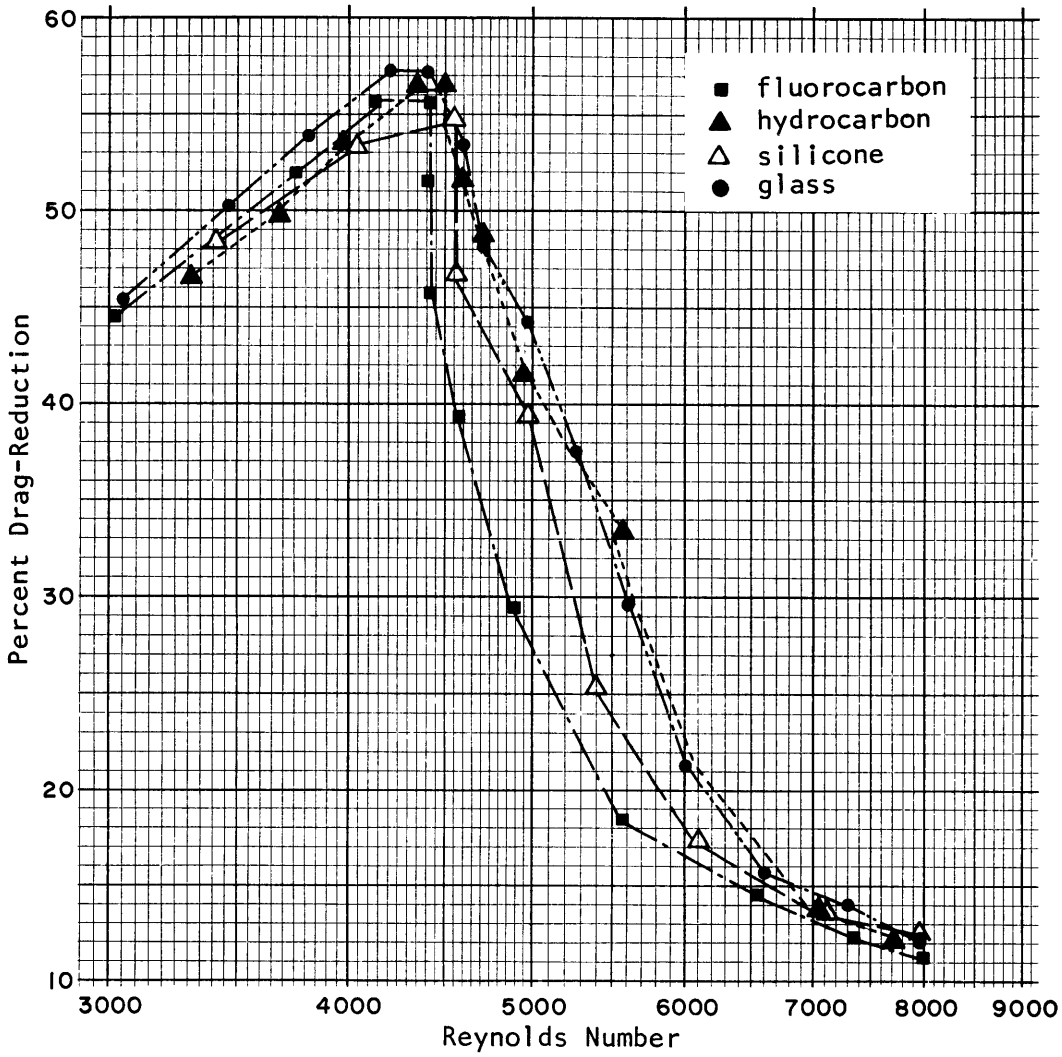

Drag-Reduction versus Reynolds Number for a 3/2 ppm "coagulant" solution in G16 series capillary tubes; replotted from Figure VI-4 with % DR=100(1-fp/f) Re.

Figure VI-17

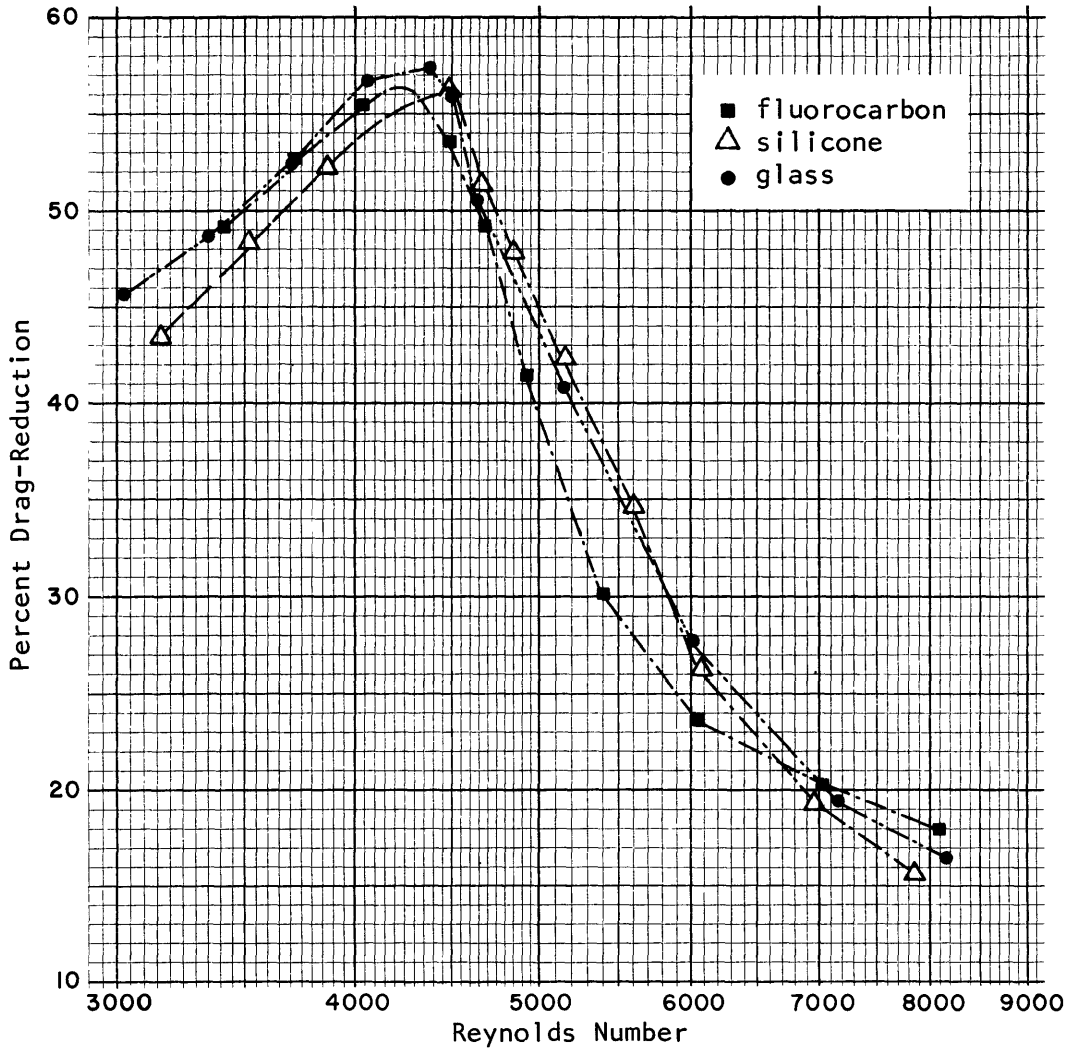

Drag-Reduction versus Reynolds Number for a 2 ppm "coagulant" solution in G16 series capillary tubes; replotted from Figure VI-5 with % DR=100(1-fp/$_f$) Re.

Figure VI-18

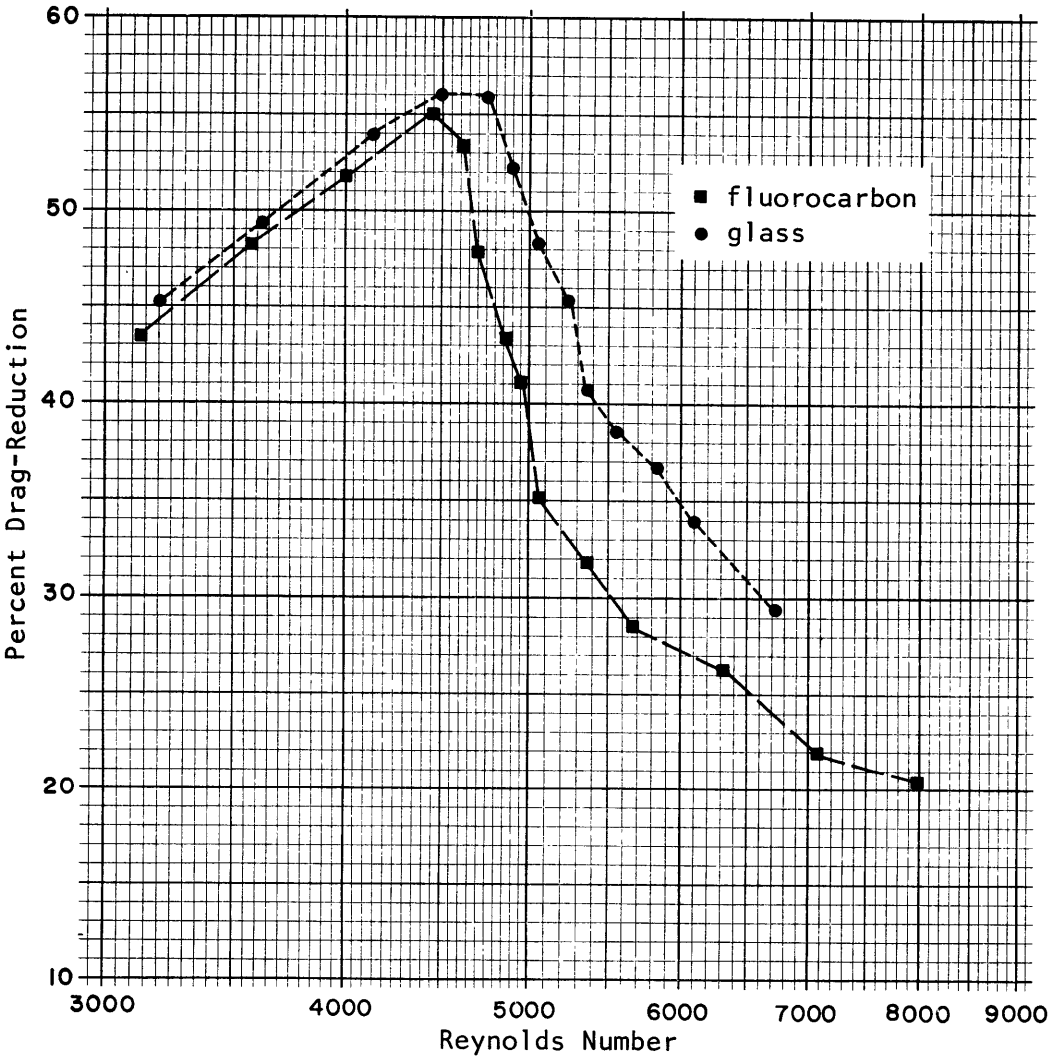

Drag-Reduction versus Reynolds Number for a 2 ppm "coagulant" solution in G16 series capillary tubes; replotted from Figure VI-6 with % DR=100(1-fp/$_f$) Re.

Figure VI-19

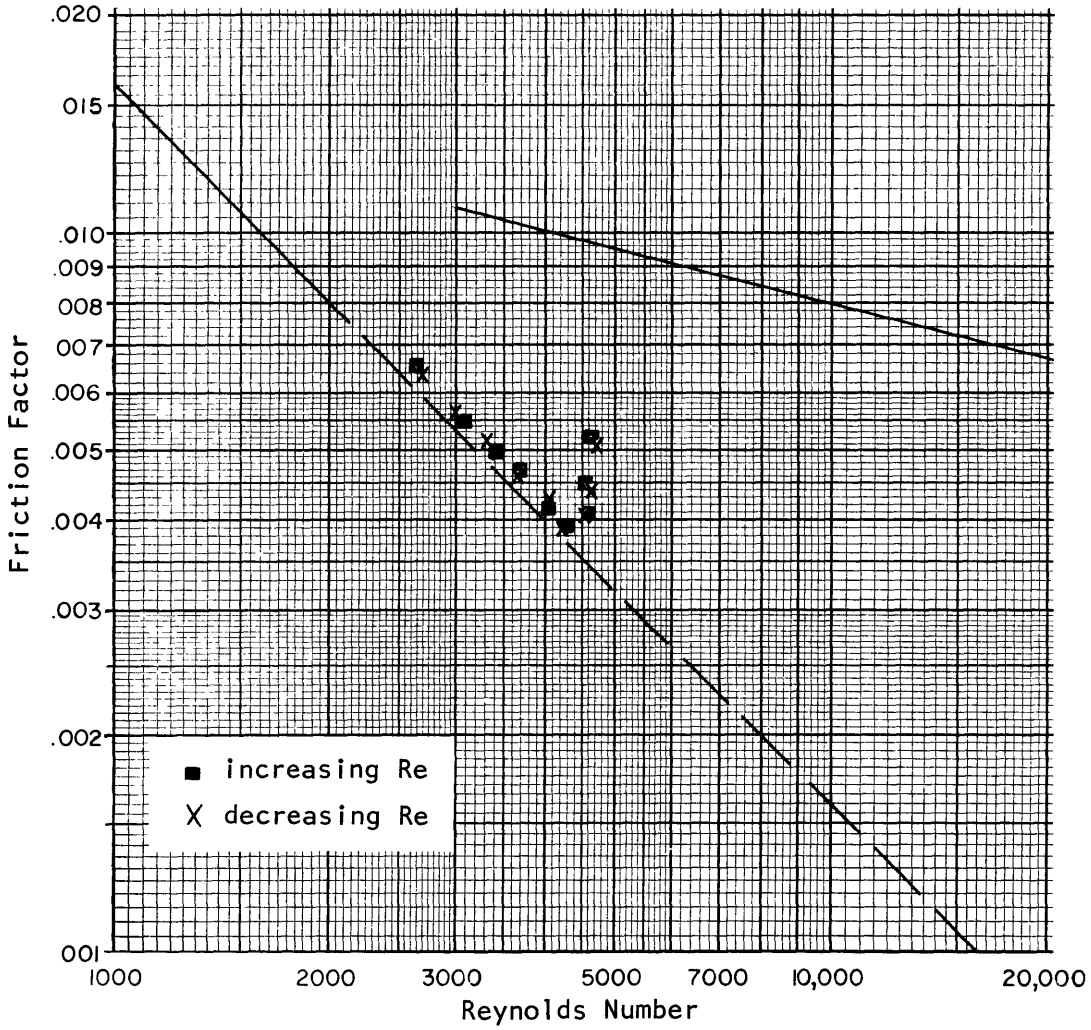

Friction Factor versus Reynolds Number for a 3 ppm "coagulant" solution in glass capillary tube G16F; hysteresis run; ■ increasing Re, X decreasing Re.

Figure VI-20

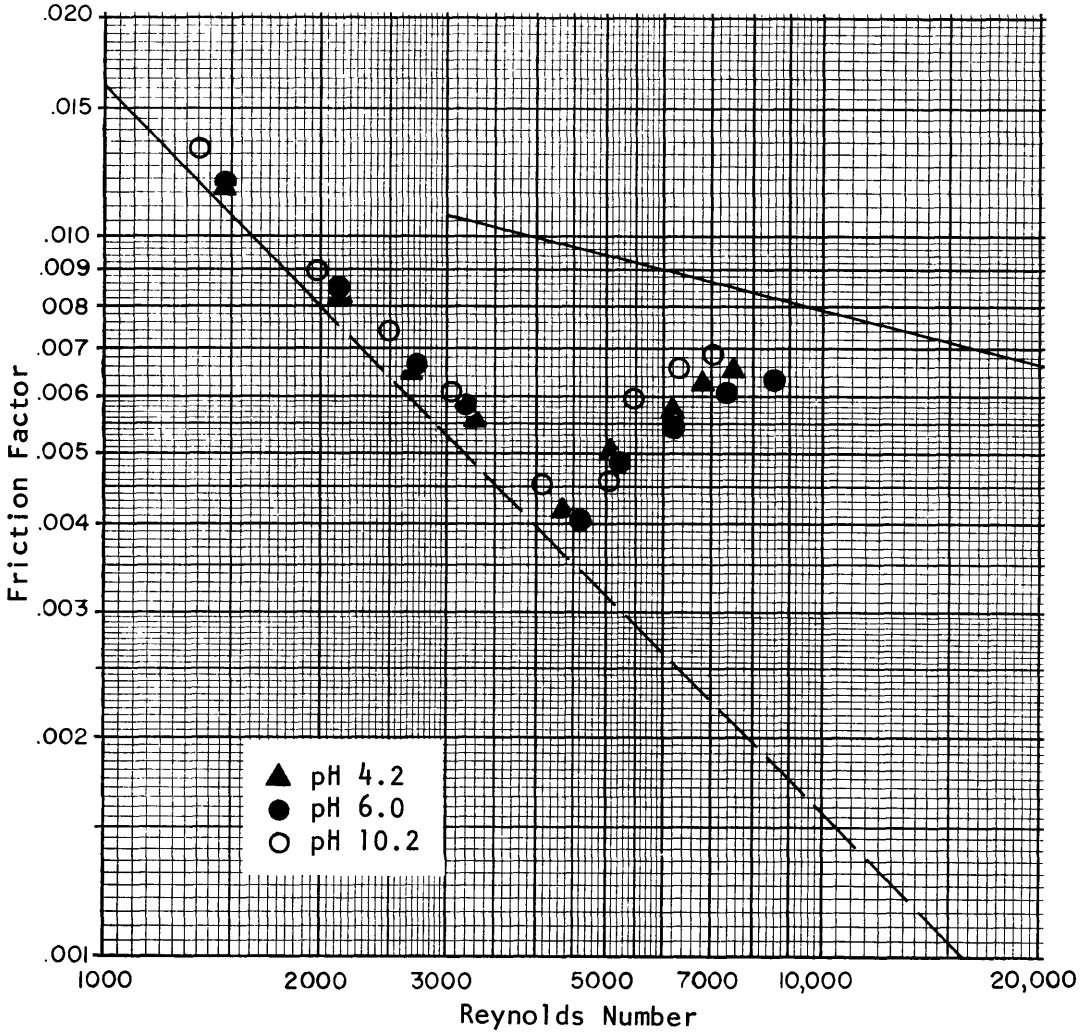

Friction Factor versus Reynolds Number for a 3 ppm "coagulant" solution in glass capillary tube G12; pH as parameter.

Figure VI-21

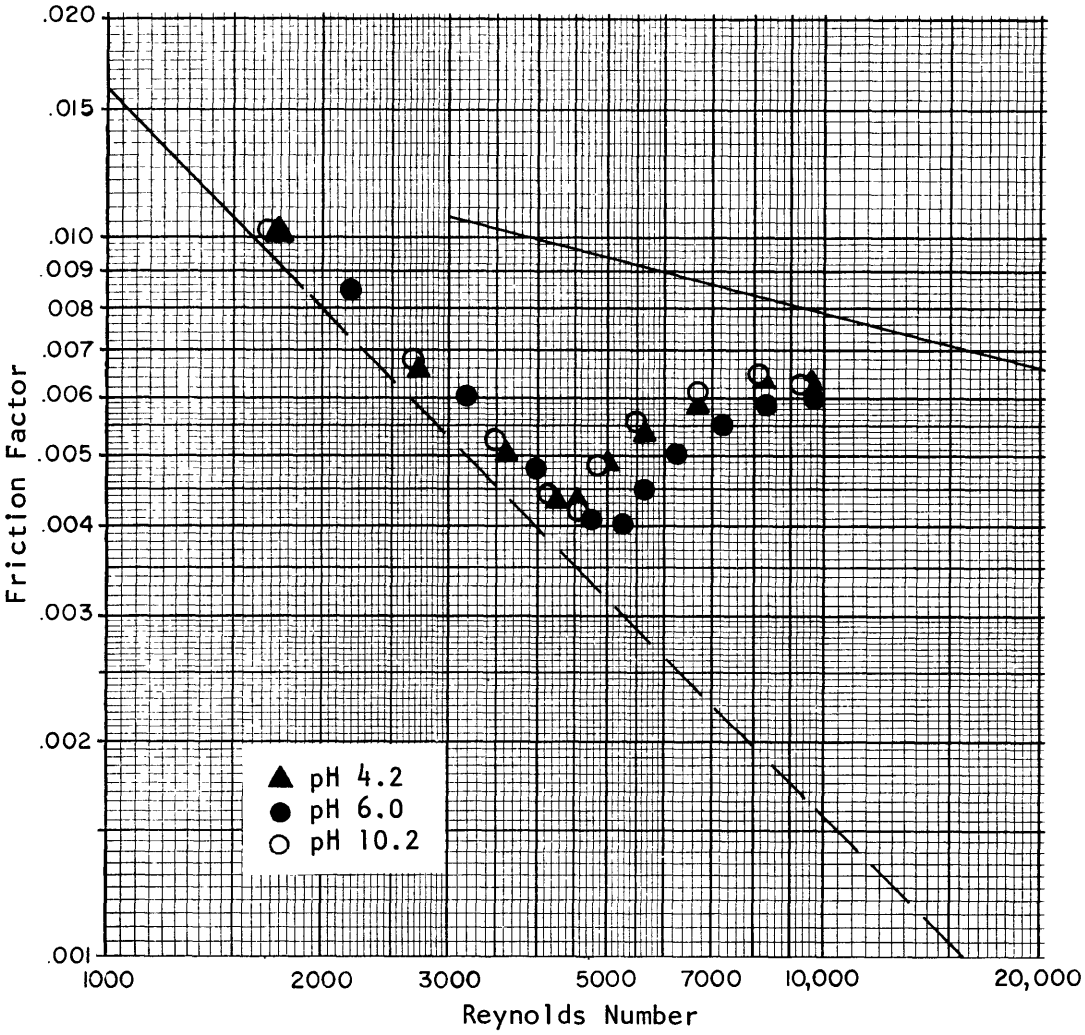

Friction Factor versus Reynolds Number for a 3 ppm "coagulant" solution in glass capillary tube G16F; pH as parameter.

Figure VI-22

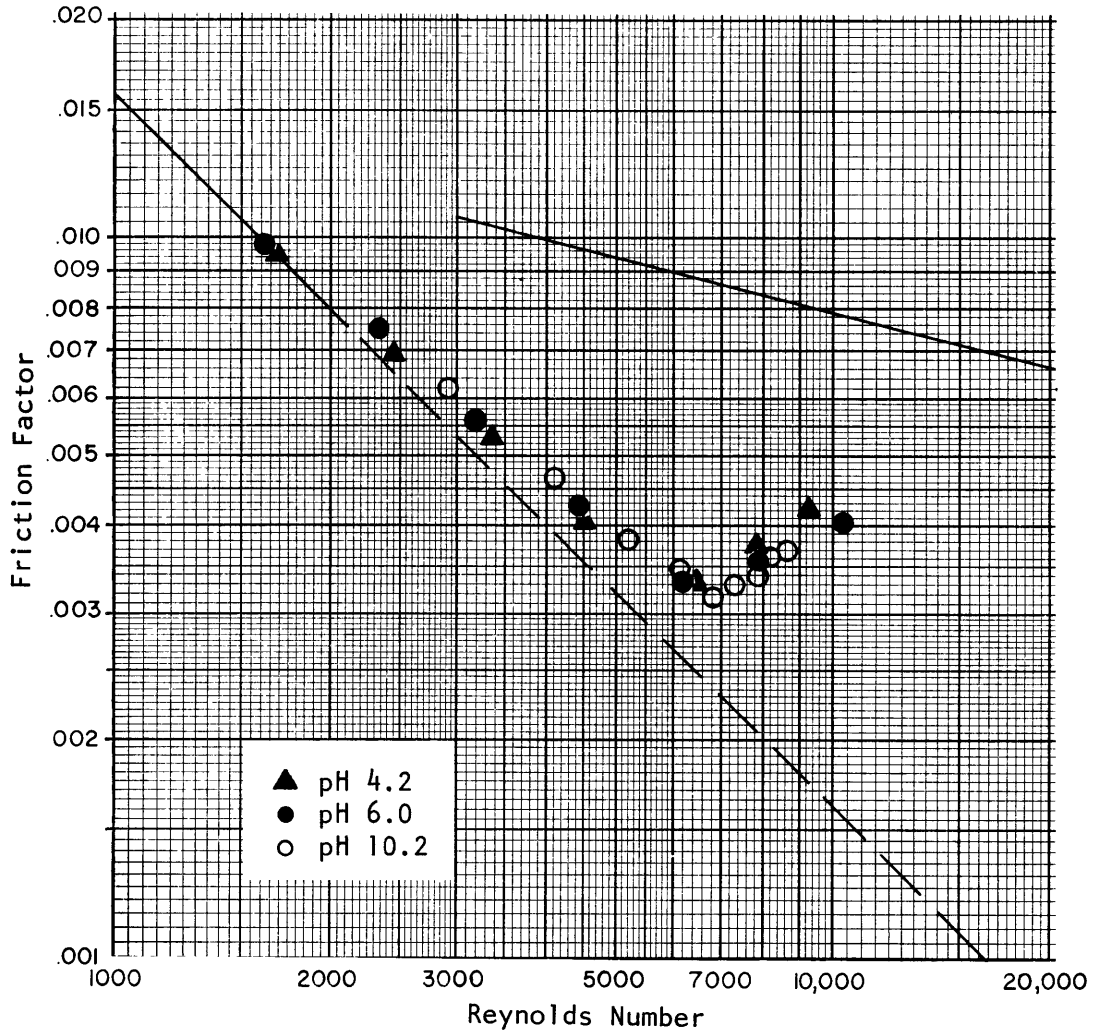

Friction Factor versus Reynolds Number for a 3 ppm "coagulant" solution in glass capillary tube G31; pH as parameter.

Figure VI-23

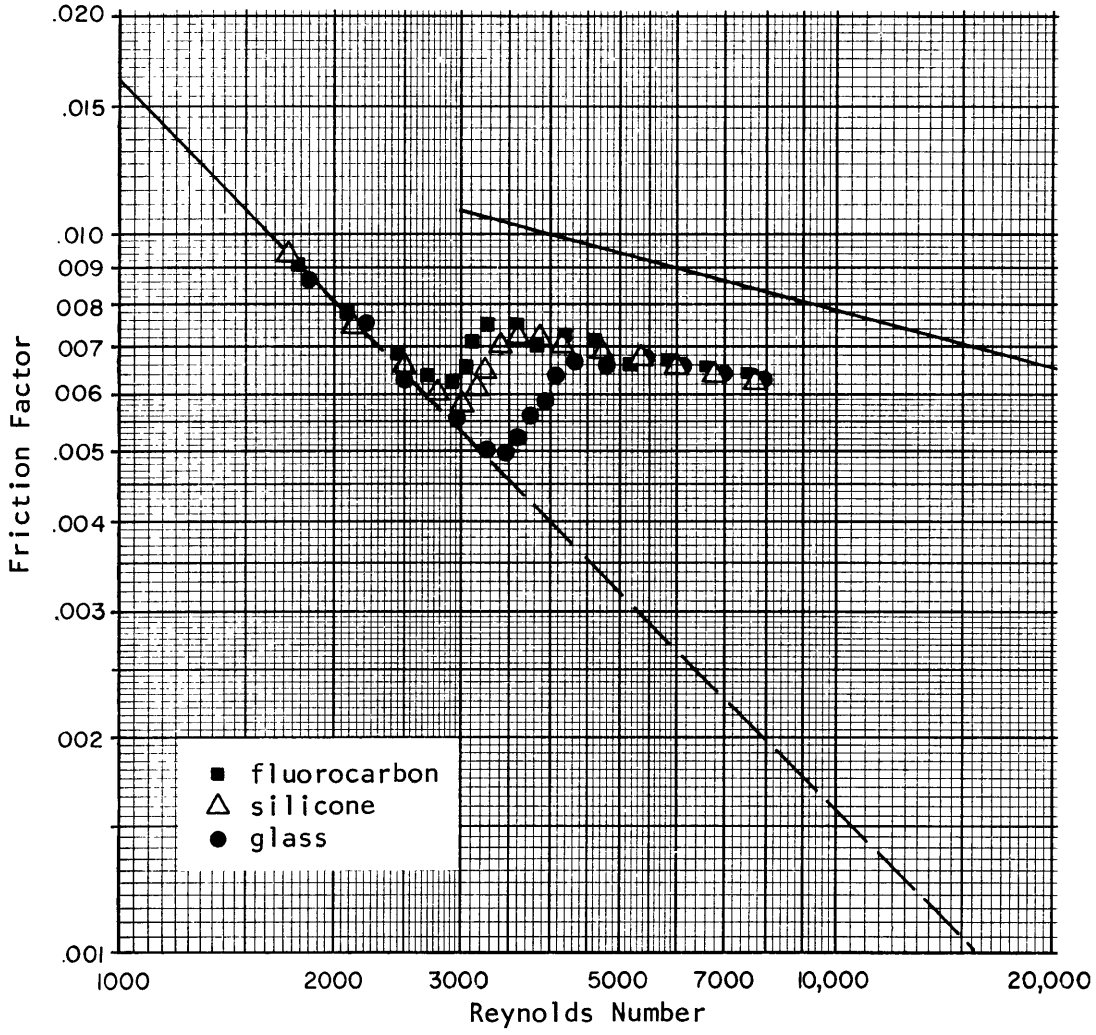

Friction Factor versus Reynolds Number for a 10 ppm "WSR-N-3000" solution in G16 series capillary tubes.

Figure VI-24

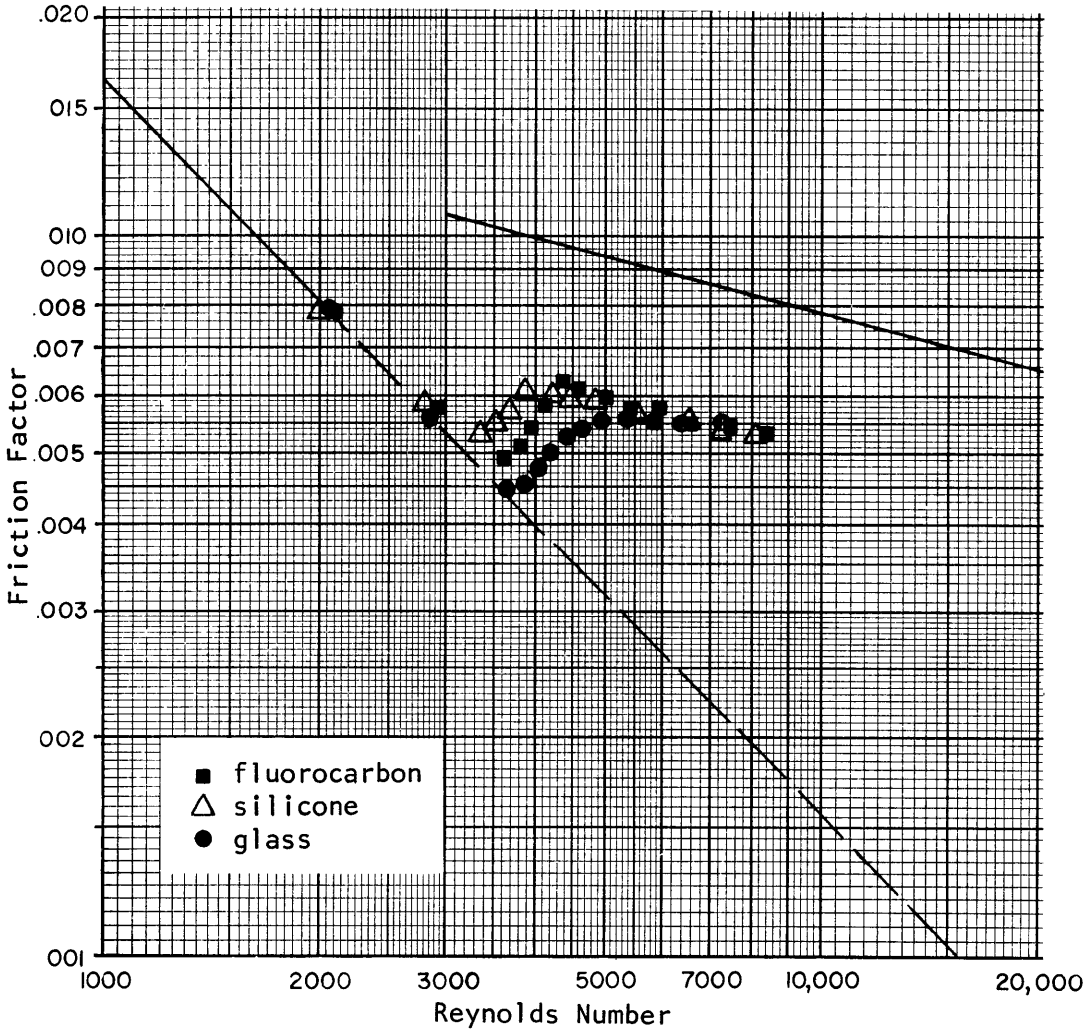

Friction Factor versus Reynolds Number for a 20 ppm "WSR-N-3000" solution in G16 series capillary tubes.

Figure VI-25

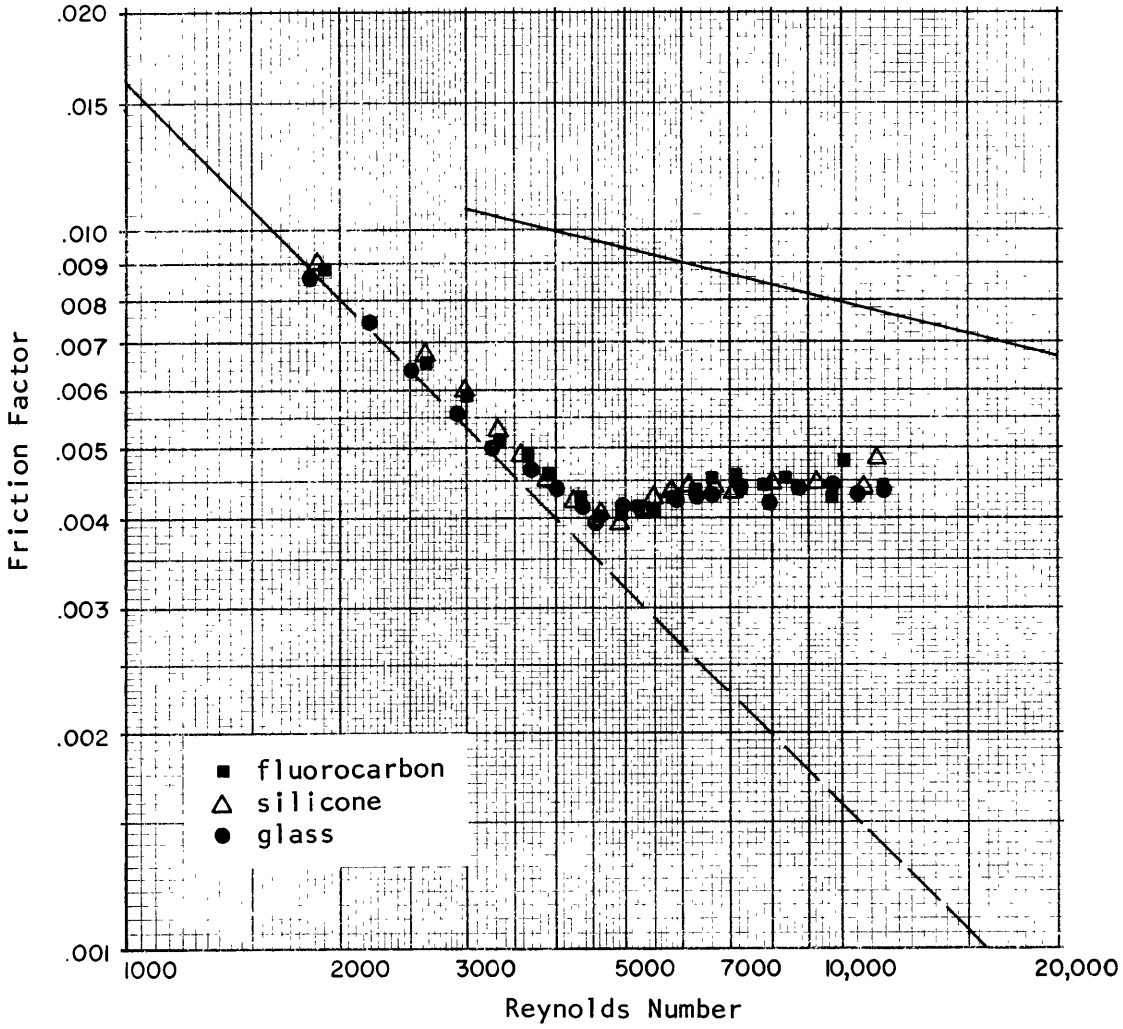

Friction Factor versus Reynolds Number for a 30 ppm "WSR-N-3000" solution in G16 series capillary tubes.

Figure VI-26

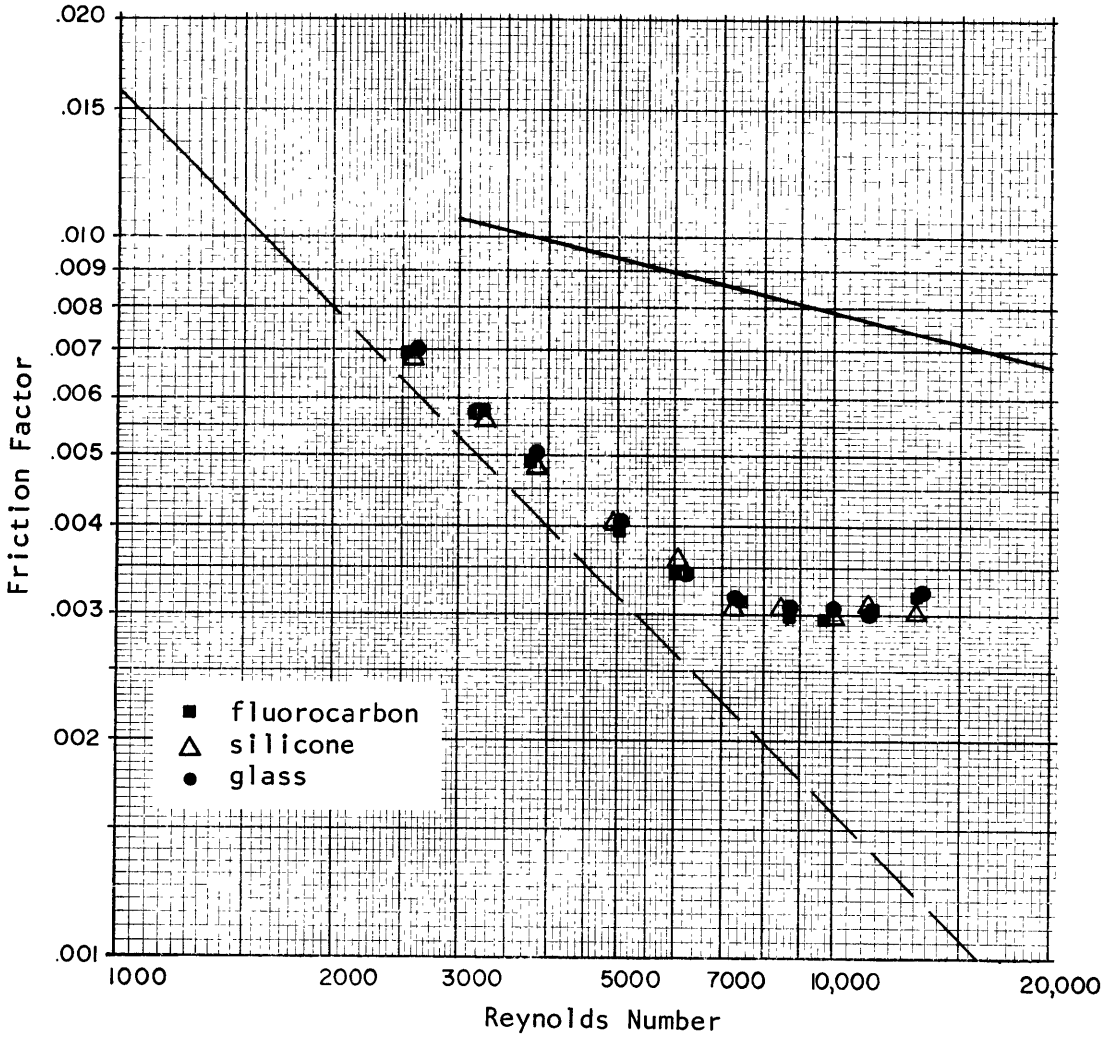

Friction Factor versus Reynolds Number for a 60 ppm "WSR-N-3000" solution in G16 series capillary tubes.

Figure VI-27

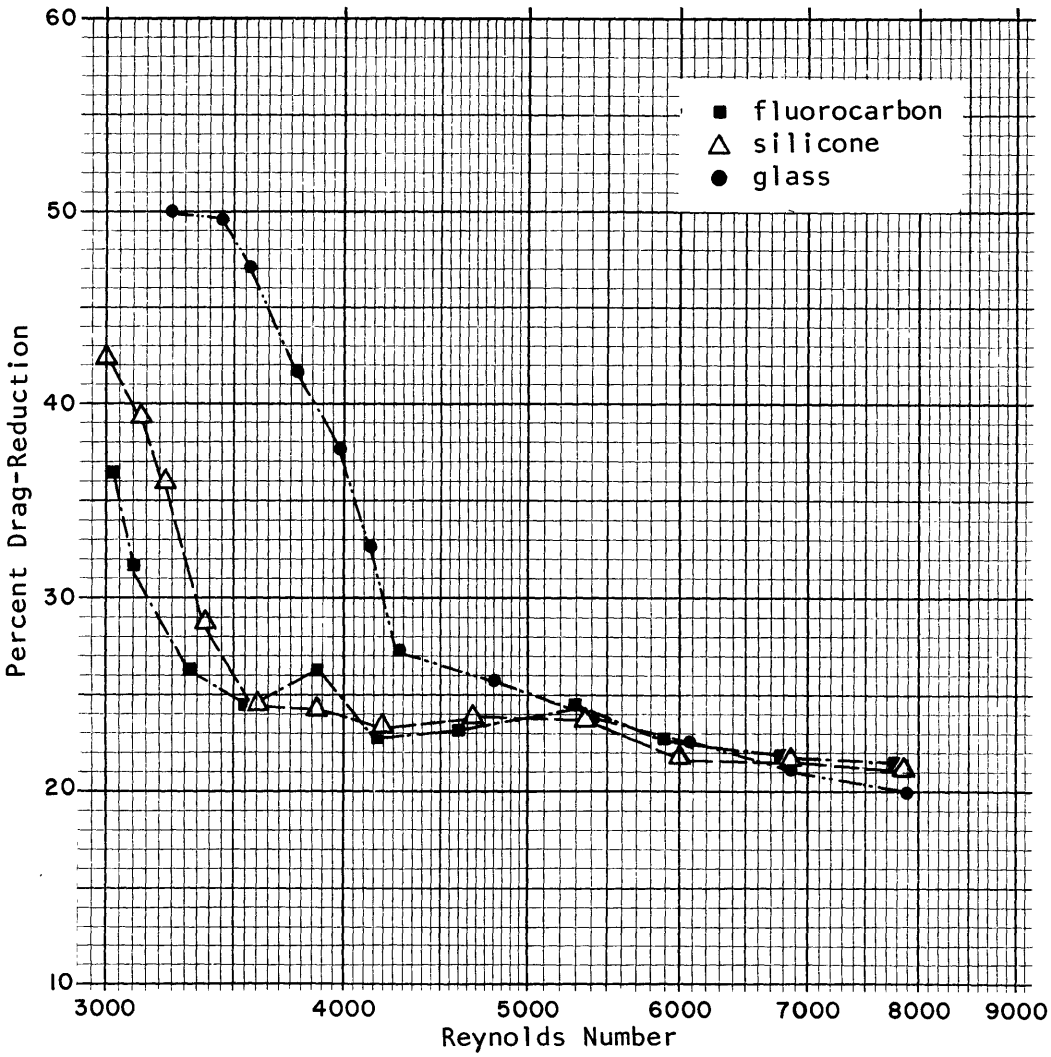

Drag-Reduction versus Reynolds Number for a 10 ppm "WSR-N-3000" solution in G16 series capillary tubes; replotted from Figure VI-24 with % DR=100(1-fp/f) Re.

Figure VI-28

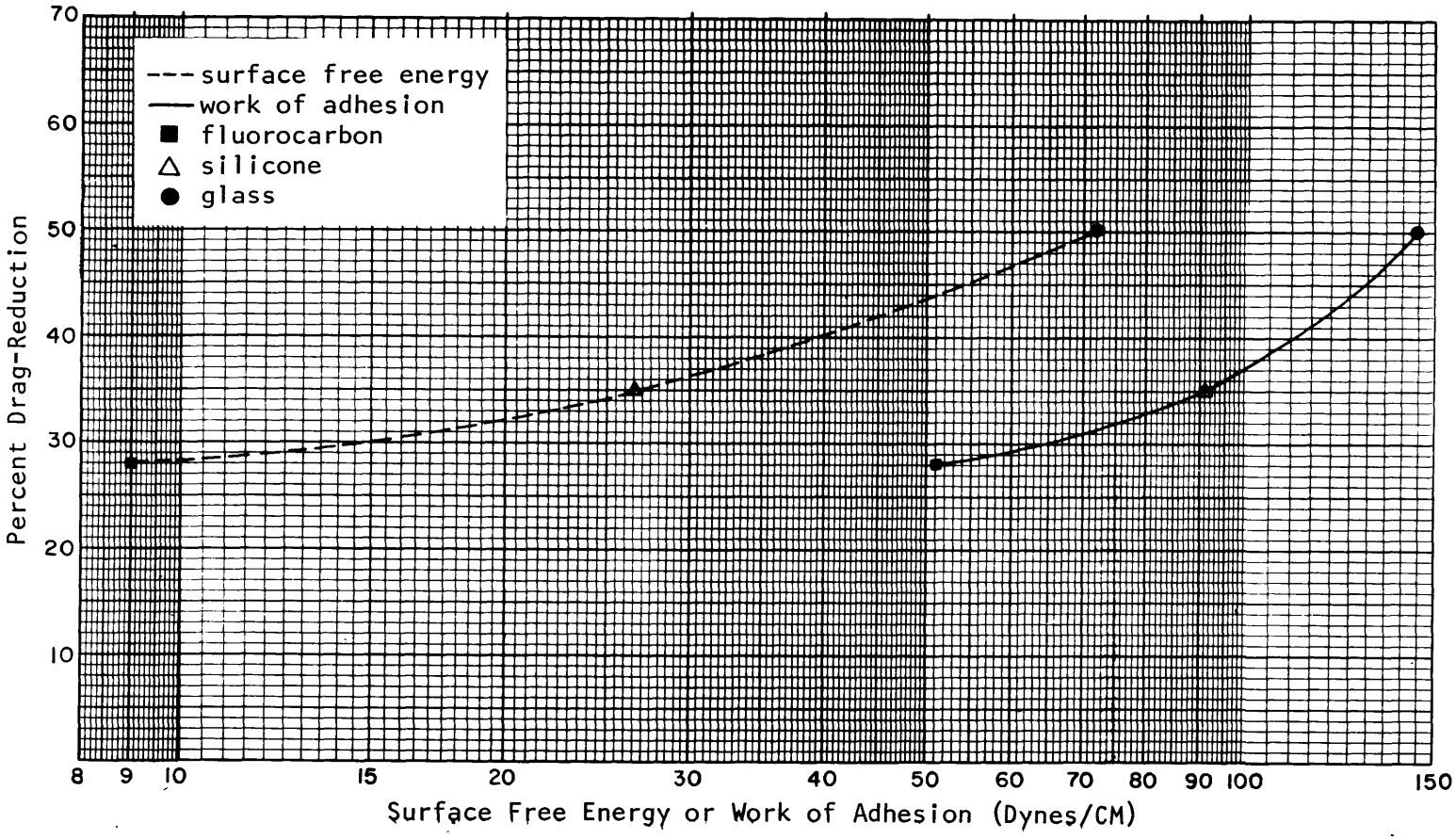

Drag-Reduction as a function of surface free energy and work of adhesion for a 10 ppm poly (ethylene oxide) "WSR-N-3000" solution in G16 series capillary tubes; Re_{max} = 3250.

Figure VI-29

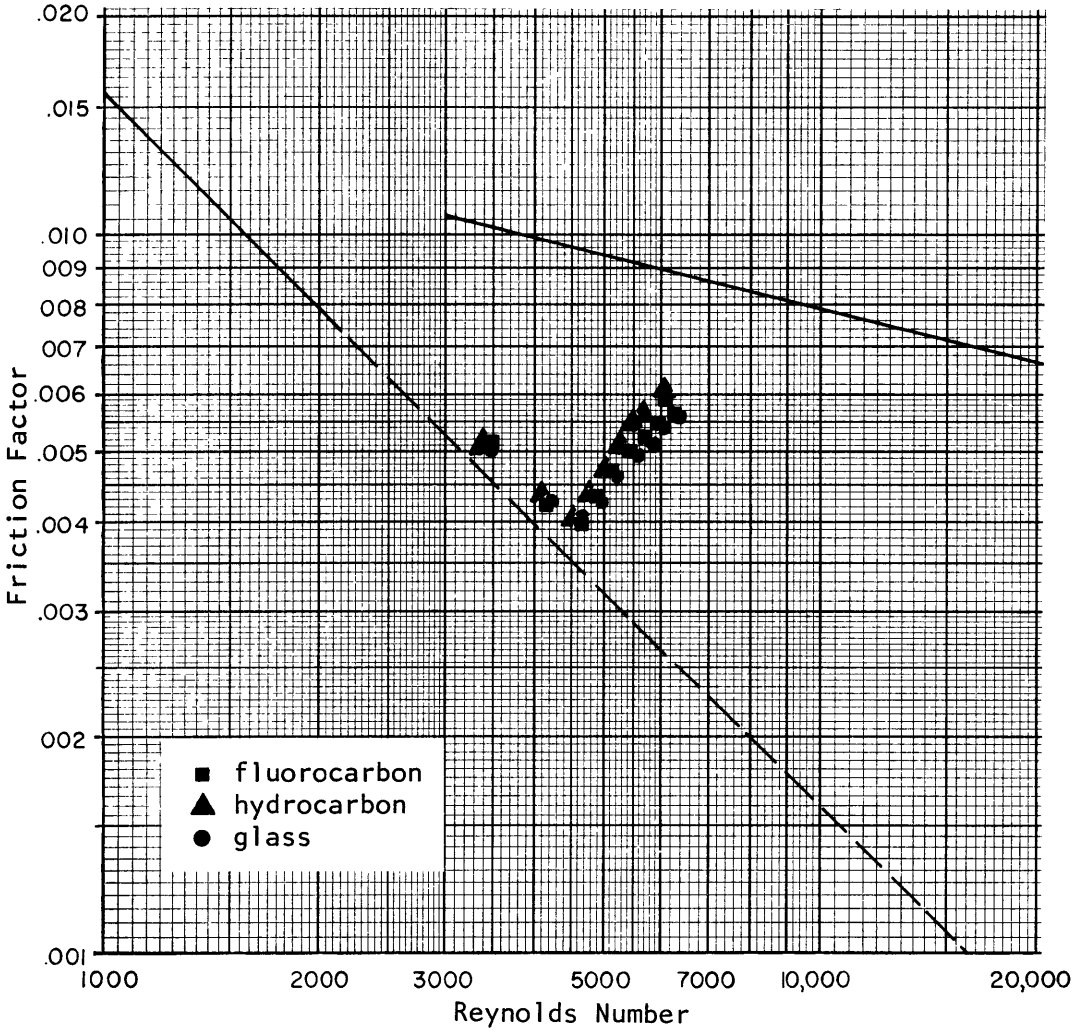

Friction Factor versus Reynolds Number for a 1 ppm "coagulant" solution in G20 series capillary tubes.

Figure VI-30

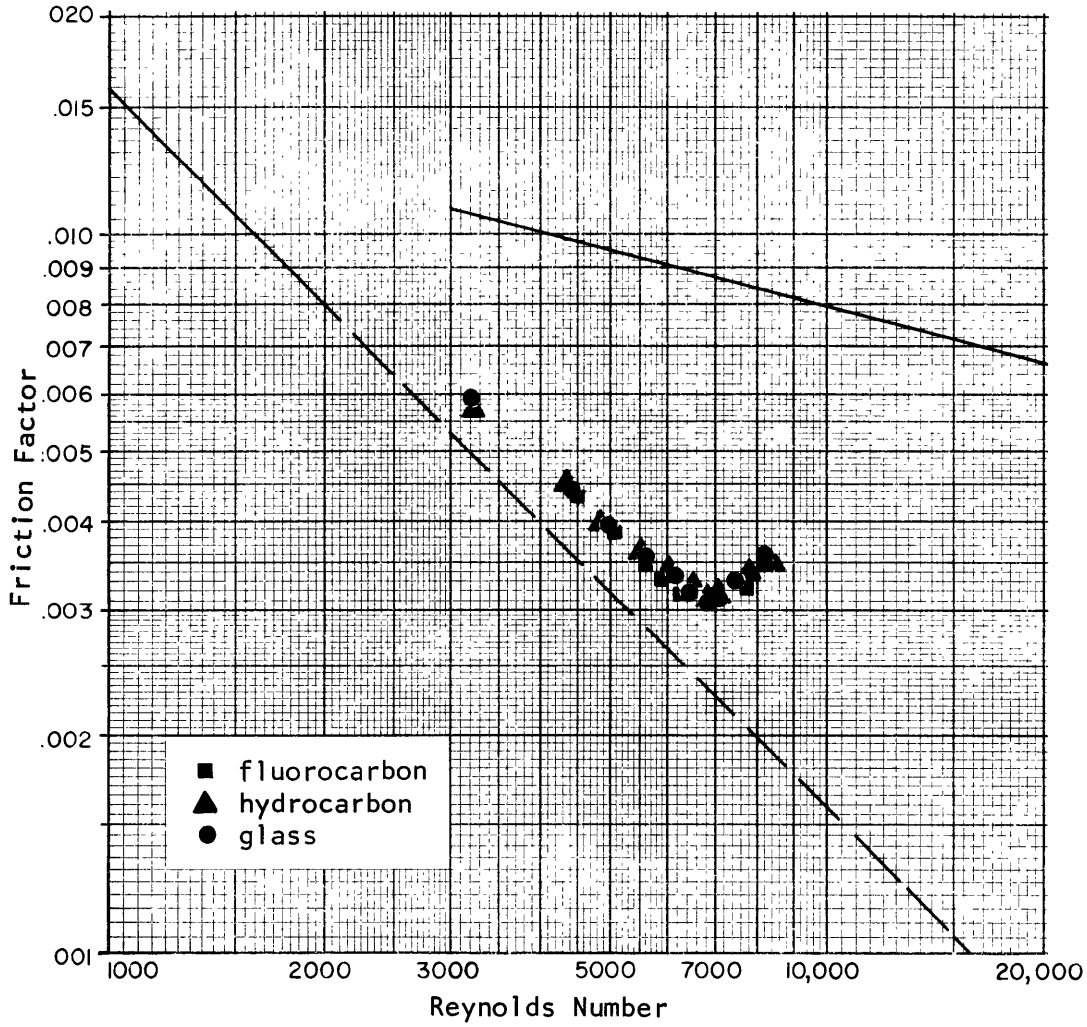

Friction Factor versus Reynolds Number for a 5 ppm "coagulant" solution in G20 series capillary tubes.

Figure VI-31

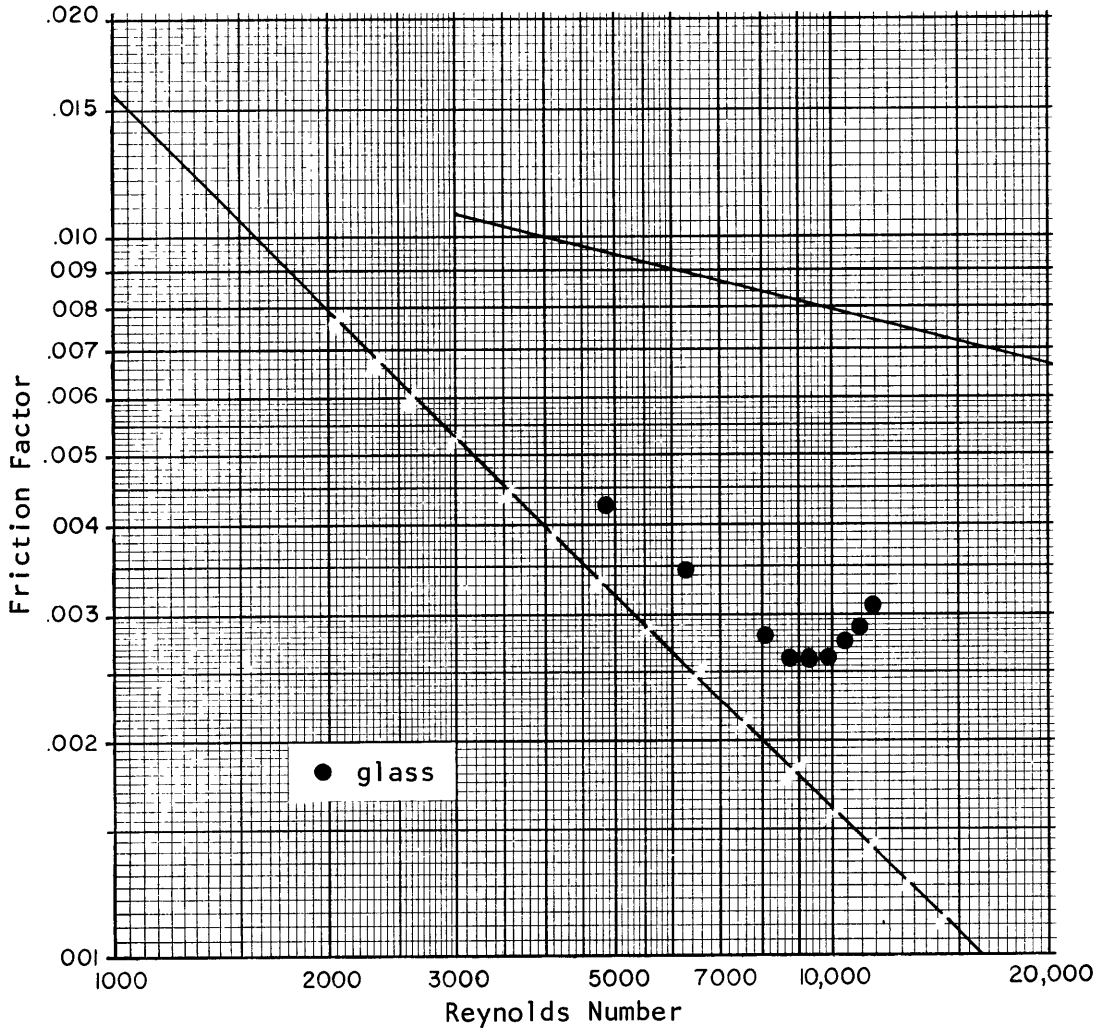

Friction Factor versus Reynolds Number for a 10 ppm "coagulant" solution in G20 series capillary tubes.

Figure VI-32

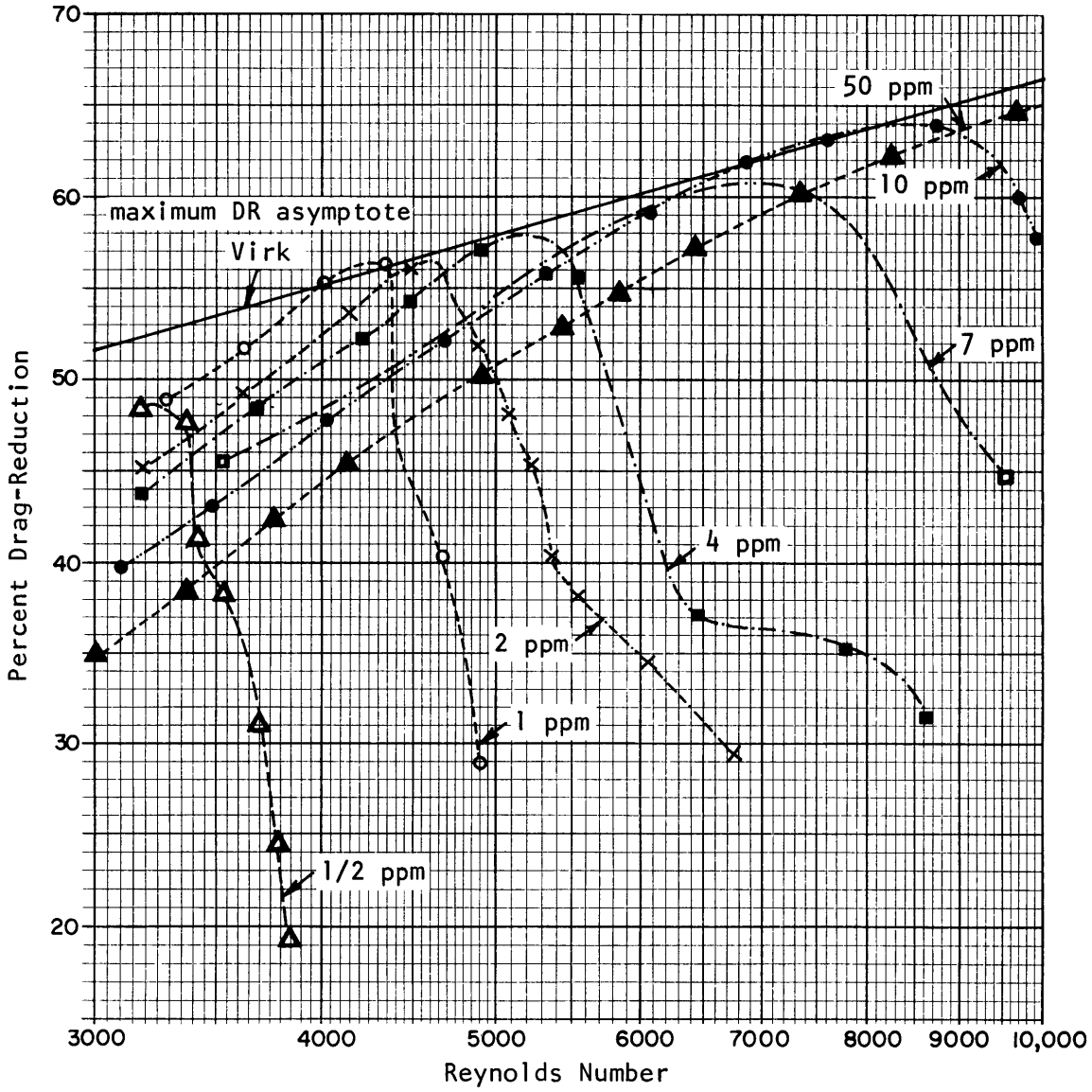

Drag-Reduction as a function of Reynolds Number for flow of "coagulant" solutions in glass capillary tube G16F; concentration as parameter.

Figure VI-33

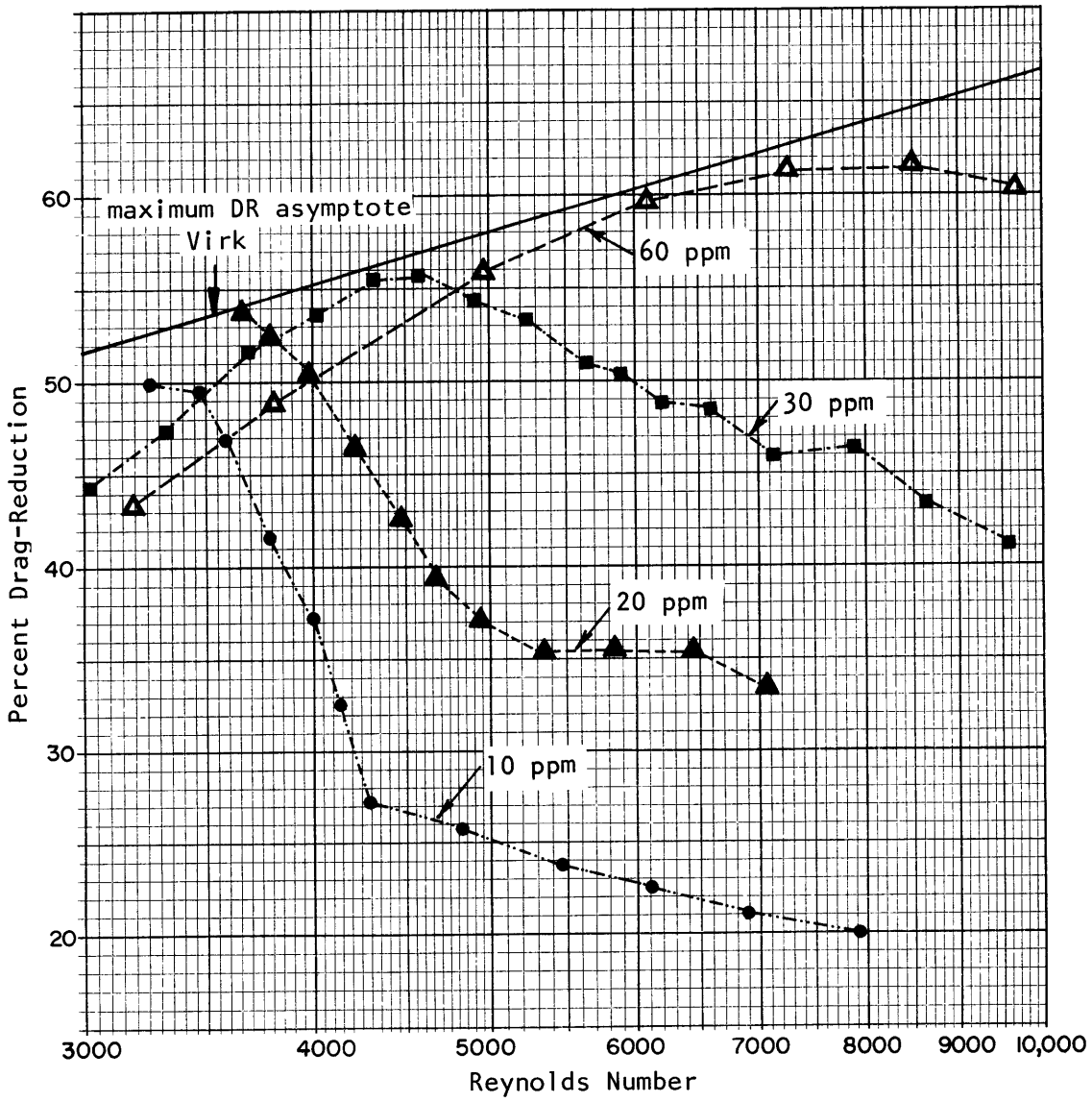

Drag-Reduction as a function of Reynolds Number for flow of "WSR-N-3000" solutions in glass capillary tube G16F; concentration as parameter.

Figure VI-34

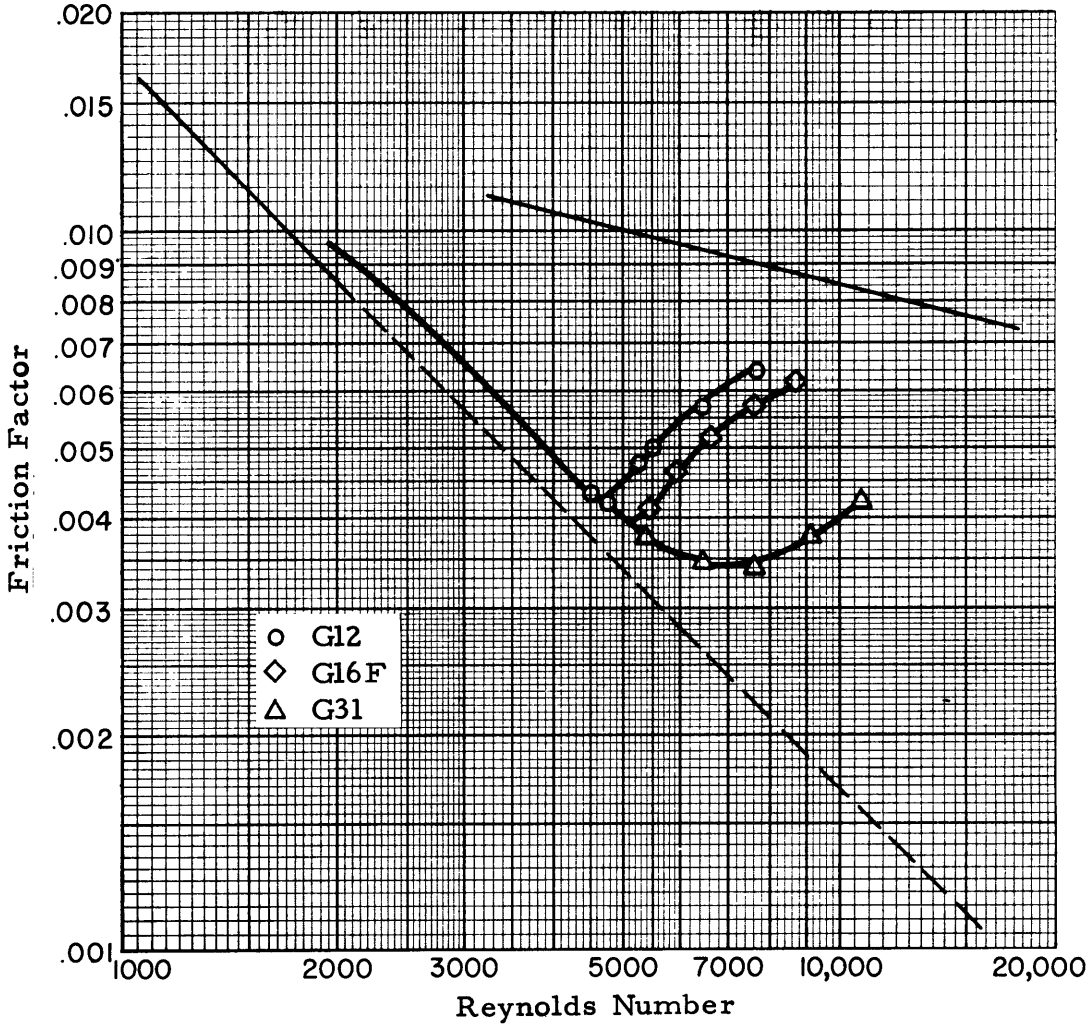

Friction Factor versus Reynolds Number for a 3 ppm "coagulant" solution in glass capillary tubes; tube diameter as parameter.

Figure VI-36

NOMENCLATURE

This list contains only those symbols which are used in more than one section of this text.

English

C	Concentration, gm/cm^3
D	Diameter, cm
DR	Drag-reduction, percent
f	Fanning friction factor, dimensionless
fp	Polymer solution friction factor
L	Length, cm
MW	Molecular weight
ΔP	Pressure drop, $dynes/cm^2$
Q	Volumetric flow rate, cm^3/sec
R	Radius, cm
R_c	Gas constant
Re	Reynolds number, dimensionless
T	Temperature
$\overline{V}$	Average velocity, cm/sec
W_A	Work of adhesion, dynes/cm

Greek

γ_{LV}^o	Surface tension, dynes/cm
γ_S^o	Surface free energy, dynes/cm

$\dot{\gamma}_w$ Wall shear rate, sec^{-1}

ϵ Shear surface viscosity coefficient, dynes-sec/cm

θ Contact angle, degrees

$\bar{\kappa}$ Dilational surface viscosity coefficient, dyne-sec/cm

μ Viscosity, dynes-sec/cm^2

μ_s $\mu_s = \bar{\kappa} + \epsilon$, surface viscosity, dynes-sec/cm

ν $\nu = \mu/\rho$, kinematic viscosity, cm^2/sec

ρ Density, gm/cm^3

τ_w Wall shear stress, dynes/cm^2

LITERATURE CITED

1. Toms, B. A., "Some Observations on the Flow of Linear Solutions Through Straight Tubes at Large Reynolds Numbers", Proc. of 1st Intnl. Congress on Rheology, Vol. II, pp. 135-141, North Holland Publishing Company, 1948.

2. Hoyt, J. W., "The Effect of Additives on Fluid Friction", U. S. Naval Ordnance Test Station Report TP 3670, Dec. 1964.

3. Hoyt, J. W., "The Friction-Reducing Effects of High Polymers", Naval Research Reviews, Oct. 1966.

4. Fabula, A. G., "The Toms Phenomenon in the Turbulent Flow of Very Dilute Polymer Solutions", Proc. of 4th Intnl. Congress on Rheology, 1963, Interscience, N. Y., 1965.

5. Schlicting, H., "Boundary Layer Theory", Fourth Edition, McGraw-Hill Book Co., Inc., New York, 1960.

6. Bird, R.,W. Stewart, and E. Lightfoot, "Transport Phenomena", John Wiley and Sons, Inc., New York, 1960.

7. Sherwood, T. K., K. A. Smith, and P. E. Fowles, "The Velocity and Eddy Viscosity Distribution in the Wall Region of Turbulent Flow", Chem. Eng. Science, Vol. 23, 1225-1236, 1968.

8. Granville, P. S., "The Frictional Resistance and Velocity Similarity Laws of Drag-Reducing Dilute Polymer Solutions", Naval Ship Research and Development Report 2502, Sept. 1967.

9. Reinhardt, H., NACA TM 1047, 1943.

10. Latzko, H., f. angen. Math. u. Mech., 1:268 (1921).

11. Paterson, R. W., "Turbulent Flow Drag-Reduction and Degradation with Dilute Polymer Solutions", Ph.D. Thesis, Harvard University, 1969.

12. Merrill, E. W., Smith, K. A., Shin, H. and Mickley, H. S., "Study of Turbulent Flows of Dilute Polymer Solutions in a Couette Viscometer", Transactions

of the Society of Rheology, 10:1, pp. 335-351 (1966).

13. Filisko, F., Private communication.

14. Hand, J. H., and M. C. Williams, "Effect of Secondary Polymer Structure on the Drag-Reducing Phenomena", Journal of Applied Polymer Science, Vol. 13, 2499 (1969).

15. Mathieson, A. R., and J. V. McLaren, J. Polymer Science, Vol. 3, 2555 (1965).

16. Little, R. C., "Flow Properties of Polyox Solutions", I.&E.C. Fundamentals, Vol. 8, No. 3, 557-9 (1969).

17. Cottrell, F. R., "An Experimental Study of the Conformation of Polyisobutylene in a Hydrodynamic Shear Field", Sc.D. Thesis Digest, (1968), M.I.T., Cambridge, Mass.

18. Stromberg, R. R., "Adsorption of Polymers", Treatise on Adhesion and Adhesives, Vol. 1, edited by R. L. Patrick, pp 69-118, Marcel Kekker, Inc., 1967.

19. Jenckel, E., and B. Rumback, F., Elektraeshem., Vol. 55, 612 (1951).

20. Frisch, H. L., and R. Simha, "Viscosity of Colloidal Suspensions and Macromolecular Solutions", J. Chem. Phys., Vol. 27, 702 (1957).

21. Forsman, W. C., and R. E. Hughes, "Adsorption Theory for Flexible Linear Polymer Molecules", J. Chem. Phys., Vol. 38, 2130 (1963).

22. Silberberg, A., "Adsorption of Flexible Macromolecules", J. Phys. Chem., Vol. 66, 1872, 1884 (1962).

23. Hoeve, C., A. J. DiMarzio, and P. Peyser, "Adsorption of Polymer Molecules at Low Surface Coverage", J. Chem. Phys., Vol. 42, 2558 (1965).

24. Roe, R. J., "Conformation of an Isolated Polymer Molecule at an Interface", Proc. Natl. Acad. Sci., M.S., Vol. 53, 50 (1965).

25. Öhrm, O. E., Arkiv, Kemi, Vol. 12, 397 (1958).

26. Rowland, F., R. Balas, E. Rothstein, and F. R. Eirich, "Structure of Macromolecules at Liquid-Solid Inter-

faces", Ind. Eng. Chem., Vol. 57, 46 (1965).

27. Rowland, F., "Flow Rates of Polymer Solutions Through Porous Disks as a Function of Solute", Ph.D. Thesis, Polytechnic Institute of Brooklyn, New York, 1963.

28. Fontana, B. J. and J. R. Thomas, "The Configuration of Adsorbed Alkyl Methacrylate Polymers by Infrared and Sedimentation Studies", J. Phys. Chem., Vol. 65, 480 (1961).

29. Stromberg, R. R., "Polymer Adsorption on Substrates", Interface Conversion for Polymer Coatings, edited by P. Weiss and G. D. Cheever, American Elsevier Publishing Co., Inc., 1969.

30. Kowalski, T., "Reduction of Frictional Drag by Non-Newtonian Additives", Naval Engineers Journal, Apr. 1966.

31. Davies, G. A., and A. B. Ponter, "Turbulent Flow Properties of Dilute Polymer Solutions", Nature, Vol. 212, No. 5057, 66, 1966.

32. Little, R. C., "Displacement of Aqueous Drag-Reducing Polymer Solutions, I.&E.C. Fundamentals, Vol. 8, 520 (1969).

33. Little, R. C., "Drag Reduction by Dilute Polymer Solutions in Turbulent Flow", NRL Report 6542, May 1967.

34. Peyser, P., Private communication.

35. Howard, G. J., and P. McConnel, "Adsorption of Polymers at the Solution-Solid Interface, 3-polyethers on Nylon", J. Phys. Chem., Vol. 71, No. 9, 2991 (1967).

36. Zisman, W. A., "Relation of Equilibrium Contact Angle to Liquid and Solid Constitution", Contact Angle, Wettability and Adhesion, edited by R. F. Gould, Advances in Chemistry Series, Vol. 43, American Chemical Society (1964).

37. Good, R. J., "Theory for the Estimation of Surface and Interfacial Energies", Contact Angle, Wettability and Adhesion, edited by R. F. Gould, Advances in Chemistry Series, Vol. 43, American Chemical Society, 74 (1964).

38. Virk, P. S., "The Toms Phenomenon - Turbulent Pipe Flow

of Dilute Polymer Solutions", Sc.D. Thesis, M.I.T., Nov. 1966.

39. Ernst, W. D., "Investigation of the Turbulent Shear Flow of Dilute Aqueous CMC Solutions", A.I.Ch.E. Journal, Vol. 12, No. 3, May 1966.

40. Shaver, R. G., and E. W. Merrill, "Turbulent Flow of Pseudo-Plastic Polymer Solutions in Straight Cylindrical Tubes", A.I.Ch.E. Journal, Vol. 5, No. 2, 191, 1959.

41. Oldroyd, J. G., "A Suggested Method of Detecting Wall Effects in Turbulent Flow Through Pipes", Proc. 1st Intnl. Congress on Rheology, Vol. II, pp 130-134, North Holland Publishing Co., 1948.

42. Meyer, W. A., "A Correlation of the Frictional Characteristics for Turbulent Flow of Dilute Viscoelastic Non-Newtonian Fluids in Pipes", A.I. Ch.E. Journal, Vol. 12, No. 3, May 1966.

43. Laufer, J., "The Structure of Turbulence in Fully Developed Pipe Flow", Report 1174, N.A.C.A. (1954).

44. Hanson, J., Personal communication.

45. Fabula, A. G., "An Experimental Study of Grid Turbulence in Dilute High-Polymer Solutions", Ph.D. Thesis, Pennsylvania State University, June 1966.

46. Fabula, A. G., Lumley, J. L. and Taylor, W. D., "Some Interpretations of the Toms Effect", Modern Developments in the Mechanics of Continua, Academic Press Inc., New York (1966).

47. Lumley, J. L., Annual Review Fluid Mechanics, Vol. 1, Annual Review Inc., Palo Alto, California (1969).

48. Savins, J. G., "Drag Reduction Characteristics of Solutions of Macromolecules in Turbulent Pipe Flow", Soc. of Petroleum Engineers Journal, pp 203-214, Sept 1964.

49. Hershey, H. C., and J. L. Zakin, "Existence of Two Types of Drag Reduction in Pipe Flow of Dilute Polymer Solutions", I.&E.C. Fundamentals, Vol. 6, No. 3, 381 (1967).

50. Hershey, H. C., "Drag Reduction of Newtonian Polymer Solutions", Ph.D. Thesis, U. of Missouri, Aug. 1965.

51. Walsh, M., "On the Turbulent Flow of Dilute Polymer Solutions", Ph.D. Thesis, C.I.T., Pasadena, California (1967).

52. Pruitt, G. T., B. Rosen, and H. R. Crawford, "Effect of Polymer Coiling on Drag Reduction", Western Company Report DTMB - 2, Aug 1966.

53. Elata, C., J. Lehrer, and A. Kahanovitz, "Turbulent Shear Flow of Polymer Solutions", Israel Journal of Technology, Vol. 4, No. 1, 87, 1966.

54. Rouse, P. E., "A Theory of the Linear Visco-Elastic Properties of Dilute Solutions of Random Coiling Polymers, J. Chem. Physics, Vol. 21, 1272, 1953.

55. Adamson, A. W., Physical Chemistry of Surfaces, Interscience Publishers, Inc., N. Y., 1967.

56. Cotton, D. J., "A General Theory of Interfacial Tension and its Application to Adsorption Phenomena", Ph.D. Thesis, Howard University, Jan 1968.

57. Lyman, D. J., W. M. Muir, and I. J. Lee, "The Effect of Chemical Structure and Surface Properties of Polymers on the Coagulation of Blood", Trans. Amer. Soc. Artif. Int. Organs, Vol. 11, 301 (1965).

58. Bischoff, K. B., "Discussion of Correlations of Blood Coagulation with Surface Properties of Materials", J. Biomed. Mater. Res., Vol. 2, pp 89-93 (1968).

59. Shin, H., "Reduction of Drag in Turbulence by Dilute Polymer Solutions", Sc.D. Thesis, M.I.T., May 1965.

60. Poreh, M., H. Rubin and C. Elata, "Studies in Rheology and Hydrodynamics of Dilute Polymer Solutions", Clearinghouse (DDC) Report No. AD690264.

61. Kanner, B., and J. E. Glass, "Surface Viscosity and Elasticity", I.&E.C., Vol. 61, No. 5, pp 31-41, May 1969.

62. Motomura, K., "Interfacial Viscoelasticity of Poly-DL-Alanine and Bovine Serum Albumin Monolayers", J. Phys. Chem., Vol. 68, 2826 (1964).

63. Inokuchi, K., "Mechanism of Agglomeration of Red Cells for High Polymer Compounds", Bull. Chem. Soc., Jap., Vol. 26, 500 (1953).

64. MacRitchie, F., and A. E. Alexander, "The Effect of Sucrose on Surface Films", J. Colloid Science, Vol. 16, 57 (1961).

65. Inokuchi, K., "Rheology of Surface Films", Bull. Chem. Soc. Jap., Vol. 28, 453 (1955).

66. Brown, A. G., W. C. Thurman, and J. W. McBain, J. Colloid Science, Vol. 8, 491 (1953).

67. Jarvis, N. L., "Surface Viscosity of poly(dimethylsiloxane) Monolayers", J. Phys. Chem., Vol. 70, 3027 (1966).

68. Whitaker, S., "Gravitational Thinning of Films", Ind. Eng. Chem. Fundam., Vol. 5, No. 3, pp 379-388, Aug 1966.

DISTRIBUTION LIST

NSRDC (Code L41) (2)
NSRDC (Code 513)
NSRDC (Code 508)
NSRDC (Code 581)
NSRDC (Code L42) (10)
NAVSHIPRANDLAB PANAMA
NAVSHIPS (SHIPS 034)
NAVSHIPS (SHIPS 03412)
NAVSHIPS (SHIPS 037)
NAVSHIPS (SHIPS 037C)
NAVSHIPS (SHIPS 08)
NAVSHIPS (SHIPS PMS 381)
NAVSHIPS (SHIPS 425)
NAVSHIPS (SHIPS 2052) (2)
NAVSHIPS (SHIPS PMS 393)
NAVSHIPS (SHIPS 0371)
NAVSHIPS (SHIPS 031)
NAVSEC (SEC 6103)
NAVSEC (SEC 6110)
NAVSEC (SEC 6114D)
NAVSEC (SEC 6111)
NAVSEC (SEC 6136)
DDC (20)
USL
ONR (Code 438)
(Mr. R. D. Cooper)
ONR Branch Office
Boston, Mass. 02210
(Dr. A. Wood)
NRL (Dr. R. C. Little)
NAVUSEARANDCEN PASADENA
(Code 2501)
(Code 254)
(Code 2543)
SSPO
NUWS (J. F. Brady, R. Nadolink)
NAVUSEARANDCEN
(H. V. L. Patrick)
AFORSR (SREM)
1400 Wilson Boulevard
Arlington, Va. 22209
Library of Congress
Science & Technology Div.
Washington, D.C. 20540

NAVORDSYSCOM (Codes 035, 054131)
Dept. of Naval Architecture
College of Engineering
Univ. of Calif.
Berkeley, Calif. 94720
(Prof. J. V. Wehausen)
Calif. Inst. of Technology
1201 E. Calif. Blvd
Pasadena, Calif. 91109
(Dr. A. J. Acosta)
(Dr. T. Y. Wu)
Univ. of Conn., Box U-37
Hydraulic Research Lab.
Storrs, Conn. 06268
(Prof. V. Scottron)
Harvard Univ., Pierce Hall
Cambridge, Mass. 02138
(Prof. G. J. Carrier)
Univ. of Illinois
College of Engineering
Theoretical & Applied
Mechanics Dept.
Urbana, Illinois 61801
(Dr. J. M. Robertson)
Brown Univ.
Providence, R.I. 02912
(Prof. R. I. Tanner)
The Univ. of Iowa
Iowa City, Iowa 52240
(Dr. H. Rouse)
The Univ. of Iowa
Iowa Inst. of Hydraulic Research
Iowa City, Iowa 52240
(Dr. L. Landweber)
(Dr. J. Kennedy)
Mass. Inst. of Technology
Dept. of Naval Architecture
& Marine Engineering
Cambridge, Mass. 02139
(Dr. A. H. Keil)
Univ. of Mich.
Dept. of Naval Architecture
& Marine Engineering
Ann Arbor, Mich. 48104
(Dr. T. J. Ogilvie)

DISTRIBUTION LIST (Cont)

St. Anthony Falls Hydraulic Lab.
Univ. of Minn.
Mississippi River &
3rd Ave., S.E.
Minneapolis, Minn. 55414
(Director)
(Mr. J. M. Killen)
(Mr. F. Scheibe)
(Mr. J. M. Wetzel)
(Mr. J. Ripkin)

U.S. Naval Academy
Annapolis, Md. 21402
(Library)
(Dr. B. Johnson)
(Dr. A. Adams)

U.S. Naval Postgraduate School
Dept. of Mechanical Engineering
Monterey, Calif. 93940
(Dr. T. Sarpkaya, Code 59)

The Pennsylvania State Univ.
Ordnance Research Lab.
University Part, Pa. 16801
(Director)
(Prof. J. Lumley)
(Dr. Sevir)

Colorado State Univ.
Dept. of Civil Engineering
Fort Collins, Colo. 80521
(Dr. J. P. Tullis)

Esso Research & Engineering Co.
Engineering Technology Dept.
Florham Park, N.J. 07932

Stanford Univ.
Stanford, Calif. 94305
(Prof. R. L. Street)

Stevens Inst. of Technology
Davidson Lab.
711 Hudson St.
Hoboken, N.J. 07030
(Dr. J. Breslin)

Hydronautics, Inc.
Pindell School Road
Laurel, Md. 20810
(Mr. P. Eisenberg)
(Mr. M. Tulin)
(Mr. J. Wu)

National Science Foundation
Engineering Div.
1800 G. St., N.W.
Washington, D.C. 20550
(Director)

Univ. of Calif. at San Diego
Dept. of Applied Mechanics
P.O. Box 109
La Jolla, Calif. 92038
(Dr. A. T. Ellis)

NAVSCIENTECHINTCEN (Code 234)

The Western Co.
2201 N. Waterview Pkwy
Richardson, Texas 75080
(N. F. Whitsitt)

Union Carbide Co.
P.O. Box 65
Tarrytown, N.Y. 10591
(Dr. F. W. Stone)

Esso Research & Engineering Co.
Government Research Lab.
P.O. Box 8, Bldg 8
Linden, N.J. 07036
(M. Lieberman)

Maritime Administration
Office of Research &
Development
441 G. St., N.W.
Washington, D.C. 20235
(Director)
(R. Falls)

Lone Star Gas
Dallas, Texas 75240
(Dr. H. Crawford)

General Electric Co.
Research & Development Center
Schenectady, N.Y. 12301
(W. B. Giles)
(F. W. Staub)
(J. C. Corman)
(S. D. Savkar)

Univ. of Delaware
Dept of Chemical Engineering
Newark, Delaware 19711
(Prof. A. B. Metzner)

DISTRIBUTION LIST (Cont)

Univ. of Missouri
Dept. of Chemical Engineering
Rolla, Mo. 65401
(Prof. G. K. Patterson)
Mobil Field Research Lab.
P.O. Box 900
Dallas, Texas 75221
(J. G. Savins)
LTV Research Center
P.O. Box 6144
Dallas, Texas 75222
(C. S. Wells)
(W. A. Meyer)
U.S. Army Mobility Equipment
& R&D Center
Fort Belvoir, Va. 22060
(K. L. Trieber)
Columbia Research Corp.
P.O. Box 485
Gaithersburg, Md. 20760
(P. A. Crowley)
(N. C. Witbeck)
North American Rockwell Corp.
3370 Miraloma Ave.
Anaheim, Calif. 92803
(E. R. Van Driest)

Security Classification UNCLASSIFIED

DOCUMENT CONTROL DATA - R & D

(Security classification of title, body of abstract and indexing annotation must be entered when the overall report is classified)

1 ORIGINATING ACTIVITY *(Corporate author)*
Naval Ship Research and Development Laboratory
Annapolis, Maryland 21402

2a. REPORT SECURITY CLASSIFICATION
Unclassified

2b. GROUP

3 REPORT TITLE
Turbulent Flow Drag-Reduction by Dilute Poly(Ethylene Oxide) Solutions in Capillary Tubes

4 DESCRIPTIVE NOTES *(Type of report and inclusive dates)*
Research and Development

5 AUTHOR(S) *(First name, middle initial, last name)*
Ira Michael Felsen

6 REPORT DATE	7a. TOTAL NO. OF PAGES	7b. NO. OF REFS
March 1971	163	68

8a. CONTRACT OR GRANT NO	9a. ORIGINATOR'S REPORT NUMBER(S)
b. PROJECT NO Task Area Z-R011 01 01	3240
c. Task 05600	9b. OTHER REPORT NO(S) *(Any other numbers that may be assigned this report)*
d. Work Unit 1-821-135A	8-717 AD 720 688

10. DISTRIBUTION STATEMENT
Approved for public release; distribution unlimited.

11. SUPPLEMENTARY NOTES	12. SPONSORING MILITARY ACTIVITY
Originally published as doctoral thesis for the University of Maryland	Naval Ship Research and Development Laboratory Annapolis, Maryland 21402

13. ABSTRACT

An experimental investigation of turbulent flow drag-reduction was conducted using dilute solutions of poly(ethylene oxide) flowing in capillary tubes. This study was initiated to investigate turbulent flow drag-reduction by dilute poly(ethylene oxide) solutions in capillary tubes and thereby elucidate the mechanism of drag-reduction through interpretation of the experimental results. Flow through capillary tubes was chosen as a means to (1) obtain a large ratio of solid surface area to fluid volume, and (2) obtain high shear stresses at low Reynolds numbers. This allowed investigation of surface effects and polymer degradation as a function of a number of variables which are known to influence drag-reduction. Small bore capillary tubes were coated with monomolecular layers having various surface free energies. Use of these tubes offered a method of distinguishing whether drag-reduction is due in part or wholly to some property(ies) or configuration of the macromolecule in solution, or to the properties and configuration of the polymer adsorbed on the solid surface and interacting with the solution flowing through and around the adsorbed polymer film. In the small-bore uncoated-glass capillary tubes used, a 1 ppm poly(ethylene oxide) Coagulant solution gives drag-reduction as high as 56%. In addition,

(over)

14 KEY WORDS	LINK A		LINK B		LINK C	
	ROLE	WT	ROLE	WT	ROLE	WT
Poly(Ethylene Oxide)						
Capillary Tubes						
Turbulent Flow						
Drag-Reduction						
Shear Stresses						
Surface Effects						
Polymer Degradation						
Polymer Film						
Surface Viscosity						
Gibbs Elasticity						

Abstract (Cont)

the Virk maximum drag-reduction asymptote is obtained, even at concentrations as low as 1 ppm for poly(ethylene oxide) Coagulant, and 10 ppm for poly(ethylene oxide) WSR-N-3000. Drag-reduction increases systematically with decreasing concentration, at constant Reynolds number, prior to the onset of degradation. The effect of increasing concentration is to allow intersection with the maximum drag-reduction asymptote at a higher percent drag-reduction. Upon reaching the asymptote, degradation begins and proceeds rapidly with increasing pressure driving force, or, for higher concentrations, the curves intersect and then run along the asymptote until degradation begins. Virk's asymptote is verified as being diameter and molecular weight independent. At equal Reynolds numbers, drag-reduction is independent of tube diameter until polymer degradation begins in the smaller diameter tube. At Reynolds numbers corresponding to equal wall shear stresses, drag-reduction decreases with increasing tube diameter. In a series of 0.016 inch diameter capillary tubes of surfaces fluorocarbon, hydrocarbon, silicone, and glass, a 1/2 ppm poly(ethylene oxide) Coagulant solution gives drag-reduction as high as 59% in the glass tube. All tubes give equal drag-reduction until the onset of degradation is approached. The maximum Reynolds number, or stability before the onset of degradation, is obtained in the uncoated glass tube. The experimental evidence shows an increase in the maximum Reynolds number at the onset of degradation with increasing surface free energy of the tube coatings. Consequently, drag-reduction increases with increasing surface free energy, at equal Reynolds numbers, at the onset of degradation. A semi-flexible film hypothesis is presented. Emphasis is placed on the importance of surface viscosity and Gibbs elasticity of an adsorbed or hydrogen bond associated polymer film, and not on turbulence suppression by individual polymer molecules. A wall associated polymer film, exhibiting optimum surface rheology characteristics, may act to inhibit turbulence in the wall region, and thus stabilize flow and retard the onset of degradation.

(Author)